



**HAL**  
open science

# The role of synaptopodin for the diffusion of membrane protein in the dendritic spine neck

Lili Wang

► **To cite this version:**

Lili Wang. The role of synaptopodin for the diffusion of membrane protein in the dendritic spine neck. Other [q-bio.OT]. Ecole normale supérieure - ENS PARIS, 2015. English. NNT : 2015ENSU0021 . tel-01771759

**HAL Id: tel-01771759**

**<https://theses.hal.science/tel-01771759>**

Submitted on 19 Apr 2018

**HAL** is a multi-disciplinary open access archive for the deposit and dissemination of scientific research documents, whether they are published or not. The documents may come from teaching and research institutions in France or abroad, or from public or private research centers.

L'archive ouverte pluridisciplinaire **HAL**, est destinée au dépôt et à la diffusion de documents scientifiques de niveau recherche, publiés ou non, émanant des établissements d'enseignement et de recherche français ou étrangers, des laboratoires publics ou privés.



*En vue de l'obtention du grade de*

**DOCTEUR de L'ÉCOLE NORMALE SUPÉRIEURE**

École Doctorale Cerveau Cognition Comportement

**The Role of Synaptopodin in Membrane Protein Diffusion  
in the Dendritic Spine Neck**

Présentée par  
Lili Wang

Soutenue le 14 septembre 2015 devant le jury composé de

Présidente	Patricia Bassereau DR, UMR168, Institut de Curie
Rapporteur	Olivier Thoumine CR, UMR5297, Université de Bordeaux2
Rapporteur	Lorenzo Cingolani DR, Italian Institute of Technology, Gênes
Examineur	Marianne Renner Professeur, Université Pierre et Marie Curie
Examineur	Serge Marty CR, Institut du Cerveau et de la Moelle Epinière
Directeur de thèse	Antoine Triller DR, Institut de Biologie de l'École Normale Supérieure



## Abstract

Lateral diffusion in and outside synapses plays a key role in the accumulation of receptors at synapses, which critically determines the efficacy of synaptic neurotransmission. Therefore, to better understand the trapping of neurotransmitter receptors in synapses, it is important to investigate the mechanisms that may affect receptors diffusion and their capacity to reach synapses. The neck of dendritic spine imposes a diffusional barrier that is considered to depend on the length and diameter of the spine neck. The origin of this barrier could be purely geometrical or could be induced by the presence of specific barriers/obstacles for diffusion. A subpopulation of spines contains a specialized form of endoplasmic reticulum in the spine neck called spine apparatus. The actin-binding protein synaptopodin (SP) is tightly associated with the spine apparatus and participates in synaptic plasticity mechanisms. The central question of my research was to assess whether the presence of the SP affects the diffusion of receptors in the spine neck and to characterize the underlying molecular mechanisms.

To study membrane diffusion, I have developed three different probes: a construct associated with the outer leaflet of the plasma membrane (GFP-GPI), a construct with one transmembrane domain and a short intracellular sequence (TMD-pHluorin), and a recombinant metabotropic mGluR5 receptor construct containing an extracellular domain tagged with pHluorin, seven transmembrane domains, as well as a large intracellular region. The diffusion properties of these molecules were measured by single particle tracking using quantum dots. My experiments revealed that the diffusion of membrane proteins was slower in the spine neck than in the dendrite as a result of the different diameter of the two compartments. Furthermore, the diffusion properties depended on the molecular size and complexity of the membrane proteins. Interestingly, the diffusion of membrane proteins with transmembrane domains was particularly slow in spine necks containing SP. This could be the result of direct molecular interactions between the membrane proteins and SP or due to spatial constraints that are related to the structural organization of spine necks expressing SP.

To address these questions further I used pharmacological treatments to change the internal organization of the spine neck, and measured their effect on the diffusion properties of mGluR5. The distribution of SP and F-actin in the spine neck was determined on the nanoscopic scale using PALM/STORM imaging. This showed that under control condition SP occupies only the central region of the spine neck. Activity-dependent depolymerization of F-actin by 4-Aminopyridine led to a simultaneous decrease of the amount of F-actin and SP and enhanced the diffusion of mGluR5 in all analyzed neck regions. Disruption of F-actin by latrunculin A

induced the re-distribution of SP and the formation of larger SP clusters, occupying an increased region within the spine neck. The recruitment of SP was accompanied by an acceleration of mGluR5 diffusion in SP-positive spines, demonstrating that the mobility of mGluR5 is not controlled by direct interactions with SP. Instead, the diffusion of mGluR5 is dependent on the organization of the spine cytoskeleton.

In conclusion, I propose that SP and the polymerization of actin filaments have a reciprocal effect on the stability of each other in the spine neck of cultured hippocampal neurons. Spine necks bearing SP have a unique F-actin cytoskeletal organization that acts as an additional diffusion barrier for neurotransmitter receptors such as mGluR5.

## Résumé

Au sein des synapses comme dans les régions extrasynaptiques, la diffusion latérale joue un rôle critique dans la densité membranaire des récepteurs. En face des zones actives, l'accumulation de récepteurs détermine en particulier l'efficacité de la transmission synaptique. Il est important de comprendre les paramètres cellulaires qui jouent sur l'accès au compartiment synaptique, qu'ils soient d'origine moléculaires ou morphologiques. Dans les synapses excitatrices, la tige de l'épine dendritique se comporte comme une barrière à la diffusion. Cette barrière pourrait être fonction de la longueur et du diamètre de la tige (paramètre géométrique), ou résider dans la présence d'éléments spécifiques constituant des obstacles à la diffusion. Une sous-population d'épines contient dans sa tige une forme spécialisée de réticulum endoplasmique, appelé appareil épineux et constituée d'un empilement de saccules de réticulum. Une protéine liant l'actine, nommée synaptopodine, est associée de façon étroite à l'appareil épineux et participe aux mécanismes de plasticité synaptique. La question centrale de ce travail de thèse était de définir si la présence de synaptopodine influait sur les caractéristiques de la diffusion dans la tige de l'épine, et d'identifier les mécanismes sous-jacents.

Afin d'étudier la diffusion membranaire, j'ai utilisé trois protéines recombinantes différentes: une protéine associée au feuillet extérieur de la membrane plasmique (GFP-GPI), une protéine avec un domaine transmembranaire et une courte séquence intracellulaire (TMD-pHluorin), et la sous-unité GluR5 du récepteur métabotrope (mGluR5) contenant 7 domaines transmembranaires et une séquence intracellulaire volumineuse. Les trois constructions portent une étiquette (GFP ou pHluorin) du côté extracellulaire. Les propriétés diffusives de ces molécules ont été mesurées par un suivi de particules uniques, à base de quantum dots. Ces expériences ont révélé que la diffusion des protéines membranaires est fonction du diamètre de la structure cylindrique considérée, et par conséquent moins rapide dans la tige de l'épine que dans le tronc du dendrite. Mais les propriétés diffusives dépendent aussi de la taille et de la complexité des molécules membranaires considérées. En effet, la diffusion de molécules comportant des domaines transmembranaires est particulièrement faible dans les tiges contenant de la synaptopodine.

Cet aspect a été approfondi par l'utilisation de traitements pharmacologiques, qui ont permis de modifier la structure interne de la tige dendritique. Les variations des tailles des

domaines occupés par l'actine-F, et par les agrégats de synaptopodine, ont été observées à l'échelle nanoscopique en utilisant l'imagerie PALM/STORM. En conditions contrôle, la synaptopodine occupe la partie centrale de la tige. La dépolymérisation indirecte de l'actine-F par le 4-Aminopyridine entraîne une diminution des zones occupées par ces deux composants, corrélée à une augmentation de la vitesse de diffusion de mGluR5. En revanche, la dépolymérisation par la latrunculin-A (effet direct sur l'actine) induit une augmentation de la taille des clusters de synaptopodine et donc de la surface occupée par ceux-ci dans la tige. Les mesures de la diffusion de la sous-unité mGluR5 réalisées dans ces conditions montrent une accélération de la vitesse de diffusion, indiquant que la mobilité de mGluR5 n'est pas régulée par une interaction directe avec la synaptopodine.

En conclusion, je propose un rôle de stabilisation mutuel pour l'actine-F et la synaptopodine dans la tige des épines dendritiques de neurones d'hippocampe en culture. Les épines contenant de la synaptopodine dans leur tige auraient une organisation unique du cytosquelette qui agirait comme une barrière additionnelle pour la diffusion de récepteurs aux neurotransmetteurs.

# Table of contents

<b>I Introduction</b>	<b>1</b>
<b>1 Synapse: structural organization and function</b>	<b>3</b>
1.1 Morphology of synapses	3
1.2 The postsynaptic membrane	4
1.2.1 The PSD at inhibitory synapses	5
1.2.2 The PSD at excitatory synapses	6
<b>2 Dendritic spines</b>	<b>8</b>
2.1 Types of spines	8
2.2 Composition of dendritic spines	9
2.2.1 Actin organization in dendritic spines	10
2.2.2 Heterogeneous distribution of actin filaments	11
2.2.3 Actin related proteins	12
2.2.4 Organelles in dendritic spines	15
2.3 The compartmentalization of the spine neck	16
2.4 Advances in the study of dendritic spines	17
<b>3 Synaptopodin</b>	<b>19</b>
3.1 Synaptopodin expression	19
3.2 Distribution of synaptopodin in hippocampal neurons	19
3.3 Synaptopodin and synaptic plasticity	21
3.4 Synaptopodin and the intracellular calcium stores	22
3.5 Synaptopodin interaction with the actin network of the spines	23
<b>4 Molecular dynamics in the neuronal plasma membrane</b>	<b>25</b>
4.1 The fundamentals of diffusion in biological membrane	26
4.2 The analysis of lateral diffusion	26
4.3 The diffusion barriers for lateral diffusion in plasma membrane	28
4.3.1 Actin cytoskeleton	28
4.3.2 Membrane-membrane junctions	29
4.3.3 Membrane-matrix junctions	29
4.3.4 Intramembranous clusters	30
4.3.5 Scaffold proteins	30
4.3.6 Membrane geometry	31
4.4 Lateral diffusion and synapses	32
4.4.1 Dynamics at inhibitory synapses	32
4.4.2 Dynamics at excitatory synapses	34
4.5 The spine neck as a barrier for lateral diffusion	37

<b>II Materials and Methods</b>	<b>43</b>
<b>1 Methods</b>	<b>45</b>
<b>2 Single molecule imaging</b>	<b>51</b>
2.1 Single particle tracking using quantum dots	51
2.2 Super-resolution STORM/PALM imaging	55
<b>III Results</b>	<b>61</b>
<b>1 Spine neck as a diffusion barrier to confine molecules diffusion</b>	<b>63</b>
1.1 The dendrite diameter influences the diffusion of molecules	63
1.2 The role of spine neck as a diffusion barrier	65
<b>2 The role of synaptopodin in molecule diffusion</b>	<b>67</b>
2.1 The distribution of synaptopodin in dendritic spines	67
2.1.1 Synaptopodin is present in a majority of spine necks	67
2.1.2 Synaptopodin occupies part of the inner volume of the spine neck	69
2.2 Synaptopodin affects the diffusion of membrane proteins in the spine neck	73
<b>3 Actin filaments are involved in the effect of SP presence on diffusion</b>	<b>75</b>
3.1 Actin depolymerization abolishes the slowing down of mGluR5 diffusion in SP-positive spines	75
3.2 Modulation of synaptopodin by actin depolymerization	75
<b>4 Neuronal activity increases diffusion of mGluR5 in the spine neck</b>	<b>80</b>
4.1 Neuronal activity regulates the amount of synaptopodin	80
4.2 Neuronal activity regulates the diffusion of mGluR5	82
4.3 Neuronal activity regulates the amount of $\alpha$ -actinin2	85
<b>5 The relationship between synaptopodin and mGluR5</b>	<b>86</b>
<b>IV Discussion</b>	<b>89</b>
<b>References</b>	<b>99</b>
<b>Annexes</b>	<b>115</b>

# List of Figures

## Introduction

1.1 From neuron to synapse.....	4
1.2 The PSD at inhibitory synapses.....	5
1.3 The PSD at excitatory synapses.....	7
2.1 Structure and composition of dendritic spines.....	10
2.2 The three pools of F-actin that underlie spine structure and plasticity.....	13
2.3 Actin-binding proteins (ABPs) regulate the dynamic actin filaments.....	15
3.1 Synaptopodin distribution in the brain.....	20
3.2 Synaptopodin as an essential component of the spine apparatus organelle....	21
3.3 Schematic illustration demonstrates synaptopodin regulate plasticity of dendritic spines in hippocampal neurons.....	22
4.1 Scheme of receptor trafficking between synaptic, extrasynaptic and intracellular compartments.....	25
4.2 The Brownian motion in the biological membrane.....	28
4.3 Physical barriers to the diffusion of membrane lipids or proteins.....	31
4.4 The geometry of dendritic spine as a regulator of molecule diffusion.....	39

## Materials and Methods

2.1 Processing and analysis of SPT data.....	53
2.2 Effect of geometry on diffusion measurements on cylindrical structures.....	55
2.3 The principle of PALM/STORM imaging.....	56
2.4 The steps of drift correction in dual-color PALM/STROM imaging.....	59

## Results

1.1 Different constructs used for the diffusion study.....	64
1.2 Effect of the diameter of dendrite on membrane proteins diffusion.....	65
1.3 Effects of spine neck and dendritic shaft on membrane proteins diffusion.....	66
2.1 Distribution of SP in dendritic spines of hippocampal cultured neurons.....	68
2.2 Respective distribution of mRFP-SP and endogenous SP.....	69

2.3 SP distribution within the spine neck.....	71
2.4 The plasma membrane at spine neck revealed by super resolution imaging....	72
2.5 Role of SP on membrane protein diffusion in the spine neck.....	74
3.1 Effect of actin depolymerization on mGluR5 diffusion.....	77
3.2 Synaptopodin recovered after latA washout.....	77
3.3 Effects of actin depolymerization on SP distribution.....	78
3.4 Effect of actin depolymerization on SP structure revealed by STORM/PALM..	79
4.1 Immunocytochemistry showed the effect of neuronal activity on SP amount.....	81
4.2 STORM/PALM imaging revealed the effect of neuronal activity on SP distribution.....	82
4.3 The reversibility of synaptopodin occurred after 4AP washout.....	83
4.4 Effect of neuronal activity on mGluR5 diffusion.....	84
4.5 Immunocytochemistry showed the effect of neuronal activity on $\alpha$ -actinin2 amount.....	85
5.1 The relationship between synaptopodin cluster and mGluR5 receptor in spines.....	87

## Discussion

1.1 Schematic illustration showing the organization of spines containing synaptopodin.....	98
---	----

## List of tables

### Introduction

4.1 Diffusion properties of molecules at inhibitory synapse, excitatory synapse and in extrasynaptic membrane sites.....	32
---	----

### Materials and Methods

1.1 Primers used for cloning.....	46
-----------------------------------	----

## Abbreviations

4-AP	4-Aminopyridine
AMPA	$\alpha$ -amino-3-hydroxy-5-methyl-4-isoxazolepropionic acid
CaMKII	Ca <sup>2+</sup> /calmodulin-dependent protein kinases II
CNS	Central nervous system
D	Diffusion coefficient
ECM	Extracellular matrix
EM	Electron microscopy
ER	Endoplasmic reticulum
FRAP	Fluorescence recovery after photobleaching
FWHM	Full width at half maximum
GABA	$\gamma$ -Aminobutyric acid
GKAP	Guanylate kinase-associated protein
IP <sub>3</sub> R	Inositoltrisphosphate receptors
latA	Latrunculin A
LTD	Long-term depression
LTP	Long-term potentiation
mGluR	Metabotropic glutamate receptors
MSD	Mean squared displacement
NMDA:	N-methyl-D-aspartate
PALM	Photoactivated localization microscopy
PKC	Protein kinase C
PSD	Postsynaptic density
PSF	Point spread function
QDs	Quantum dots
RyR	Ryanodine receptors
TARP	Transmembrane AMPAR regulatory proteins
SA	Spine apparatus
SAP	Synapse-associated protein
SER	Smooth endoplasmic reticulum
SP	Synaptopodin
SPT	Single particle tracking
STED	Stimulated emission depletion microscopy
STORM	Stochastic optical reconstruction microscopy



# I Introduction



## 1 Synapse: structural organization and function

In the mammalian brain, billions of neurons interconnect into the functional neural networks that underlie all our behaviors in the central nervous system (CNS). Neurons are the basic structural and functional units of the CNS, which is the fundamental idea of the '*Neuron doctrine*' theory, described by S. Ramón y Cajal in 1888. By using Golgi's silver-staining technique to show the neuron morphology, Cajal experimentally demonstrated that nerve cells are independent cells not continuous but contiguous (Fig. 1.1A). The communication of neurons with each other is mediated via specialized cell junctions called synapses. The term "synapse" was coined by Charles Sherrington in 1897 to refer the specific connection of one nerve cell with another that facilitated the transmission of a nervous impulse [Cowan and Kandel 2001]. In the following manuscript, the term synapse will only refer to chemical synapses.

### 1.1 Morphology of synapses

All chemical synapses share common structural and functional features, in spite of great morphological and molecular variability. The ultrastructure of a chemical synapse was shown in electron microscopy (Fig. 1.1B). The synapse consists of three elements: the pre- and postsynaptic elements and the intervening synaptic cleft (Fig. 1.1C) [Cowan and kandel 2001]. The presynaptic compartment contains neurotransmitter-filled synaptic vesicles. The active zone, localized at the presynaptic terminus, facilitates vesicle fusion and the release of neurotransmitter content to synaptic cleft. The synaptic cleft is packed with electron-dense material [Harris and Weinberg 2012] and contains both standard extracellular matrix proteins and specific synaptic proteins [Dityatev et al. 2010]. In the postsynaptic compartment, the electron-dense postsynaptic densities (PSDs) are in front of the presynaptic active zone. PSDs guarantee that receptors are in close proximity to presynaptic neurotransmitter release sites. Hundreds of proteins have been identified in the PSD including neurotransmitter receptors, scaffold proteins and many downstream signaling molecules. The association of pre- and postsynaptic compartments supports the synaptic transmission and ensures the signal communication from one neuron to another.

Also, chemical synapses can be classified as inhibitory synapses or excitatory synapses according to the neurotransmitter released. Excitatory synapses are found mainly on dendrites and on the protrusions they bear, the dendritic spines in the pyramidal neurons, medium spiny neurons and the Purkinje cells [Rochefort and Konnerth 2012]. Inhibitory synapses are present

on the cell soma and often on the axonal initial segment, and also distribute along both spiny and non-spiny dendrites, in the shafts of the dendrites.

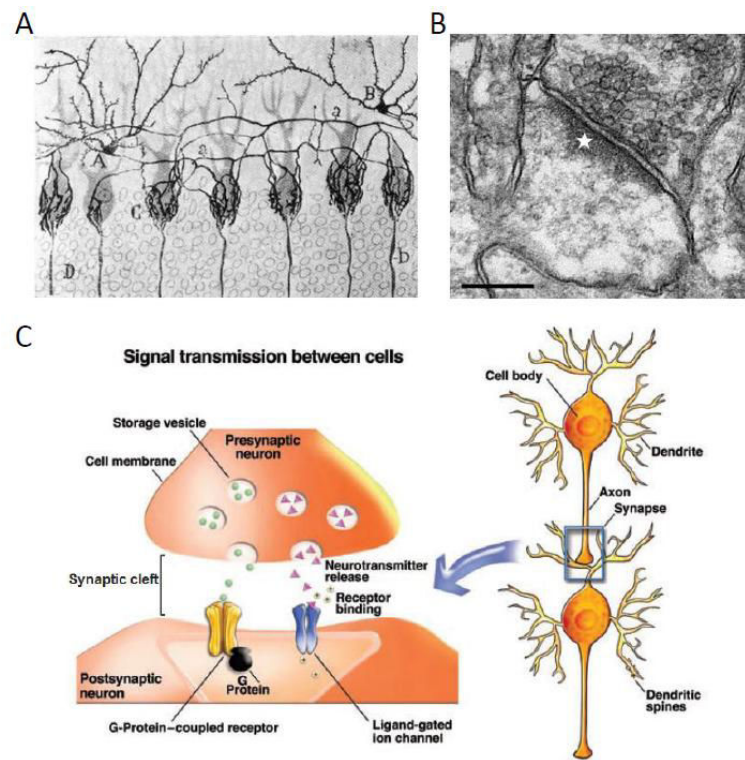


**Figure 1.1 From neuron to synapse.**

**A.** Original drawing by Cajal illustrating independence and connections of neuronal structure of a lamina of cerebellum. A and B, and star-shaped cells from the molecular layer (cells in baskets), whose axon (a) generates terminal nests around the Purkinje cells (c); b, axon of these corpuscles". From [López-Muñoz and Alamo \[2009\]](#). **B.** Electron microcopy image shows the anatomy of a typical synapse in CNS. The presynaptic compartment filled with synaptic vesicles apposes to the postsynaptic density (white star). Scale bar: 200 nm. Adapted from [Rostaing et al. \[2006\]](#). **C.** Scheme of the composition of a chemical synapse: the apposition of pre-and postsynaptic compartment, separated by the synaptic cleft. From [Clapp et al. \[2008\]](#).

## 1.2 The postsynaptic membrane

The PSD has been proposed to concentrate and organize neurotransmitter receptors in the postsynaptic membrane, which is considered to be specialized for postsynaptic signaling and plasticity. The typical size of PSDs is on the order of 200 to 500 nm wide and 30 to 60 nm thick [\[Harris and Stevens 1989\]](#). As a complex machine, the PSD demonstrates dynamic modifications in its structure and composition during the different states of development and synaptic activity.

### 1.2.1 The PSD at inhibitory synapses

Glycine receptors (GlyRs) and A-type GABA ( $\gamma$ -Aminobutyric acid) receptors (GABA<sub>A</sub>Rs) are the two main receptor families mediating fast-chloride-dependent inhibition at inhibitory synapses in the CNS and spinal cord [Moss and Smart 2001]. The accumulation of GlyRs and GABA<sub>A</sub>Rs at postsynaptic membranes depends on a subsynaptic scaffold. Gephyrin acts as a core protein of the scaffold that provides binding sites for the synaptic localization of inhibitory receptors. The interaction of gephyrin with GlyR is mediated by an 18-amino-acid amphipathic helix present on its intracellular domain of the  $\beta$  subunit. Deletion of gephyrin in mice caused the reduction of GABA<sub>A</sub> receptor synaptic clustering in cultured neurons and brain sections [Kneussel et al. 1999]. Recent studies have shown that gephyrin directly interacts with the intracellular loops of GABA<sub>A</sub>R $\alpha$ 1,  $\alpha$ 2 and  $\alpha$ 3 subunits and the binding affinities of these interactions have been characterized [Tretter et al. 2012]. Other molecules directly binding to gephyrin or inhibitory receptors have been identified, such as GABARAP (GABA receptor-associated protein), Raft1 (rapamycin FKB12 target protein) or Pin1 (Peptidyl-prolyl isomerase NIMA-interacting 1). Although these proteins are not structural components of the subsynaptic scaffold, they may contribute to the regulation of receptor trafficking and subsequently receptor amount at synapse [Triller and Choquet 2003]. Adhesion proteins (i.e. cadherins, neuroligin-2) are also present at inhibitory synapses. Lastly, gephyrin interacts with microtubules and, indirectly, with the actin cytoskeleton. Thus, it stabilizes the receptor-scaffold molecular complex at inhibitory synapses (Fig. 1.2).

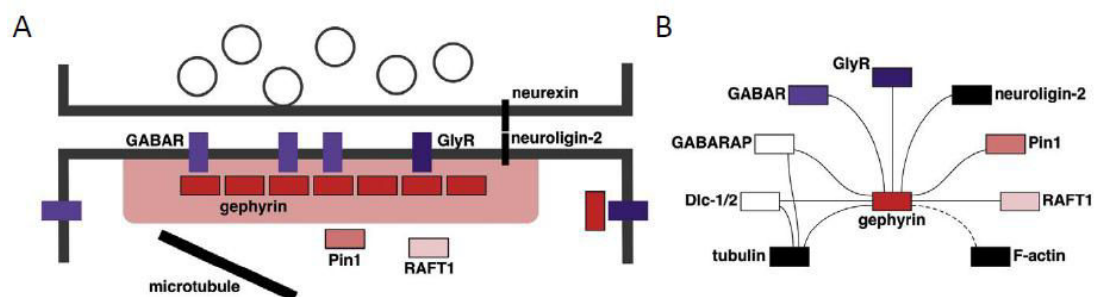


**Figure 1.2 The PSD at inhibitory synapses.**

**A.** The scaffold at inhibitory synapses is largely composed of gephyrin (red), which offers binding sites for the clustering at synapses of the main types of inhibitory receptors (GlyRs and GABA<sub>A</sub>Rs; purple). Gephyrin also interacts with the cytoskeleton and adhesion proteins (black), proteins that are involved in trafficking (white) as well as with synaptic regulatory proteins (light red tones). **B.** Network of interactions between the components of inhibitory PSDs. Black and dashed lines indicate the direct and indirect interactions, respectively. From Renner et al. [2008].

### 1.2.2 The PSD at excitatory synapses

The PSD at excitatory synapses is thicker and much more complex than that at inhibitory synapses. In the CNS, excitation is mostly mediated by glutamate through fast ionotropic receptors or through slower metabotropic receptors coupled to G proteins. There are two main ionotropic glutamate receptors, namely AMPA ( $\alpha$ -amino-3-hydroxy-5-methyl-4-isoxazolepropionic acid) receptors (AMPA) and NMDA (N-methyl-D-aspartate) receptors (NMDARs), which open to allow influx of positively charged  $\text{Na}^+$  ions (and additionally  $\text{Ca}^{2+}$  ions in the case of NMDARs and GluA1-containing AMPARs), thereby depolarizing electrically the postsynaptic neuron. AMPARs and NMDARs are present in high densities at PSDs adjacent to glutamatergic terminal boutons [Nusser 1994]. The metabotropic receptors (mGluR1 and mGluR5) are enriched in an annulus surrounding the PSD. The mGluRs also are found at a distance from PSD, such as in dendritic and somatic membrane [Luján et al. 1997].

Glutamate receptors have interactions with a plenty of intracellular proteins directly or indirectly that accumulate at PSDs (Fig. 1.3) [Boeckers 2006; Okabe 2007]. Scaffolding proteins hold sequences like PDZ, SH3 or proline-rich domains that allow protein-protein interaction. PSD-95 interacts directly with NMDARs, as well as GRIP (Glutamate receptor-interacting protein) with AMPARs and Homer with mGluRs [Kornau et al. 1995; Brakeman et al. 1997; Dong et al. 1997]. However, GKAP (guanylate kinase-associated protein) interacts with both PSD-95 and Shank indirectly coupling the NMDA/PSD-95/GKAP complex [Brakeman et al. 1997]. NMDARs, as calcium-permeable receptors, can directly interact with signaling molecules like CAMKII [Wyszynski et al. 1997]. Stargazin regulates the amount of AMPARs at synapse by its interaction directly with PSD-95 and AMPARs [Chen et al. 2000].

Besides glutamate receptors, the PSDs contain tyrosine kinases receptors, ion channels, and cell adhesion molecules. Adhesion protein neuroligin-1 can associate indirectly with NMDARs via binding to PSD-95, and subsequently modulates NMDA mediated synaptic transmission [Kornau et al. 1995; Irie et al. 1997; Khosravani et al. 2005]; cadherins can recruit kainate receptors and also modify spine shape and function [Coussen et al. 2002; Mysore et al. 2007]. Electron microscopic immunogold analysis revealed a laminar distribution of scaffold proteins within the PSD [Valtschanoff and Weinberg 2001; Petralia et al. 2005]. The organization of these molecules is related to their functions in synaptic plasticity: PSD-95 locates close to the postsynaptic membrane ( ~12 nm from the extracellular side of the plasma membrane), whereas GKAP, Shank, and Homer proteins reside in a deeper position ( ~24-26 nm) near the cytoplasmic face of the PSD. PSD-95 is thus well-suited as a scaffold to interact with

transmembrane receptors and channels. By contrast, Shank promotes maturation of spines through interacting with regulatory proteins of the actin cytoskeleton [Sala et al. 2001].

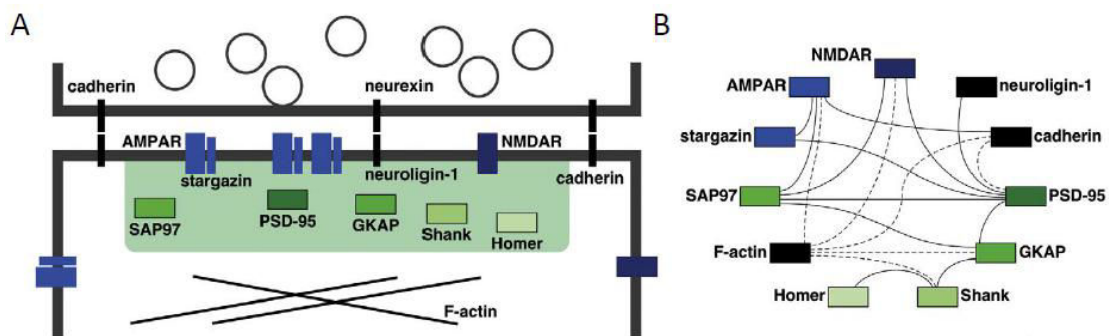


**Figure 1.3 The PSD at excitatory synapses.**

**A.** High complexity characterizes the scaffold at excitatory synapses. The model shows only a limited number of scaffold or adaptor proteins (green shades) that provide binding sites for excitatory receptor types (AMPA and NMDARs, blue) as well as actin cytoskeletal, adhesion and adaptor proteins. **B.** Network of interactions between the components of excitatory PSDs. Direct and indirect interactions are represented as black and dashed lines, respectively. From Renner et al. [2008]

## 2 Dendritic spines

Dendritic spines are actin-rich protrusions that harbor the postsynaptic sites of synapses and receive most of the excitatory synaptic inputs in the central nervous system. The alterations in density, morphology and maturation of dendritic spines are strongly correlated with the strength of excitatory synaptic connections and associated with many neuronal disorders.

### 2.1 Types of spines

Dendritic spines, described by *Ramón y Cajal* in 1888 [Bennett 1999], are tiny membranous protrusions (typically 0.5-2  $\mu\text{m}$  in length) from dendritic shaft of various types of neuron including the pyramidal neurons of neocortex, the medium spiny neurons of the stratum and Purkinje cells of the cerebellum. Most of the excitatory synaptic inputs in the central nervous system develop dendritic spines, allowing regulation of synaptic strength on a synapse-by-synapse basis. The number of spines normally is 1-10 spines per micrometer of dendrite length on principal neurons and the volume ranges from 0.01  $\mu\text{m}^3$  to 1  $\mu\text{m}^3$  [Hering and Sheng 2001]. A prominent characteristic of spines is their dynamic shape and size, suggesting a high degree of functional diversity.

Dendritic spines contains three separate compartments: a bulbous head containing the PSD, a thin neck, and the spine base with delta-shape at the joint with the parental dendritic shaft. Spines identified in electron microscopy studies are typically categorized based on their morphology: thin spines (with a thin, long neck and a small bulbous head), stubby spines (short spines lacking an identifiable neck), mushroom spines (with a larger head) and branched spines (with a cup-shaped head) (Fig. 2.1-A) [Bourne and Harris 2008]. However, by using stimulated emission depletion (STED) imaging, one recent study argues against the presence of stubby spines and indicates that stubby spines are wrongly detected as a result of limited spatial resolution [Tønnesen et al. 2014]. Taken together, though the spine shapes and size are diversified, these spine types can be observed in same dendrite segment. They display continuous dynamic motion and in general large spines are more stable and functionally stronger in response to synaptic activity, whereas small spines are more flexible in their response to subsequent activation. In addition, filopodia, thin protrusions without a bulbous head, are found on dendrites of developing neurons. They are transient structures that might develop into spines through synaptic inputs [Fiala et al. 1998; Hering and Sheng 2001].

## 2.2 Composition of dendritic spines

Dendritic spines, as the postsynaptic compartment of excitatory receptors, contain the elements of the PSD, actin cytoskeleton, as well as multiple membrane-bound organelles, like smooth endoplasmic reticulum (SER), mitochondria, and endosomes (Fig. 2.1-B) [Sheng and Hoogenraad 2007].

Due to the particular morphology of dendritic spines, spine heads provide a local biochemical compartment and concentrate ions and signaling molecule in response to synaptic activation. The PSD is usually found at the tip of the spine head adjacent to the presynaptic active zone. As described in the section [1.2], hundreds proteins are clustered at the PSD, such as receptors, scaffold proteins and adhesion proteins, as well as a variety of signaling proteins assembled at the postsynaptic membrane [Sheng and Hoogenraad 2007]. The PSD plays roles in physical link and communication with the presynaptic compartment as well as the postsynaptic signal transmission. Lateral to the PSD region in extrasynaptic regions, there is a stable membrane associated with clathrin-cated vesicles (CCV) and recycling endosomes, named endocytic zone. The endocytic zone is dedicated to endocytosis of postsynaptic receptors near the postsynaptic membrane [Blanpied et al. 2002]. More precisely, the endocytic zone is essential to degrade and recycle the mobile AMPARs pool at synapses [Lu et al. 2007; Petrini et al. 2009].

In addition to the molecular composition of the synapse, the morphology of spines is also thought to be critical for synaptic function. Spine head size positively correlates with the area of PSD and the strength of synaptic transmission, and undergoes changes during synaptic plasticity [Arellano et al. 2007]. In addition, the length of spine neck is also related to synaptic strength, specifically for the compartmentalization of calcium signaling [Majewska et al. 2000; Yuste et al. 2000] and the filtering of membrane electrical potentials [Araya et al. 2006]. Among the PSD scaffold proteins, the Shank family and PSD-95 scaffold protein play a critical role in spine morphology [Sala and Segal 2014]. However, spine morphogenesis is largely dependent on the remodeling of its underlying actin, the primary cytoskeleton within spines. Actually, in mature spines, actin stabilizes postsynaptic protein and modulates spine head structure in response to postsynaptic signaling [Okamoto et al. 2004]. Induction of long-term potentiation (LTP) causes depolymerization of actin, characterized by a long-lasting increase in F-actin levels, while the preservation of LTP and the maintenance of spine enlargement need polymerization of F-actin [Fukazawa et al. 2003]. Conversely, long-term depression (LTD) causes the depolymerization of actin and the elongation or shrinkage of spine heads [Bourne and Harris 2008; Zhou, Homma,

and Poo 2004]. Moreover, the regulation of actin dynamics drives the morphological remodeling in dendritic spines that are associated with the modulation in synaptic efficacy [Matus 2000; Cingolani and Goda 2008].

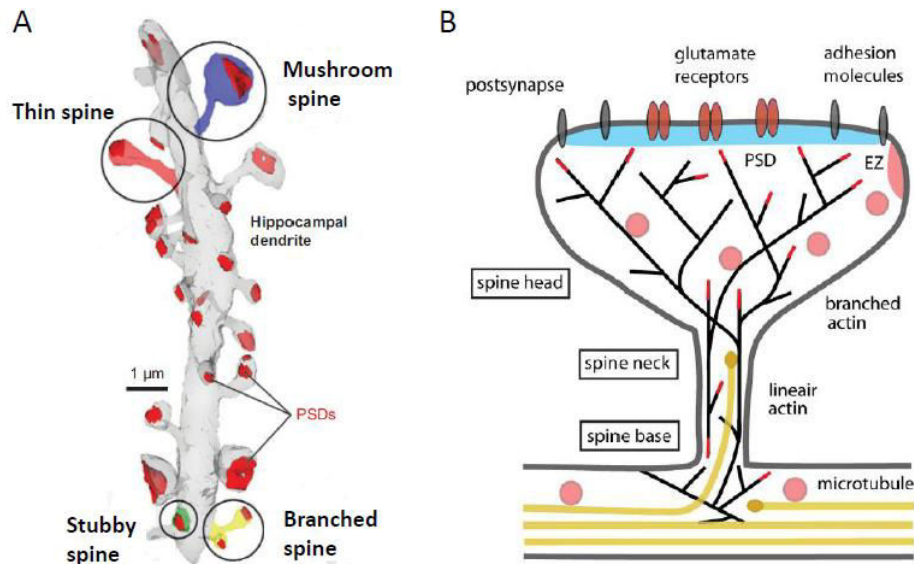


**Figure 2.1 Structure and composition of dendritic spines.**

**A.** Three-dimensional EM reconstruction of a hippocampal dendrite illustrating different spine shapes containing mushroom (blue), thin (red), stubby (green), and branched (yellow). PSDs (red) also display the dynamic in size and shape. From [Bourne and Harris \[2008\]](#). **B.** Schematic view of the composition of a mushroom-shaped spine containing the postsynaptic density (PSD; blue), adhesion molecules (gray) and glutamate receptors (reddish brown), the actin (black lines) and microtubule (yellow) cytoskeleton. Dendritic spines are enriched with straight and branched actin filaments (black lines). The spine neck contain longitudinal, constricted actin filaments, while the spine head hold more branched filaments. The dendritic shaft is full of stable microtubule arrays not actin filaments. EZ: endocytotic zone. From [Hotulainen and Hoogenraad \[2010\]](#).

### 2.2.1 Actin organization in dendritic spines

Dendritic shafts are enriched with microtubules, while the main cytoskeletal component dendritic spines is actin [[Hotulainen and Hoogenraad 2010](#)]. Spines contain about 6 times more actin than the dendritic shafts [[Honkura et al. 2008](#)]. Actin filaments (filamentous actin, F-actin) are formed by the polymerization of actin monomers (globular actin, G-actin). F-actin is the main formation of actin in dendritic spines where only about 12% of total actin being

monomeric [Star et al. 2002; Honkura et al. 2008]. Actin is in a dynamic equilibrium and these polymer filaments generally turnover by continuous “treadmilling” with a time constant of ~1 min [Star et al. 2002]. This process is due to the addition and removal of dynamic subunits at the two ends of actin filaments, which involves the depolymerization of F-actin at the pointed end of the filament and the polymerization of G-actin at the barbed end.

Dendritic spines contain a complex, highly branched and dynamic actin cytoskeleton that mediate spine morphology in response to synaptic activity. The most likely role of actin in mature spines is to anchor postsynaptic receptors at synapses by interacting with a myriad of scaffolding proteins [Kuriu et al. 2006; Renner et al. 2009], adjusting the structure of spine head in response to synaptic plasticity [Fischer et al. 1998; Star et al. 2002; Okamoto et al. 2004], as well as modulate the receptor trafficking [see section 4, molecular diffusion]. Thus, actin regulation is crucial to the formation, maturation, and plasticity of dendritic spines.

### 2.2.2 Heterogeneous distribution of actin filaments

The distribution of actin filaments within single spines is not homogeneous. Electron microscopy has revealed that longitudinal, confined actin filaments are present in the spine neck and more branched filaments are localized in the spine head just underneath the PSD [Korobova&svitkina 2010]. Photoactivated localization microscopy (PALM) has demonstrated that actin filaments display heterogeneous treadmilling rates, with a size shorter than ~200 nm [Frost et al. 2010].

Using a photoactivatable green fluorescent protein (PAGFP) fused to  $\beta$ -actin, two distinct pools of F-actin based on their turnover rate have been identified in spines at rest by two-photon microscopy [Honkura et al. 2008] (Fig. 2.2). The dynamic pool lies at the tip of the spine and shows a fast turnover rate with a time constant <1 min, whereas the stable pool with a slower turnover rate (~17 min) localizes at the base of spine head. The size of a stable F-actin pool is related to spine volume. Usually, larger spines contain higher proportion of stable F-actin pool at the base [Star et al., 2002; Honkura 2008]. Actin polymerization inhibitor latrunculin A can rapidly reduce the actin concentration of the dynamic pool as well as the shrinking of spine head volume [Honkura et al. 2008]. Thus, the dynamic F-actin pool support the volume of spine head by continuous polymerization. Following LTP induction, an enlargement pool of actin is formed into dendritic spines and the maintenance of this third actin pool is necessary for LTP stabilization. The establishment of a long-term enlargement pool requires confinement of this pool by the spine neck in a  $\text{Ca}^{2+}$ /calmodulin-dependent protein kinases II (CaMKII)-dependent manner, and therefore the release of F-actin from the enlargement pool was limited into

dendritic shaft [Honkura et al. 2008]. Interestingly, the mature spine necks contain complex filament organization of mix directionality, which might manage both spine morphology and various actin functions in the spine [Frost et al. 2010].

The stable pool of F-actin may serve as a scaffold for the dynamic pool to generate an expansive force, thereby stable the dendritic spines. The F-actin pool in large spines is more stable than that of small spines, which could explain the transient change in larger mushroom spines but persistent in small spines after long term enlargement and LTP induced [Matsuzaki 2004]. Electron micrographs shows F-actin distribution around the lamellae of the spine apparatus [Capani et al. 2001; Cohen et al 1985]. The spine apparatus is preferentially located nearly the base of large spines head and partially extends into the spine neck [Spacek and Harris 1997]. This suggests that the similar localization exists between spine apparatus and the stable F-actin pool. Synaptopodin, an actin- and  $\alpha$ -actinin-binding protein in the spine neck, is closely associated with the spine apparatus [Deller et al 2000a]. This apparatus and its associated molecules may thus play a role in the localization and size of the stable F-actin pool in the spine.

Taken together, the morphology and plasticity of dendritic spines are mechanically modulated by the three pools of F-actin fibers and the dynamic motion of actin filaments.

### **2.2.3 Actin related proteins**

The dynamic actin cytoskeleton is highly regulated by an abundance of actin binding proteins that can affect the treadmilling rate of the filaments as well as the stability and organization of dendritic spines actin. A number of actin binding proteins have been implicated in development, morphology and function of the spine (Fig. 2.3). It is the case of drebrin (stabilization of actin filament and formation of stable spine morphology), ADF/cofilin (soluble pool of actin monomers and maintenance of spine morphology [Shirao and González-Billault 2013]. Arp2/3 (formation and polymerization of new actin branches) and VASP /Formin (elongation of actin filaments) [Chazeau and Giannone 2014]. It is also the case of the following proteins, which in addition have been shown to play a role in the regulation of lateral diffusion of membrane protein and the anchoring of the PSD complex to actin cytoskeleton.

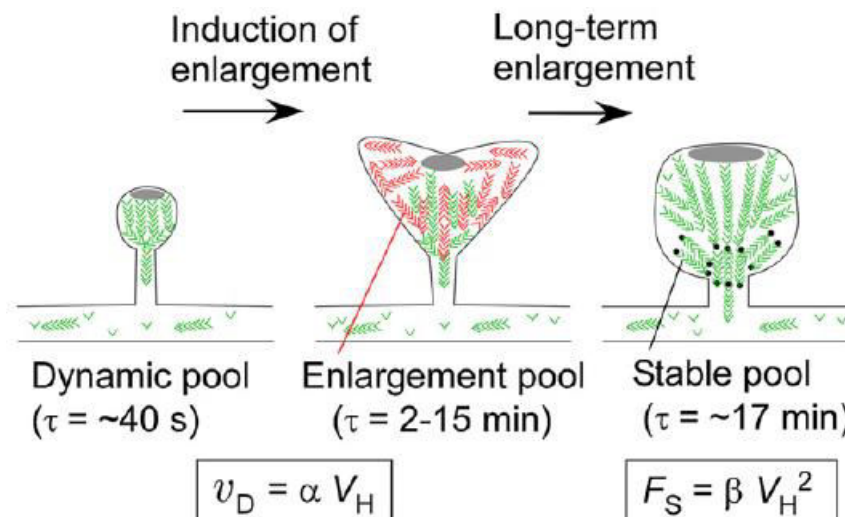


**Figure 2.2 The three pools of F-actin that underlie spine structure and plasticity.**

In the rest of spine, the dynamic pool turns over with a time constant ( $\tau$ ) of  $\sim 40$  s. The velocity ( $v_D$ ) of the flow is relative to the spine-head volume ( $V_H$ ). The stable pool is located at the base of the spine head and has a turnover time constant of  $\sim 17$  min. The amount of the stable pool ( $F_S$ ) is relative to the square of the spine-head volume ( $V_H$ ). After a stimulation in a calmodulin-dependent manner, the enlargement pool is established during spine enlargement and has a turnover time constant of 2-15 min. The maintenance of long-term spine enlargement requires the confinement of the enlargement pool, which is regulated by the stability of the spine neck and CaMKII. The establishment of long term enlargement also requires an increase in the size of the stable pool. From [Honkura et al. \[2008\]](#).

**$\alpha$ -actinin:**  $\alpha$ -actinin belongs to the spectrin/dystrophin family protein that bundles actin filaments [[Grazi et al. 1992](#)]. The  $\alpha$ -actinin family contains four conserved members and among them only  $\alpha$ -actinin3 is not found in the brain.  $\alpha$ -actinin is concentrated in the postsynaptic density of excitatory synapses [[Wyszynski et al. 1998](#)].  $\alpha$ -actinin acts as regulator of spines morphology and density. Overexpression of  $\alpha$ -actinin2 induces the increase of the length and density of dendritic protrusions and the motility of these structures in cultured hippocampal neurons [[Nakagawa et al. 2004](#)].  $\alpha$ -actinin2 can interact directly with a diverse set of postsynaptic proteins including NMDARs, CaMKII and spine associated Rap GTPase GAP (SPAR). It is believed that  $\alpha$ -actinin2 binds by its central rod domain to the cytoplasmic tail of both the NR1 and NR2B subunits of NMDARs and PSD-95 in the rat brain, and this binding can be directly inhibited by calcium/calmodulin [[Wyszynski et al. 1997, 1998](#)]. In addition,  $\alpha$ -actinin2 also competes the binding sites of CaMKII with calcium/calmodulin and thus negatively alters CaMKII activity [[Robison et al. 2005a](#)]. SPAR and  $\alpha$ -actinin are engaged in bidirectional structural plasticity of dendritic spines: SPAR induces the enlargement of spine heads while

$\alpha$ -actinin favors elongation and thinning of dendritic spines [Hoe et al. 2009]. The study of Schulz et al [Schulz et al. 2004] suggests that  $\alpha$ -actinin is involved in the process of AMPARs transport. RIL (reversion-induced LIM protein) binds to the AMPARs subunit GluA1 C terminus and also to  $\alpha$ -actinin2 via its PDZ domain. Also, RIL triggers the transport of GluA1-containing AMPARs to dendritic spines in an  $\alpha$ -actinin/actin-dependent manner, and such trafficking function promoted the synaptic accumulation of the receptors.

Based on these interactions,  $\alpha$ -actinin could play a vital role in the alteration of spine morphology and the connection of postsynaptic membrane complexes with the actin cytoskeleton. The actin bundling activity of  $\alpha$ -actinin can be modulated by other molecules, such as synaptopodin, which is involved in the morphology of dendritic spines and synaptic plasticity [Fukazawa et al. 2003; Asanuma et al. 2005; Kremerskothen et al. 2005].

**CaMKII:** CaMKII is a serine/threonine protein kinase critically involved in synaptic plasticity in the brain. It is highly concentrated in the postsynaptic density membrane [Kelly et al. 1984]. The major isoforms of CaMKII in neurons are  $\alpha$  and  $\beta$  family membranes, and both of them play a role in modulating spine morphology. CaMKII $\alpha$  can bind to  $\alpha$ -actinin to modulate actin dynamic and organization [Robison et al. 2005b]. Via directly binding to F-actin, down regulation of CaMKII  $\beta$  leads to a reduction of spine volume, while its overexpression slows down actin turnover and promote the formation of mature spines [Okamoto et al. 2007]. Also, CaMKII is essential for the process of group I mGluR-dependent protein synthesis and associated LTD [Mockett et al. 2011].

**Synaptopodin:** Synaptopodin, a spine neck-specific actin-binding protein, is thought to modulate actin bundling via its interaction with  $\alpha$ -actinin and F-actin [Asanuma et al. 2005; Kremerskothen et al. 2005]. For a detailed introduction on synaptopodin please see Introduction section 3 [Synaptopodin].

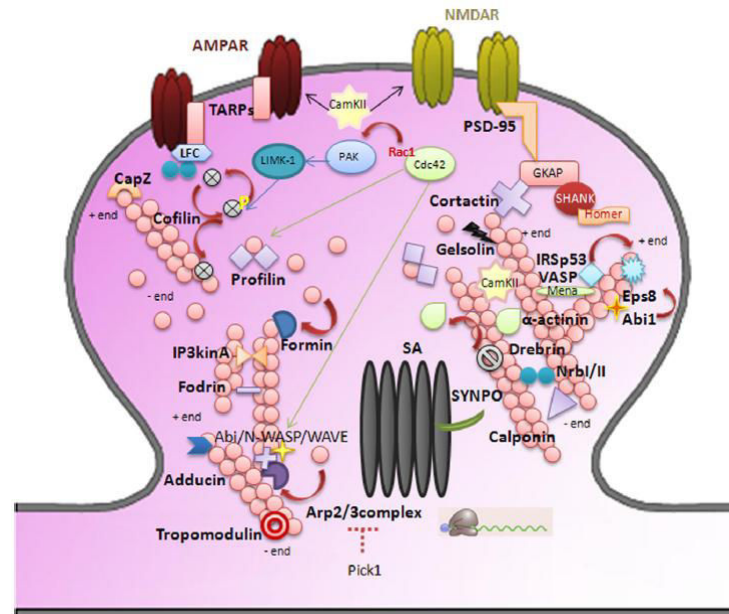


**Figure 2.3 Actin-binding proteins (ABPs) regulate the dynamic actin filaments.**

ABPs in a dendritic spine are involved in actin nucleation (Arp2/3 complex, Formin, N-WASP, WAVE-1, Abp1, Abi2 and cortactin), actin polymerization (Profilin I/II), actin capping (Capz, Adducin and Tropomodulin), actins severing (ADF/cofilin and gelsolin) and actin bundling ( $\alpha$ -actinin, CamKII $\beta$ , SYNPO, Fodrin and DerbinA). SA: spine apparatus; SYNPO: synaptopodin. Adapted from [Bellot et al. \[2014\]](#).

## 2.2.4 Organelles in dendritic spines

There are multiple membrane-bound organelles in dendritic spines. Smooth endoplasmic reticulum (SER) is present around 50% of hippocampal spines [[Spacek 1985](#); [Spacek and Harris 1997](#)]. The dynamic, continuous network of SER is formed in the dendritic shaft, and extends into a subset of dendritic spines, sometimes closely to the PSD [[Spacek and Harris 1997](#)]. The most crucial function of SER is thought to modulate the storage and release of calcium and the transport of materials constituting of the plasma membrane and synapses [[Fifková et al. 1983](#); [Verkhatsky 2005](#)]. The elevated calcium thereby modulates the dynamic of the actin cytoskeleton in spines [[Oertner and Matus 2005](#)]. The spine apparatus, a specialized compartment containing stacks of SER and electron dense plates, is found in ~20% of hippocampal and cortical spines. However, more than 80% of large mushroom spines have a spine apparatus, typically in the spine neck [[Spacek and Harris 1997](#)]. Spine apparatus may serve as a regulator of spine calcium kinetics [[Fifková et al. 1983](#)] and the post-translational modification and transport of locally synthesized proteins [[Kennedy and Ehlers 2006](#)]. The formation and/or stability of spine apparatus depends on the presence of the actin-binding

protein synaptopodin, as synaptopodin-deficient mice exhibit a loss of spine apparatus and subsequent defects in LTP in the hippocampus [Deller et al. 2003].

In addition, polyribosomes are required for local translation in dendrites [Steward and Schuman 2003], and can be found in a subset of dendritic spines. After induction of LTP by tetanic stimulation, polyribosomes can redistribute into spines with larger PSDs to synthesize proteins (like CaMKII and PSD95) to maintain LTP [Ostroff et al. 2002; Bourne and Harris 2007]. Finally, on the postsynaptic, mitochondria are abundant in the dendritic shaft but scarce in dendritic spines of adult brains, and produce ATP to provide the energy needed for signal transduction. Mitochondria undergo translocation into spines during synaptic stimulation and seem to be essential for the morphogenesis and plasticity of dendritic spines [Li et al. 2004].

## 2.3 The compartmentalization of the spine neck

Spines serve as an electrical compartment and the spine neck plays a role in the transmission of membrane potentials, isolating synapses electrically. Synaptic potentials generated inside the spine head are filtered by spine neck when they travel to the dendritic shaft [Araya et al. 2006a; Yuste 2013]. What effects contribute to the compartmentalization of synaptic potentials in spines? Spine neck resistance, as one of most debated relevant parameters, can not be direct measured due to technical problems. The reported values on spine neck resistance are highly variable and strongly influenced by the methods. One more recent report has reveals that half of all spines have the spine neck resistance value larger than 56 M $\Omega$ , and 5% of that larger than 500 M $\Omega$  [Tønnesen et al. 2014]. The huge range is consistent with measurement based on EM and diffusional coupling between spine head and dendrite [Harris and Stevens 1989; Svoboda et al. 1996]. However, The typical resistance of the spine neck does not reach agreement. Another good candidate is the morphology of spine neck. In single spines, the induction of plasticity not only enlarges the spine head [Matsuzaki 2004; Tanaka et al. 2008], but also remodels the spine neck [Grunditz et al. 2008]. In support of this, STED imaging precisely reveals that spines necks gradually becomes shorter and wider in a spine-specific LTP model [Tønnesen et al. 2014].

Biochemical compartment depends sensitively on spine neck geometry. The width of spine neck is the most influential determinant of compartmentalization, potentially facilitating fast and cost-efficient regulation of synaptic activity. Previous studies reveals that spine necks act as a barrier to compartmentalize signaling events within individual spines by restricting the diffusion of molecules in and out of spine head [Adrian et al. 2014]. The enlargement of spine

head is strongly correlated with the shortening and broadening of spine neck after LTP [Tønnesen et al. 2014], which may facilitate molecules access to the spine from the dendrite and thereby have the capability to sustain plasticity and stronger synaptic currents. In addition, the excitatory postsynaptic potential (EPSP) amplitudes are inversely correlated with the length of spine necks [Araya et al. 2014]. The length of the spine neck may also control the kinetics and magnitude of the postsynaptic calcium responses. Calcium response in spines with a longer neck have a shorter latency and slower decay kinetics [Majewska et al. 2000]. Short spine neck can elevate the speed of calcium diffusion from the spine head into the parent dendrite [Korkotian et al. 2004]. Besides calcium, spine neck also serves as a barrier to the diffusion of other second messengers (cAMP, cGMP and IP<sub>3</sub>) and thereby compartmentalize the signal transmission [Sabatini et al. 2002; Noguchi et al. 2005; Grunditz et al. 2008], and regulate diffusion across the neck during activity [Bloodgood and Sabatini 2005].

## 2.4 Advances in the study of dendritic spines

Critical advances in science have depended on the development of new methods. The rapid development of molecular and cellular imaging techniques boosts our knowledge about the localization and dynamic morphology of dendritic spines and the functional analysis of molecular interactions and spine activity. Dendritic spines were firstly described by the application of then-novel Golgi stain (Ramón y Cajal 1888), and demonstrated as being synaptic units by the introduction of electron microscopy (EM) [Gray 1959]. In particular, serial-section EM allowed the full morphology description of dendritic spines undergoing modifications in response to specific stimuli [Bourne and Harris 2008]. Indeed, EM provides the highest resolution currently, but it is applicable only with fixed samples and is inherently incompatible with live-cell imaging.

Several fluorescence light microscopy techniques developed recently advance the study of spines. The biochemical compartmentalization and motility of dendritic spines has been discovered by two-photon microscopy [Yuste and Denk 1995], which has the advantages of deeper tissue penetration, efficient light detection and less phototoxicity [Denk et al. 1990]. The spatial resolution of two-photon imaging is typically limited to ~250nm. Due to diffraction limit, structures closer than half the wavelength of light cannot be distinguished. For instance, the widths of spine necks vary between 40 and 500 nm for spines in CA1 pyramidal neurons [Harris and Kater 1994].

Fortunately, the development of super-resolution imaging techniques can overcome the

diffraction limit and offer a combination of live-cell compatibility. Super resolution microscopy produce very clear imaging of living neurons and reveal unprecedented details about the dynamic morphology and molecular structures of dendritic spines. For example, based on patterned illumination STED which has been applied to image spines at a nanoscale resolution (28 nm) [Hell 2003], revealing the shape and dynamics of dendritic spines in live cells [Nägerl et al. 2008]. STED has also been established to image spines in vivo in living brain [Berning et al. 2012]. On the other hand, based on single molecule switching, Photoactivated Localization Microscopy (PALM) [Betzig et al. 2006] and Stochastic Optical Reconstruction Microscopy (STORM) [Rust et al. 2006] are have been applied successfully to detect the internal architecture of dendritic spines. The resolution of them can achieve around 20 nm in the lateral dimension and 50 nm in the axial dimension. In live cells, using genetically encoded fluorophores label or bind to actin, PALM demonstrate the heterogeneous actin dynamics in spines [Frost et al. 2010] and the dynamic image of dendritic spines [Izeddin et al. 2011]. Using multiple fluorescent colors in three dimensional (3D) STORM, Dani et al. map the protein organization within individual synapses, revealing the nanoscale distribution of pre- and post-synaptic markers, like Shank and Homer proteins, from fixed mouse brain sections [Dani et al. 2010]. Recently, using dual-color 3D-PALM/STORM, the nano organization of inhibitory synapse at spinal cord has been characterized, revealing the densities of GlyRs and scaffold protein gephyrin molecules, and the stoichiometry of their binding sites [Specht et al. 2013]. More information about PALM/STORM, please see Methods section.

### 3 Synaptopodin

Synaptopodin, an actin-binding protein, accumulates at a strategic position in necks of dendritic spines of mature cortical and hippocampal neurons where is closely associated with the spine apparatus [Mundel et al. 1997; Deller et al. 2000a]. Previous studies indicated that synaptopodin contributes to the morphological regulation of dendritic spines relevant to the maintenance of synaptic plasticity.

#### 3.1 Synaptopodin expression

Synaptopodin is a 100-kDa proline-rich protein, firstly described by Mundel group [Mundel et al. 1997]. The name was chosen because synaptopodin (SP) was found in close association with telencephalic synapses as well as in the processes of renal podocytes. Three isoforms of synaptopodin have been identified: one neuronal (SP-short, 685 amino acid residues) and two in kidney cells (SP-long, 903 residues; SP-T, 181 residues). All three isoforms specifically interact with  $\alpha$ -actinin and elongate  $\alpha$ -actinin-induced actin filaments [Asanuma et al. 2005].

In the brain, throughout the molecular sequence, synaptopodin shows no significant homology to any known proteins and does not contain functional domains found in receptor-clustering PSD proteins. It contains several potential phosphorylation sites and contains two PPXY motifs (amino acid residues 310-313 and 329-332 of the mouse protein) involved in protein-protein interaction [Mundel et al. 1997]. During postnatal maturation of rat brain, synaptopodin gene expression is differentiation-dependent. Indeed, SP was first detected by Western blot around day 15, increases thereafter, and reaches its maximum level of expression in the adult animal. The expression of SP is only restricted to regions of high synaptic plasticity : olfactory bulb, cerebral cortex, striatum, and hippocampus (Fig. 3.1A), and it is not detected in the cerebellum [Mundel et al. 1997].

#### 3.2 Distribution of Synaptopodin in hippocampal neurons

Light microscopic analysis reveals SP-immunoreactive puncta primarily in the dendritic layers of the hippocampus, where SP shows a regional and laminar-specific distribution (Fig 3.1B). The highest percentage of SP-puncta is found in the outer and middle molecular layer of the dentate gyrus, whereas *stratum oriens* of CA1 contains lower percentage of SP-puncta [Orth et al. 2005]. This regional and laminar-specific distribution indicated that the arrangement of SP within hippocampal dendrites dependent on the afferent synaptic activity. This hypothesis

is supported by several studies that showed activity-dependent modification in the distribution of SP in the hippocampus. For instance, SP expression is upregulated during the last-phase of LTP in vivo [Yamazaki et al. 2001]. Excitotoxic lesions of the hippocampus cause a loss of SP labeling [Orth 2007].

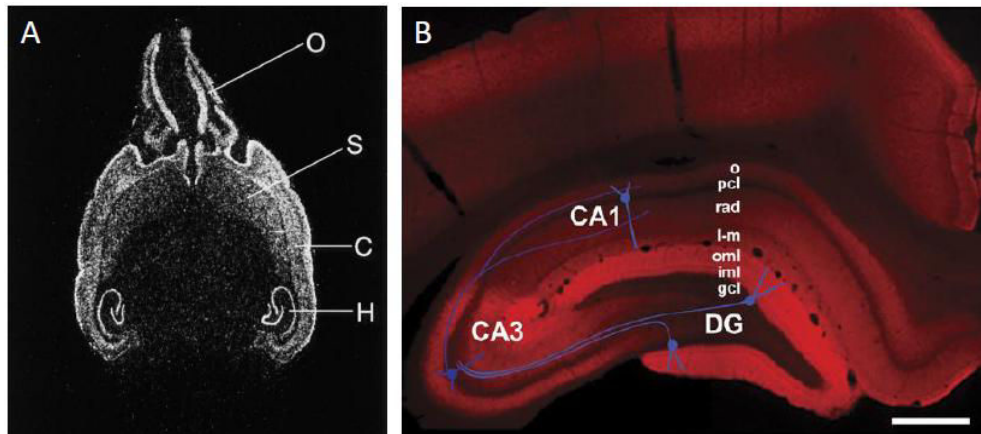


**Figure 3.1 Synaptopodin distribution in the brain.**

**A.** The distribution of synaptopodin mRNA in mouse brain. The signal can express in the olfactory bulb (O), cortex cerebral (C), striatum (S), and hippocampus (H). This expression pattern matches the immunohistochemical distribution of the protein. From Mundel et al. [1997]. **B.** The distribution of synaptopodin displays a layer- and region-specific pattern in frontal section of the rat hippocampus. Blue line indicates the connectivity between DG, CA3 and CA1. DG, dentate gyrus; gcl, granule cell layer; iml, inner molecular layer; l-m, stratum lacunosum-moleculare; o, stratum oriens; oml, outer molecular layer; pcl, pyramidal cell layer; rad, stratum radiatum. Scale bar: 500 nm. From Jedlicka et al. [2008].

Electron microscopy reveals SP were primarily located in dendritic spines (>95%) and only rarely in dendritic shafts [Deller et al. 2002; Orth et al. 2005]. Within spines, the majority of SP is present in the spine neck, where it was normally associated with the spine apparatus organelle (Fig. 3.2A-C). To assess the potential function of synaptopodin in vivo, mice homozygous for a targeted deletion of the SP gene are generated and analyzed [Deller et al. 2003]. SP-deficient mice are viable and develop normally. The number and length of dendritic spines on cortical neurons is similar to controls. However, an extensive electron microscopic analysis reveals that telencephalic neurons of these mice do not form spine apparatuses in the striatum, cortex, and hippocampus (Fig. 3.2D). These SP-deficient mice also exhibit an impaired ability to express LTP and show deficits in spatial learning [Deller et al. 2003].

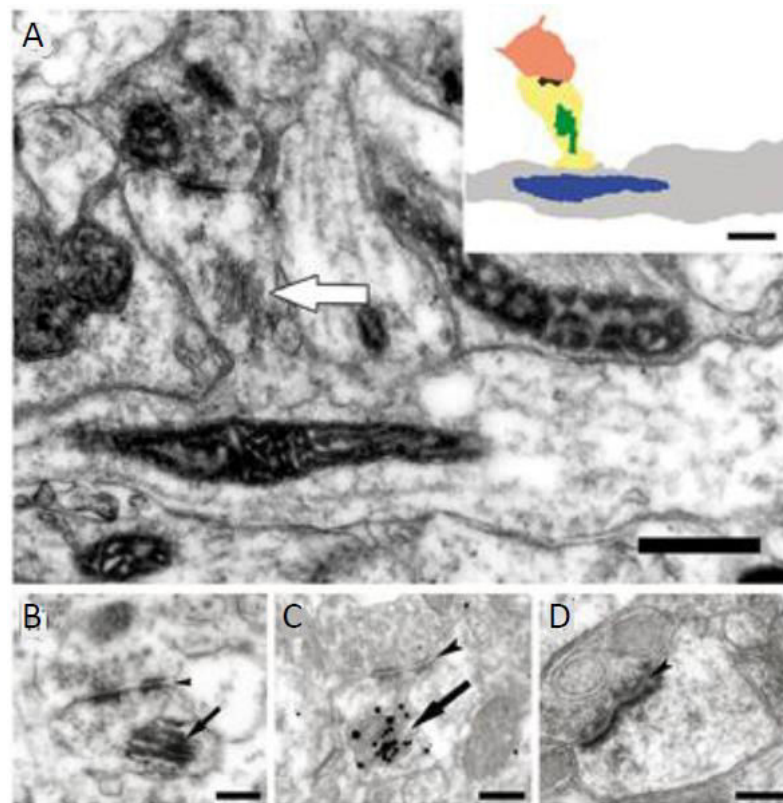


**Figure 3.2 Synaptopodin as an essential component of the spine apparatus organelle.**

**A.** A spine apparatus (arrow) are present in the neck of a dendritic spine. A schematic representation of structures seen in the electron micrograph is illustrated in the inset (top right; dendrite: gray, dendritic spine: yellow, mitochondrion: blue, presynaptic terminal: orange, postsynaptic density: black, spine apparatus: green). **B,C.** Electron micrographs of SP-immunoreactive spines located in the outer molecular layer of the normal mouse dentate gyrus. SP immunoreactivity is strongest in the spine neck and closely associated with the spine apparatus (arrows). SP structures are heavily labeled with DAB-immunoprecipitate (B) or immunogold particles (C). **D.** The SP-deficient mouse losses the spine apparatus (and SP protein) in a hippocampal neuron. Scale bars: 1 $\mu$ m in A, 0.2  $\mu$ m in B-D. Adapted from [Jedlicka et al. \[2008\]](#).

### 3.3 Synaptopodin and synaptic plasticity

Remarkably, not all spines in the CNS contain SP and a spine apparatus. A. Vlachos [[Vlachos et al. 2009](#)] showed around 30% of the spines contained a clearly discernable SP cluster in hippocampal cultured neurons. T. Deller [[Deller et al. 2003](#)] showed that most of mushroom-shaped spines had a spine apparatus which colocalized with SP puncta. This assumes SP is preferentially present in mushroom spines, where it is involved in mature and functional

synapses. How are SP-positive spines distinguishable from neighboring SP-negative spines? Studies reveals that although SP can be found in different classes of spines (thin, stubby, mushroom), the presence of SP is more prevalent in spines with a larger head volume, whereas spine length did not significantly differ between the two spine populations. It is worth mentioning that SP puncta are not a static clusters in dendritic spines, and individual SP cluster dynamics entering and exiting spines are accompanied by changes in spine head size [Vlachos et al. 2009]. Also, the spines containing SP generate greater responses to flash photolysis of caged glutamate and induce the accumulation of GluR1 in the spine head through a NMDAR mediated chemical LTP. Spines endowed with SP are more stable to release calcium from stores in the spines, which will amplify the calcium response and allow activation of downstream molecular cascades [Korkotian et al. 2014]. These data further suggest that synaptopodin contributes to the regulation of dendritic spine dynamic and synaptic plasticity, as well as homeostatic regulation (Fig. 3.3) [Vlachos et al. 2009, 2013].

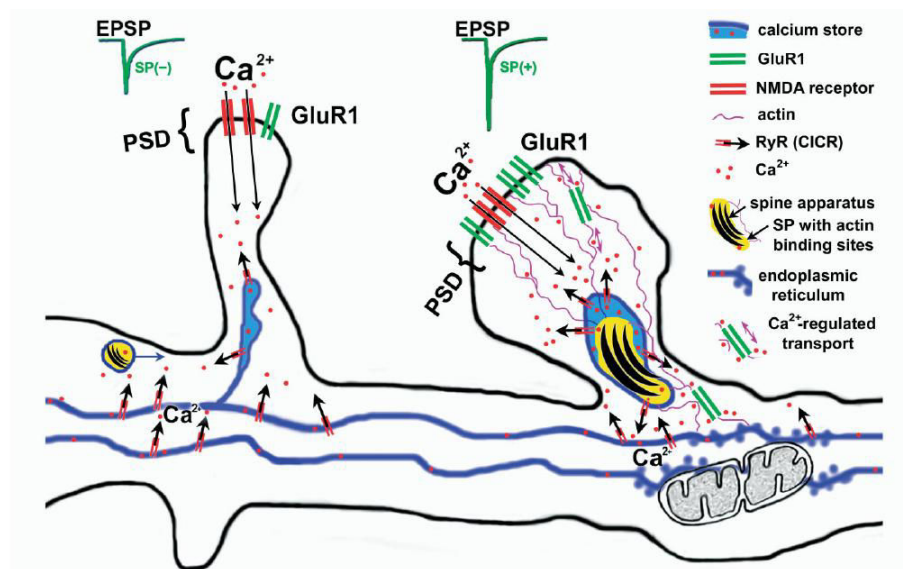


**Figure 3.3 Schematic illustration demonstrates synaptopodin regulate plasticity of dendritic spines in hippocampal neurons.** Transient synaptic activation of NMDA-Rs induces the accumulation of GluR1 in dendritic spines, which is affected by ryanodine receptor (RyR) that are associated with SP in the same spine. RyR regulates calcium release from internal stores, which is a vital step in postsynaptic spine plasticity. This suggests a potential role of SP in the regulation of plasticity. From Vlachos et al. [2009].

### 3.4 Synaptopodin and the intracellular calcium stores

Spine calcium plays a critical role in the induction of synaptic plasticity [Bliss and

[Collingridge 1993](#)]. There are several mechanisms underlying calcium influx from the extracellular space, including glutamate-mediated opening of AMPA and NMDA receptors, voltage-gated calcium channels (VGCC), nicotinic acetylcholine receptors (nAChR), and transient receptor potential type C (TRPC) channels [[Grienberger and Konnerth 2012](#)]. The concentration of calcium inside neurons is also regulated by the calcium release from intercellular calcium stores by inositoltrisphosphate receptors (IP<sub>3</sub>R) and ryanodine receptors (RyR). Interestingly, in the hippocampus, RyR distribute throughout the endoplasmic reticulum in spines and dendrites, whereas IP<sub>3</sub>R is believed to exist mainly in dendritic shafts. RyR stores associated with synaptopodin have been revealed recently by immunocytochemistry. Spines that were stained for RyR also contained SP cluster. The accumulation of GluR1 in dendritic spines mediated by NMDA mediated chemical LTP, is affected by intracellular calcium receptor (RyR) that are associated with SP in the same spine [[Vlachos et al. 2009](#)]. Similar results showed RyR-mediated conversion of STP (short-term potentiation) to LTP is lacking in synaptopodin-deficient mice [[Maiti et al. 2015](#)]. Thus, SP plays an essential role in the ability of neurons that undergo long-term plasticity.

Another study [[Korkotian et al. 2014](#)] reveals that presence of SP facilitates the expansion of spines after flash photolysis of caged glutamate or cLTP. This effect is mediated by calcium release from stores. The colocalization of STM-1 (the sensor of calcium concentration in stores) with SP and the association of Orai-1 (the calcium-induced calcium entry channel) with SP in the same spines could be the mechanism that SP may promote plasticity. This indicates that SP may adjust the functionality of calcium stores by connecting them with the STIM/Orai channels, thereby regulating synaptic plasticity.

### 3.5 Synaptopodin interaction with the actin network of the spines

Synaptopodin regulates  $\alpha$ -actinin-dependent actin-bundling and the formation of stress fibers in renal podocytes [[Asanuma et al. 2005](#)]. Electron microscopy shows that actin filaments are in close contact with the spine apparatus and could act as a link between this compartment and the postsynaptic density [[Cohen et al 1985](#)], possibly through interaction with  $\alpha$ -actinin [[Deller et al. 2000b](#)]. F-actin is the major cytoskeletal element of dendritic spine neck where synaptopodin is present. LTP induced a long-lasting increase in F-actin content in molecular layer in the dentate gyrus, while the disruption of actin filaments impaired late phase of LTP [[Fukazawa 2003](#)]. Interestingly, LTP also increases synaptopodin immunoreactivity in molecular layers [[Yamazaki et al. 2001](#)]. This means the upregulation of SP is concomitant with the

upregulation of cytoskeletal molecules in the same layers. All these suggest that SP may serve as regulator of spine morphology. Some recent studies examines this hypothesis. In neurons, SP overexpression persistently maintains spine volume enlargement mediated by pharmacological activation of NMDA receptors, while the augmentation is transient in control neurons [Okubo-Suzuki et al. 2008]. In acute slices, exposure to NMDA induces a slow, 25-30 min expansion of dendritic spines, which is not observed in SP knockout slices [Zhang et al. 2013]. Although synaptopodin is not involved in F-actin formation, SP immunoreactivity in spines positively correlates with phalloidin staining labeling F-actin in hippocampal neurons. Additionally, SP prevents F-actin from disruption in Ptk2 cells by an unknown mechanism. Therefore, SP is involved in the stabilization of spine volume during late-phase LTP [Okubo-Suzuki et al. 2008]. However, A Vlachos [Vlachos et al. 2009] group showed different results on the relationship between SP and actin filaments. Blocking actin polymerization by latrunculin did not cause a disappearance of SP clusters from spine necks, nor a relocation outside the necks. And the SP-positive spines were less likely to change their morphology, retract or elongate. Thus, they assumes that the location of SP clusters in the neck does not rely on actin polymerization is spite of being connected to the actin network. For drawing conclusions about the detailed interaction of SP and actin filaments, further investigation is needed.

## 4 Molecular dynamics in the neuronal plasma membrane

Neuronal synapses are membrane domains that allow neural cells to transmit signals to other cells in a directed fashion. Probably the most important feature of synapses is their ability to remain stable for long periods of time (several weeks or even months) without losing their ability to remodel [Holtmaat et al. 2006; Yang et al. 2009]. Synapses must comply with the paradoxical long-term stability to store previous information and at the same time remain dynamic for the fast encoding of new information [Choquet and Triller 2013].

The number of neurotransmitters at synapses is a key element determining synaptic transmission efficacy. Receptors can enter and exit synapse by a combined process: membrane insertion from intracellular pools, removal by endocytosis, and lateral diffusion on the cell surface (Fig.4.1) [Triller and Choquet 2005]. In this section, I will concentrate on the dynamic properties of receptors at the plasma membrane.

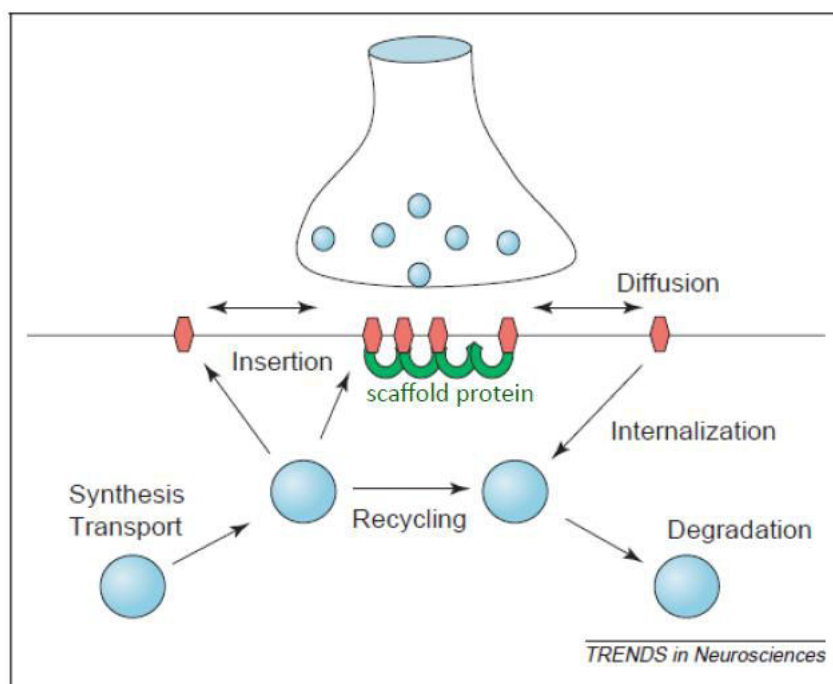


**Figure 4.1 Scheme of receptor trafficking between synaptic, extrasynaptic and intracellular compartments.** The extrasynaptic receptors (blue) are enriched at synapses and stabilized (red) by scaffolding proteins (green). The extrasynaptic receptors are exchanged with the intracellular pool by insertion (exocytosis) and internalization (endocytosis). Receptors also keep trafficking in the intracellular pool, including synthesis, transport, recycling and degradation. From Triller and Choquet [2005].

## 4.1 The fundamentals of diffusion in biological membrane

Before reviewing lateral diffusion of molecules in plasma membrane, let's firstly recall that Brownian motion of molecules is at the basis of molecular diffusion. Brownian motion is the random motion that particles display: due to thermal agitation processes, molecules are continuously moving, colliding with each other and bouncing back and forth [Berg 1983]. Diffusion is simply the macroscopic effect of Brownian motion. Therefore diffusion processes obey the following rules: (i) the diffusion rates are temperature-dependent; (ii) the molecules at higher density have lower diffusion rate ; (iii) molecules undergo random-walks due to the collisions with solvent molecules.

Based on the Brownian motion of molecules, the fluid mosaic model (Fig. 4.2A) was proposed by Singer and Nicolson [Singer and Nicolson 1972]. In this initial model, biological membranes are considered as a two-dimensional homogeneous which lipid and protein molecules appear as monomers located randomly at low concentrations and diffusing freely. However, in cell membranes, membrane molecules do not move freely throughout the whole surface of the cell membrane. Indeed, the diffusion coefficient observed in biological membranes is more than one order of magnitude lower than measurements in reconstituted artificial bilayers [Kusumi et al. 2005]. Engelman updated the model proposing that membranes are more mosaic than fluid (Fig. 4.2A) [Engelman 2005]. In this model, membranes are pretty crowded with proteins, which can also interact between themselves. This implies that the diffusion of membrane proteins and/or lipids in the membrane can be constrained by molecular crowding.

## 4.2 The analysis of lateral diffusion

Fluorescence recovery after photobleaching (FRAP) is the most often used method to study the mobility of proteins in the cell membrane over time. To achieve this measurement, a fluorophore, such as GFP, must be attached to the protein of interest. A small subset of the fluorescent molecules are focused on and its starting level of fluorescence has been measured. Then a very intense light is applied to this small region of molecules that leads to the photobleaching of fluorescent molecules. This creates separated regions of the same protein: a dark spot due to the loss of fluorescence and the surrounding brighter region with the active fluorophores. As Brownian motion proceeds, the active fluorophores will diffuse throughout the sample and replace the photobleached-fluorophore in the dark region according to their diffusion properties. Two main parameters can be determined as the ability of protein diffusion:

the time constant and the percent of fluorescence recovery at the end of the experiment. However, FRAP measurements are complicated by spatial and anisotropic constraints that make difficult to calculate the diffusion coefficients in complex morphologies such as those of neuronal cells [Triller and Choquet 2008]. Moreover, FRAP gives average estimates of protein mobility and its spatial resolution is limited by the point spread function, thus it is impossible to measure movements in areas smaller than optical resolution (~250 nm).

Recently single particle tracking (SPT) techniques has been successfully applied to measure the diffusion of individual receptors in neurons. Probes (latex bead, a fluorophore or quantum dot) have been used to attached to diffusing molecules and detected by optical imaging, thereby the movement of single molecule can be monitored over time. It has been revealed that molecules undergo a variety of motion, such as Brownian, anomalous, confined or directed [Triller and Choquet 2008]. The analysis of SPT data generally considers several parameters such as the diffusion coefficient (area explored per unit of time), the diffusion behaviors (free, confined, etc.) or the dwell time (residency time) [Lévi et al. 2012]. Compared to FRAP, The advantage of SPT using quantum dots (QDs) is that it provides long trajectories allowing the detection of different diffusive behaviors for the same molecule in a function of time. More importantly, it localizes and tracks of molecules with higher spatial resolution (10-50 nm) thanks to the fact that the size of probes is smaller than the common diffraction limit (~250 nm) [Triller and Choquet 2008]. However, the size of the antibody-QDs complexes may partly hinder diffusion in narrow spaces such as the synaptic cleft [Groc et al. 2007]. For detailed information about SPT, please check Methods section.

Various analysis techniques have been developed to extract meaningful properties from the trajectories of single molecules. In general, computing the mean square displacement (MSD) as a function of time permits a rapid determination of the mode of motion (Brownian, confined or directed) and yields associated parameters (diffusion coefficient, transport velocity, confinement area and others) [Triller and Choquet 2008]. The diffusion coefficient ( $D$ ) characterizes the rate at which a molecule spreads over a surface region, and is derived from the initial slope of MSD vs. time interval ( $\tau$ ) plot (assuming  $MSD=4D\tau$ ). Different types of motion can be distinguished from the time dependence of the MSD [Saxton and Jacobson 1997]. In the case of Brownian motion, the MSD plot is linear with the slope of  $4D$ . If the MSD plot tends toward a constant value  $L$ , the diffusion is confined in a domain of size~  $L$ . If an additional directed motion with velocity ( $v$ ) is present, MSD plot is on average equal to  $4D\tau+(v\tau)^2$  (Fig. 4.2B).

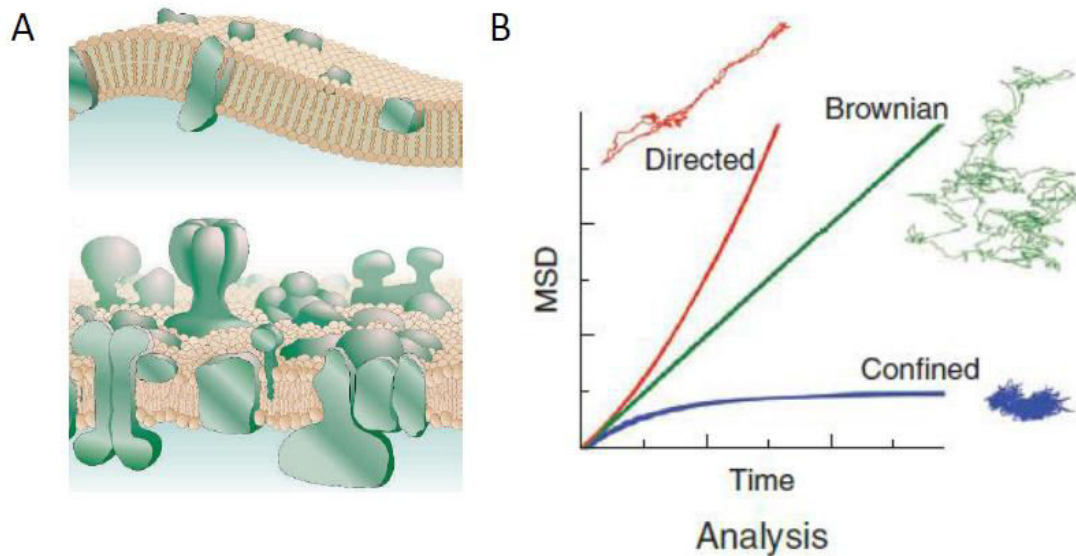


**Figure 4.2 The Brownian motion in the biological membrane.**

**A.** Scheme represents membrane structures model. Up: the fluid mosaic model from Singer and Nicolson. Bottom: an amended and updated version. The membrane, more mosaic than fluid, is a crowded environment associated with proteins and lipids irregularly. From [Engelman \[2005\]](#). **B.** Classification of the behaviors of molecules using MSD analysis, including Brownian motion (random diffusion in the membrane), confined motion (entry into membrane domains) or directed motion (linear transport owing to molecular motors). The classification is based on the shape of the MSD function over time. From [Pinaud et al. \[2010\]](#).

### 4.3 The diffusion barriers for lateral diffusion in plasma membrane

In addition to molecular crowding, other physical obstacles embedded in the membrane or present in its periphery, may affect lateral diffusion of membrane molecules. The following prototypical cases are considered [\[Trimble and Grinstein 2015\]](#):

#### 4.3.1 Actin cytoskeleton

Actin cytoskeleton is adjacent to the inner side of the plasma membrane. Removing of actin skeleton increases the diffusion coefficient of phospholipids by a factor of  $\sim 20$ , compared to that of the intact plasma membrane [\[Fujiwara et al. 2002\]](#). Actin filaments can slow down or stop diffusion by three different mechanisms: i) acting as physical barriers themselves, reducing the mobility of membrane proteins bearing a cytoplasmic tail; ii) due to transient interactions of membrane molecules with actin (scaffolding effect); iii) indirectly creating obstacles by anchoring transmembrane proteins ("pickets") which can even reduce the diffusion of lipids located in the outer leaflet of the plasma membrane ("picket-fence" hypothesis) [\[Fujiwara et al.](#)

2002; Kusumi et al. 2005; Suzuki et al. 2005] (Fig. 4.3A).

In the "picket-fence" hypothesis, the actin-based membrane skeleton creates "fences" whereas transmembrane proteins that are anchored to actin skeleton act as "pickets". Pickets further increase the confinement induced by fences. As a result, molecules are transiently confined in corrals, moving to adjacent corrals, "hopping" through gaps in the cytoskeleton. Diffusion within corrals is high, however the presence of fences and pickets strongly impairs long range diffusion [Suzuki et al. 2005]. Thus this hypothesis conciliates the expected Brownian fast diffusion (observed only inside the corrals) with the observed relatively slow diffusion in biological membranes.

As expected, the regulation of actin polymerization affects the diffusion of a variety of molecules. For example, in synapses, cytoskeleton regulates the Glycine receptor number at synapses and their lateral diffusion in the plasma membrane. Disruption of F-actin by latrunculin reduces the amount of synaptic receptors at synapse and decreases their dwell time at synapse [Charrier et al. 2006].

#### 4.3.2 Membrane-membrane junctions

Zones where two separate membranes are kept in close apposition can be seen as to form physical obstacles (Fig. 4.3B). For instance, tight junctions can immobilize membrane proteins and generate impenetrable barriers through the stable contacts formed by the extracellular surfaces of two cells [Meer and Simons 1988]. Similar effects can occur at sites of contact between organellar membranes. The endoplasmic reticulum is increasingly appreciated to form intimate contacts with the plasma membrane to control signaling (e.g.  $\text{Ca}^{2+}$ ) and metabolic processes [Carrasco and Meyer 2011], as well as connects with the membranes of mitochondria and endolysosomal system [Rowland and Voeltz 2012; Hönscher and Ungermann 2014].

#### 4.3.3 Membrane-matrix junctions

Membrane components can also be immobilized or slow down by the extracellular matrix (ECM) (Fig. 4.3C). The ECM is a collection of extracellular molecules secreted by cells that provides structural and biochemical support to the surrounding cells. Indeed, many synapses in the mature CNS are covered by a dense ECM. The diffusion of some membrane molecules may be hampered, when adhesions molecule (e.g. integrins) and other receptors binding tightly to matrix components are accumulated at sufficiently high densities. When the matrix is removed, AMPARs diffusion increases, as well as exchange rates between synaptic and extrasynaptic

membrane [Frischknecht et al. 2009]. Probably acting as scaffolding molecules, integrins hinder the lateral diffusion of AMPA receptors in dendrites and modulates short-term plasticity [Pozo et al. 2012]. Signaling via integrins, the glial-secreted ECM molecule Thrombospondin-1 (TSP-1), increases the diffusion of AMPAR. This effect is no longer observed if actin cytoskeleton is stabilized by jasplakinolida [Hennekinne et al. 2013]. Thus, ECM and related molecules can regulate lateral diffusion in membranes.

#### 4.3.4 Intramembranous clusters

Mobility can also be decreased by the intrinsic clustering of membrane components (Fig. 4.3D). In the Saffman–Delbrück model [Saffman and Delbrück 1975], the diffusion coefficient of membrane-embedded particles depends upon the size of particles and the size of the membrane in which particles are embedded. Using phospholipid bilayers, Ramadurai et al. have generally validated its basic conclusions. They measured the lateral diffusion of proteins with different radius, such as trimeric glutamate transporter (lateral radius ~4 nm), the monomeric lactose permease ( ~2 nm), and revealed the lateral diffusion of proteins is dependent on their sizes [Ramadurai et al. 2009]. More importantly, as their size increases, molecular aggregates are more easily confined in the corrals described earlier [Iino, et al. 2001].

#### 4.3.5 Scaffold proteins

In dendritic spines, most of neurotransmitter receptors display free Brownian motion in extrasynaptic domains and confined diffusion at synapses. The dynamic exchange of receptors between synaptic and extrasynaptic domains is dependent upon their direct or indirect interaction with synaptic scaffold proteins [Renner et al. 2008]. Gephyrin can bind to both GlyRs and GABARs receptors directly, and hinders their surface dynamics at inhibitory synapses [Dahan et al. 2003; Tretter et al. 2012]. At excitatory synapses, PSD-95 interacts with NMDAR and also stabilize AMPA receptors indirectly via binding to auxiliary subunit stargazin [Sans et al. 2000; Bats et al. 2007]. The couple Neuroligin1/Neurexin play a important role in targeting AMPARs to synapses. This process involves the binding between Neuroligin1 and the PSD-95 scaffold which captures diffusing AMPARs in the surface [Mondin et al. 2011]. More detailed information about the barrier role of scaffold proteins on receptors, please see next section [4.4 lateral diffusion and synapses].

### 4.3.6 Membrane geometry

Another prediction of the Saffman-Delbrück model is the dependence of lateral diffusion upon the membrane size. This postulate was recently demonstrated in case of cylindrical membranes: the lateral diffusion of lipids and proteins is slower in tubular membranes with smaller radii [Domanov et al. 2011]. This means the diffusion mobility of molecules can be influenced by the local geometry of the tubular membranes, such as axons, dendrites or the neck of dendritic spines. Due to the variability of the radius of these tubular membranes, the lateral diffusion of molecules in this case can be evaluated incorrectly by this deviation. To avoid this error, new analysis methods are developed that diffusion efficiency is only calculated from the components of displacements in the axis of the tubular structure [Renner et al. 2011].

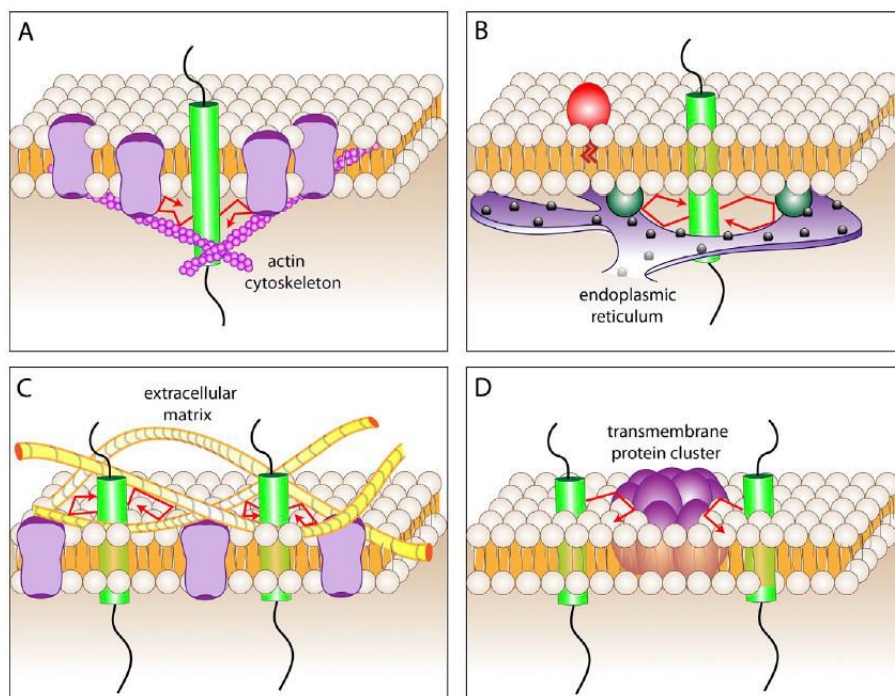


**Figure 4.3 Physical barriers to the diffusion of membrane lipids or proteins.**

**A.** The actin-based membrane skeleton forms microdomains with anchored transmembrane proteins and tightly associated lipids, named picket fences and lipid rafts. **B.** Areas of close contact between two organellar membranes can block the diffusion of molecules. An example of contact between the ER and the plasma membrane is illustrated. Blue-green spheres indicate the protein that links the plasma membrane and ER. **C.** The contact of extracellular matrix components (yellow fibers) with membrane receptors can generate a network to hinder the molecules' diffusion. **D.** The crowding and size of membrane proteins and lipids can limit the mobility of diffusing components. Green cylinder: freely mobile transmembrane proteins; Red arrows: trajectory of this protein. From Trimble and Grinstein [2015].

## 4.4 Lateral diffusion and synapses

Lateral diffusion of neurotransmitter receptors is one of the important parameters regulating synaptic efficacy. In neuronal synapses, neurotransmitter receptors are stabilized at the postsynaptic membrane by interaction with scaffold proteins. However, their stabilization is transient. Previous studies reveal that inhibitory glycine, GABA<sub>A</sub> receptors [Meier et al. 2001; Dahan et al. 2003; Lévi et al. 2008; Bannai et al. 2009] and glutamatergic AMPA, NMDA and mGluR5 [Sergé et al. 2002; Tardin et al. 2003; Groc et al. 2004] receptors can exchange between synaptic and extrasynaptic domains through lateral diffusion in the plasma membrane. Moreover, the synaptic scaffold proteins are also highly dynamic [Calamai et al. 2009; Gray et al. 2006]. Each receptor subtype shows different features in its lateral diffusion (Table 4.1) [Gerrow and Triller 2010]. The regulations of their diffusion are mediated by cytoskeleton, lipid domains, neuronal activity, and are receptor-specific [Gerrow and Triller 2010; Triller and Choquet 2008].

	Inhibitory						Excitatory							
	Gly <sup>a,b</sup>		GABA <sub>A</sub> <sup>c,d</sup>		GM1 <sup>d</sup>		AMPA <sup>e,d</sup>		NMDA <sup>e</sup>		mGluR <sup>f</sup>		GM1 <sup>d</sup>	
$D$ ( $\times 10^{-2}$ m <sup>2</sup> /s)	<b>0.1</b>	0.7	<b>1.2</b>	2.2	<b>1.3</b>	15.4	<b>2.8</b>	8.4	<b>2.1</b>	3.7	<b>1.0</b>	5.0	<b>2.0</b>	15.4
Confinement ( $\mu$ m)	<b>0.15</b>		<b>0.26</b>		<b>0.33</b>								<b>0.46</b>	
Dwell time (s)	<b>15</b>		<b>4.9</b>		<b>0.66</b>				<b>0.24</b>				<b>0.45</b>	
Changes in $D$														
Increased activity	↓		↑	↑			↑		–					
Actin disruption	↑	↑			↑	↑							↑	↑
Cholesterol depletion			↑	–	↑	↓	–	↓					↑	↓

**Table 4.1 Diffusion properties of molecules at inhibitory synapse, excitatory synapse and in extrasynaptic membrane sites.** The diffusional properties of neurotransmitter receptors and GM1 (a lipid enriched in lipid rafts) are measured by SPT experiments. Values : synaptic (bold, left) and extrasynaptic (right) sites. The changes in  $D$  (diffusion coefficient) are noted under conditions of increase neuronal activity, actin disruption and cholesterol depletion. Arrow: up (increase), down (decrease). Dashes: no change. From Gerrow and Triller [2010].

### 4.4.1 Dynamics at inhibitory synapses

#### *Glycine receptors*

Early SPT experiments using latex beads coupled to antibodies against GlyRs showed that GlyRs display lateral movement in young spinal cord neurons [Meier et al. 2001]. Basically, two distinct movements of GlyRs are recognized: free (Brownian) diffusion in the absence of gephyrin and long confinement on the top of synaptic gephyrin cluster. This means that receptors are free to move outside of gephyrin clusters even when most receptors are

stabilized. A great improvement on the study of membrane GlyRs behavior came later on from the use of quantum dots (QDs) coupled to antibodies [Dahan et al. 2003]. QDs are nanometer-sized semiconductor crystals for molecular labeling that provide long-lasting fluorescence emission. Trajectories of QDs recorded on living spinal cord neurons revealed that GlyRs exchanges rapidly between extrasynaptic and synaptic domains and display confined diffusion at synapses.

Although the mobility of receptors is greatly reduced at synapses, the large distribution of diffusion coefficient values indicated the existing of a large heterogeneity of behaviors [Ehrensperger et al. 2007]. Two synaptic population of GlyRs were distinguished: those that are tightly bound to gephyrin and those that are slowed down at synapses because of steric constraints. The diffusion behavior of extrasynaptic GlyRs depends on the gephyrin-bound form, and around at least 40% of GlyRs diffusing outside of synapse are bound to gephyrin.

Besides regulated by the actin cytoskeleton and ECM [Charrier et al. 2006, 2010; Hennekinne et al. 2013], the diffusion mobility of GlyRs are modulated by neuronal activity. The stimulation via activation of NMDARs leads to slow down diffusion rates and increases its clustering at synapse. This allows the GlyRs at inhibitory synapse to be liable to a rapid homeostatic regulation in response to increased excitatory activity [Lévi et al. 2008]. Moreover, a protein kinase C (PKC) phosphorylation site is found within the cytoplasmic domain of the  $\beta$  subunit of the GlyRs [Specht et al. 2011]. The phosphorylation sites reduces the binding affinity between GlyRs and gephyrin. Therefore, the diffusion of receptor accelerates and the accumulation of GlyRs decreases at synapse. These data indicate that the PKC could play a role in regulation dynamic of GlyRs and inhibitory synaptic plasticity.

### **GABA receptors**

FRAP revealed that GABA<sub>A</sub>Rs exhibit lower rate of mobility at synapse as compared to their extrasynaptic counterparts due to the presence of the scaffolding protein gephyrin [Jacob et al. 2005]. Bogdanov et al. [Bogdanov et al. 2006] labeled pHluorin-GABA<sub>A</sub>Rs with fluorescent  $\alpha$ -bungarotoxin to study the surface trafficking of receptors, facilitating the visualization of receptor endocytosis, exocytosis and delivery to synaptic sites. This approach revealed that synaptic GABA<sub>A</sub>Rs are directly recruited from their extrasynaptic counterparts. Electrophysiological methods were also applied to study the dynamic mobility of receptors in the surface, by introducing a specific and irreversible inhibitor to receptors. The recovery of the activity was an indication of the replacement of blocked receptors with active ones. By this approach it was shown that the cell surface population of GABA<sub>A</sub>Rs had no fast recovery (30-40

min) after irreversible inhibition. However, the synaptic population rapidly recovered by the import of new functional entities within minutes after selective inhibition [Thomas et al. 2005].

It is well established that the scaffold protein gephyrin plays a crucial role in GABA<sub>A</sub>R stabilization and GABA<sub>A</sub>R surface dynamics at inhibitory synapses [Tretter et al. 2012]. Recent studies have shown that gephyrin directly interacts with the intracellular loops of GABA<sub>A</sub>R $\alpha$ 1,  $\alpha$ 2 and  $\alpha$ 3 subunits and the binding affinities of these interactions have been characterized [Tretter et al. 2008; Saiepour et al. 2010; Mukherjee et al. 2011]. The lateral diffusion of GABA<sub>A</sub>R is regulated by neuronal activity. A SPT study on GABA<sub>A</sub>R in hippocampal neurons revealed that enhanced excitatory activity increased diffusion coefficients and the confinement domain of GABA<sub>A</sub>R at synapse, and that they were correlated with reduced cluster size of GABA<sub>A</sub>R and GABAergic mIPSC (miniature inhibitory postsynaptic currents) [Bannai et al. 2009]. These major findings demonstrate that GlyR and GABA<sub>A</sub>R diffusions were modulated by network excitatory activity in opposite directions, highlighting a functional regulatory difference between the two inhibitory receptors. Interestingly, with NMDA excitatory activity no effect of on the lateral diffusion of GABA<sub>A</sub>R in mixed inhibitory synapses (containing both GlyR and GABA<sub>A</sub>R) of spinal cord neurons was observed [Lévi et al. 2008]. Moreover, this regulation of GABA<sub>A</sub>R required Ca<sup>2+</sup> influx via NMDA receptors and activation of the phosphatase calcineurin. The mobility of individual GABA<sub>A</sub>R are dependent on serine 327 within the intracellular loop of the GABA<sub>A</sub>R $\gamma$ 2 subunit [Muir et al. 2010].

The surface trafficking of the receptors can be influenced itself by GABA<sub>A</sub>R activity. The GABA<sub>A</sub>R agonists and antagonists have opposite effects on the lateral diffusion and synaptic accumulation of GABA<sub>A</sub>R [Gouzer et al. 2014]. Even more, the influence GABA<sub>A</sub>R activity on GABA<sub>A</sub>R trafficking is differentially modulated depending on subunit composition, and those receptors compete for the same binding slots [Gerrow and Triller 2014].

#### **4.4.2 Dynamics at excitatory synapses**

##### ***AMPA receptors***

The mobility of AMPARs at the plasma membrane was initially demonstrated using latex beads. It was revealed that AMPARs in the extrasynaptic membranes are very mobile and can enter synapses where they decrease their mobility [Borgdorff and Choquet 2002]. Later, the diffusion mobility of AMPARs was confirmed by labeling with QDs or organic fluorophores [Groc et al. 2004; Tardin et al. 2003]. 50% of surface AMPARs are mobile between synaptic and extrasynaptic domains. Other global methods FRAP and electrophysiological tagging further support the lateral diffusion of AMPARs [Ashby et al. 2004; Adesnik et al. 2005].

Due to the critical role of AMPARs in the expression of synaptic plasticity, the regulation of AMPARs surface trafficking depends on many aspects, such as, neuronal activity, actin cytoskeleton, AMPARs subunit, LTP/LTD [Huganir and Nicoll 2013]. In this section, the role of interacting proteins on AMPARs surface trafficking is discussed.

AMPARs have been showed to interact with plenty of intracellular, transmembrane and extracellular proteins. Most of these interactions control the targets and signaling properties of AMPARs within the postsynaptic membrane [Opazo et al. 2012]. In the intracellular domain, AMPARs are stabilized primarily by scaffold proteins. Besides PSD-95, many other PDZ domain-containing proteins have been discovered at the synapse including three other proteins highly homologous to PSD-95, PSD-93, synapse-associated protein (SAP) 102, and SAP 97, collectively called MAGUK protein (membrane associated guanylate kinase) [Elias and Nicoll 2007]. These MAGUK protein share overlapping functions in terms of targeting AMPARs to synapses. The overexpression PSD-95 could increase synapse formation and increase AMPA levels at synapses. Increasing or decreasing the level of PSD-95 and PSD-93 increase and decrease synaptic AMPARs, respectively. However, SAP 97, which interacts directly with GluA1 AMPAR subunit, can fully rescue the deficits in synaptic AMPARs in PSD-93/95 knockout neurons [Howard et al. 2010; Huganir and Nicoll 2013]. These results indicate a complex relationship between the MAGUK protein and synaptic plasticity.

On the other hand, AMPARs has been shown to interact with extracellular matrix (ECM) and adhesion molecules. The ECM can restrict AMPARs movements, likely through non-specific interaction [Frischknecht et al. 2009] but also through direct interaction as shown for the extracellular neuronal pentraxin (NP1) which are required for GluA4 synaptic recruitment [Sia et al. 2007]. Postsynaptic adhesion protein NLs (Neuroligins) and LRRTMs (leucine-rich repeat transmembrane proteins) have specific role in AMPARs trafficking. Decreasing the expression levels of LRRTM1 and LRRTM2 blocks AMPAR-EPSCs (excitatory postsynaptic currents) in the neonate and impair the enhancement of synaptic AMPARs after cLTP induction [Soler-Ilavina et al. 2013]. Overexpression of NL3 selectively enhances AMPARs currents [Shipman et al. 2011].

Finally, perhaps among the most important partners to regulate AMPARs surface trafficking, TARP (transmembrane AMPAR regulatory protein) contain a PDZ domain binding motif at its C-terminus that associates directly with PSD-95-like MAGUKs, and this binding ligand is considered to responsible for clustering of AMPARs at the synapse [Tomita et al. 2005]. Thus, PSD-95-TARPs interaction defines the minimal components to regulate AMPARs surface diffusion. Stargazin stabilizes AMPAR at synapses through its specific interaction with PSD-95 [Bats et al. 2007].

***NMDA receptors***

Using electrophysiological and imaging approaches, it has been demonstrated a decade ago that surface NMDARs can move laterally in synaptic and extrasynaptic membranes [Tovar and Westbrook 2002; Groc et al. 2004]. The rate of recovery was approximately 65% within 7 min, indicating the most of NMDARs exchange quickly between the two compartments [Tovar and Westbrook 2002]. Indeed, SPT experiments revealed that NMDARs were less mobile than AMPARs [Groc et al. 2004]. The surface diffusion of NMDARs depends on their subunit composition, with GluN2A-containing NMDARs being more stable than GluN2B-containing ones [Groc et al. 2006]. Following chemical LTP induction, the GluN2B-NMDAR but not GluN2A-NMDAR rapidly changed through an increase in surface diffusion requiring the direct binding of CaMKII to GluN2B [Dupuis et al. 2014]. This is consistent with the decrease of NMDARs mobility during synaptogenesis due to the increased NR2A/NR2B ratio in mature synapses. Compared to AMPARs, the mobility of NMDARs is not sensitive to the change of neuronal activity [Groc et al. 2004].

The trafficking and function of NMDAR are modulated by multiple processes. For instance, the mobility of NMDA depends on the ECM [Groc et al. 2007], the activity of protein kinase C (PKC) [Groc et al. 2004] and the physical interaction with Dopamine receptor D1 [Scott et al. 2006; Ladépêche et al. 2014]. Regarding scaffolding molecules, interactions with MAGUKs play distinct roles in the modulation of NMDA surface diffusion during synaptogenesis and synapse maturation. The switch from GluN2B- to NR2A-NMDAR during spine maturation is temporally coincident with the switch from SAP 102 to PSD-95 [van Zundert et al. 2004]. SAP 102, but not PSD-95, mediates synaptic trafficking of NMDAR during synaptogenesis in vivo, whereas PSD-95 is necessary for synaptic maturation of NMDAR-mediated synaptic transmission [Elias et al. 2008]. The extracellular matrix (ECM) protein Reelin controls the lateral diffusion of NR2B subunits while the inhibition of Reelin decreases the surface mobility of NR2B-containing NMDARs and increases synaptic dwell time [Groc et al. 2007]. A potential mechanism could involve the changes in the levels of scaffolding proteins during synapse development, such as SAP 102 and PSD-95, while the changes in PSD-95 and SAP 102 reflect preferred associations with NR2A and NR2B, respectively [Sans et al. 2000].

***mGluR5***

Although the group I metabotropic glutamate receptor 5 (mGluR5) is concentrated in an annulus around the postsynaptic density (PSD) [Nusser 1994], up to 75% of the receptors can be found in the extrasynaptic membrane [Luján et al. 1997]. This distribution could result from the

dynamic mobility of mGluR5 in the plane of neuronal membrane. Using both of SPT and FRAP, it was revealed that mGluR5 molecules underwent a dynamic equilibrium between a freely diffusive state in extrasynaptic domains and a confined state at synapses, by binding to Homer or other scaffolding protein. The mobility of mGluR5 is upregulated by its activity and downregulated by its associated scaffold Homer [Sergé et al. 2002]. Agonist DHPG induces an increase of mGluR5 diffusion in both diffusive and confined events and a reduction of the confinement index during confined events. Full-length Homer causes the accumulation of mGluR5 and shifts mGluR5 movement toward confined states [Sergé et al. 2002]. Cytoskeletal elements also contribute to the highly variability of mGluR5 diffusion [Serge et al. 2003]. Depolymerization of actin and microtubule suppress the mGluR5 movement on the surface. In a pathological context, Alzheimer disease-related A $\beta$  oligomers reduce the diffusion mobility of mGluR5 at both synaptic and extrasynaptic membranes by acting as an extracellular scaffold [Renner et al. 2010]. As a consequence, there is an increase in the synaptic accumulation of mGluR5 inducing deleterious effect on synapses [Renner et al. 2010]. Interestingly, A $\beta$  oligomers binding to the plasma membrane of astrocytes induces the release of ATP that contributes to the diffusional trapping of mGluR5 and a strong enrichment of mGluR5 on astrocytes [Shrivastava et al. 2013].

#### 4.5 The spine neck as a barrier for lateral diffusion

The spine neck, by its small diameter (~75-300 nm in diameter, 1  $\mu$ m long) [Bourne and Harris 2008] constitutes a natural barrier for the diffusion of intracellular molecules isolating the spine head from dendritic shaft. Spine neck is generally thought to confine biochemical signals within the spine compartment. This function is shaped and dynamically regulated by nanoscale spine morphology.

Some reports suggest that the spine neck may act as a barrier for the diffusion of membrane molecules (Fig. 4.4). For instance, the spine neck morphology can affect lateral diffusion of AMPARs from the dendrite into the synapse, leading to a marked suppression of receptor exit rate out of spines with decreasing neck radius. Mushroom shaped spines with a thin neck are significantly more effective at retaining receptors at the spine head [Ashby et al. 2006; Kusters et al. 2013]. This is a particularly interesting, because the radius of the neck of mushroom spines is in that same range with the cylindrical membranes studied in Domanov et al. [Domanov et al. 2011], meaning that geometry could be the origin of a "diffusion barrier" in spine necks.

In addition to spine neck geometry, particular molecules present in the spine neck could contribute to its compartmentalizing function. The particular localization of some proteins in spine necks is intriguing, as it has been reported for few proteins such as DARPP-32 [Blom et al. 2013], septin-7 [Tada et al. 2007; Ewers et al. 2014], ankyrin-G [Smith et al. 2014] and synaptopodin [Deller et al. 2000b]. DARPP-32 (dopamine- and cAMP-regulated phosphoprotein of 32KDa) is an important component in the molecular regulation of postsynaptic signaling in neostriatum [Greengard et al. 1999]. Dual color STED microscopy revealed the postsynaptic distribution of DARPP-32 in dendritic spines. Larger clusters of DARPP-32 located in the spine head might be involved in the regulation of synaptic transmission. Additional DARPP-32 clusters present along the neck could contribute to the compartmentalized and confined function of spine necks [Blom et al. 2013]. Septin-7 (a marker of the septin cytoskeletal GTPase complex) has recently been found to stably localize at the base of neck of most spines (~80%). Single particle tracking revealed that the diffusion of transmembrane proteins (AMPARs) is significantly hindered in septin-7 positive spines, while membrane molecules explored larger membrane areas when septin7 expression was suppressed by RNA interference [Ewers et al. 2014]. These results indicate that septin7 contributes to the function of the spine neck as the barrier, preventing molecules to enter the spine neck from the dendritic shaft, or preventing molecules on the neck to reach the dendrite. Ankyrin-G (a scaffolding adaptor that links membrane proteins to the actin/ $\beta$ -spectrin cytoskeleton [Bennett and Healy 2009] forms distinct nanodomain structures within the spine head surrounding the PSD, and in the spine neck [Smith et al. 2014]. Interestingly, the presence of an ankyrin-G nanodomains in the spine neck is associated with the accumulation of AMPARs in the spine head. Ankyrin-G overexpression increases the levels and stability of AMPARs at synapses, increasing also the neck width [Smith et al. 2014].

Synaptopodin, an actin-binding protein, is almost exclusively present in spine neck which is full of longitudinal actin filaments. Actin cytoskeleton is the scaffold of the spine morphology and can be connected to a myriad of molecules to influence the lateral diffusion of membrane protein. Thus, SP is a very interesting candidate for the regulation of lateral diffusion in spine necks. The question whether synaptopodin contributes to the limitation of diffusion in spine necks was the focus of my study.

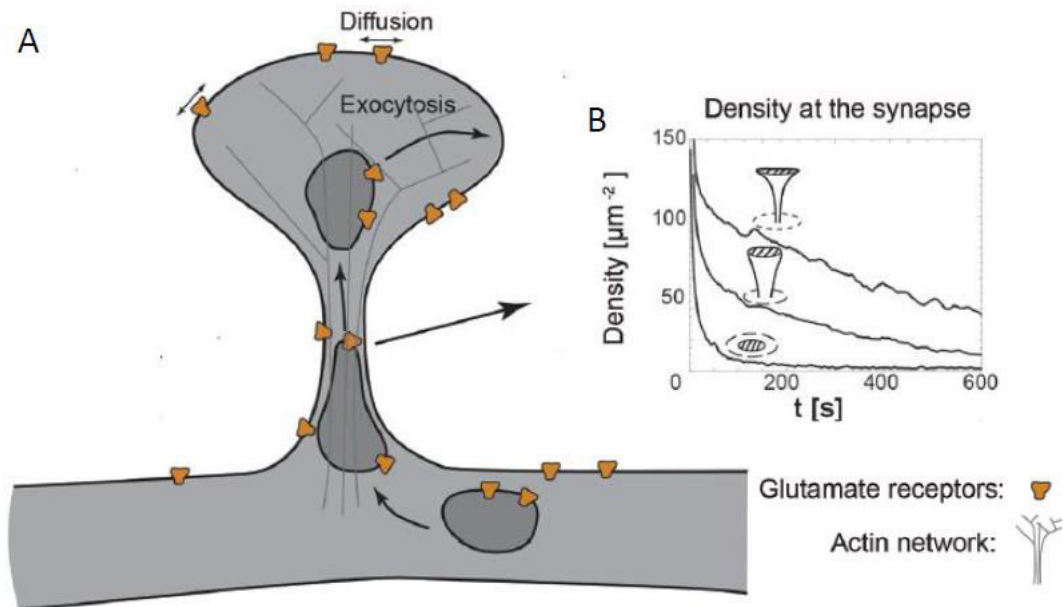


**Figure 4.4 The geometry of dendritic spine as a regulator of molecule diffusion.**

**A.** Schemew of a dendritic spine including recycling endosomes, glutamate receptors and actin cytoskeleton. The receptors display lateral diffusion in the membrane surface and the trafficking from dendritic shaft to the spine head. **B.** Spine shape influences the exit rate of receptors out of spines. The retention of receptors at the synapse is converse with the radius of the neck, indicated by the time-evolution of receptor density at the synapse (dashed area) for a planar, stubby and mushroom shaped spine. From Kapitein et al [Adrian et al. 2014].



## **Objectives**

The aim of my doctoral research project was to investigate what is the origin of the diffusional barrier in the spine neck. With respect to geometry, I have studied the diffusion behaviors of membrane proteins in dendrites and the spine necks. More importantly, I have examined whether synaptopodin contributed to the formation of a functional barrier in the spine neck. The behavior of different membrane proteins in spine necks was thus investigated in terms of diffusion dynamics and correlated with super-resolution imaging techniques using cultured hippocampal neurons in standard conditions or after manipulation of activity levels and cytoskeleton integrity.



## **II Materials and Methods**



## 1 Methods

### 1.1 Expression constructs

The GFP-GPI plasmid was kindly provided by Dr. S. Mayor (India, Bangalore; [Sharma et al. 2004]). The TMD-pHluorin plasmid driving the expression of a single transmembrane domain (TMD) from syntaxin fused to an extracellular (C-terminal) pHluorin tag was described in Ribault et al. [2011]. The pHluorin-mGluR5 plasmid containing the coding sequence of rat mGluR5a (isoform 1, UniProt accession number P31424-2) with an extracellular (N-terminal) pHluorin tag was generated from plasmid pcDNA3.1-Myc-mGluR5a- Venus [Perroy et al. 2008]. PCR fragments of the coding sequence of mGluR5 were amplified with mGluR5-PCR7s and mGluR5-PCR8a primers (Table1), digested by *Sal I/Pst I*, and cloned into a pRK5 backbone containing pHluorin sequence. The backbone was derived from a pHluorin-GABA<sub>A</sub> receptor subunit (gift from Steve Moss) by removing the GABA<sub>A</sub> sequence with *Xho I/Pst I* enzymes. Finally, the plasmid pHluorin-mGluR5 was obtained through ligation.

The mRFP-SP construct contained the mouse synaptopodin sequence (isoform 3, UniProt Q8CC35-3) and was derived from pEGFP-SYNPO [Asanuma et al. 2005] by replacing the N-terminal tag with the mRFP (made by Laetitia Hennekinne). mRFP fragment is obtained from pSERT-mRFP by PCR with primers mRFP-Synpo-1 and mRFP-rev3 (Table1) containing enzyme sites *Age I/BsrG I*. Plasmid dendra-SP is generated from mRFP-SP by replacing mRFP with dendra using enzymes *Age I/BsrG I* similarly. Finally, to generate FU-dendra-SP, the dendra-SP coding sequence was digested by *Age I/Apa I* enzymes, while the backbone FUGW replicon plasmid [Lois et al. 2002] was cut by *Age I/EcoR I*. To ligate of the insert and backbone, a short adaptor (AD-ApaEco) was used to fill the gap between the *Apa I* and *EcoR I* overhangs. Plasmid FU-dendra-SP was used to produce lentiviral particles for infection. All constructs were verified by DNA double standard sequencing.

### 1.2 General description of cloning

#### *Polymerase chain reaction*

cDNA fragments containing the coding sequences (CDS) of mGluR5a were generated by polymerase chain reaction (PCR). This was performed in 25  $\mu$ L reaction system, containing 10 ng template DNA (pcDNA3.1-Myc-mGluR5a- Venus), 10 pmol of each primer, 5  $\mu$ mol nucleotide mix, 25  $\mu$ mol MgCl<sub>2</sub>, 2.5  $\mu$ L 10x KOD polymerase PCR buffer (Novagen) and 1 U KOD polymerase (Novagen). Cycling started with a denaturing step (96°C / 5 min, hot start to prevent

primer-dimer formation), followed by 25 cycles of denaturing (96°C / 15 s), annealing (60.7°C / 10 s) and polymerization steps (72°C / 50 s). PCR products were purified by gel extraction, and subjected to restriction digestion prior to subcloning.

**Table 1.1 Primers used for cloning.**

Name	Sequence	sites
mGluR5-PCR7s	AATTGTCGACGGTCAAAGTAGTGAGAGGAGGGTGGTG	<i>Sal</i> I
mGluR5-PCR8a	TTTTCTGCAGTCACAACGATGAAGAACTCTGCG	<i>Pst</i> I
mRFP-Synpo-1	CCCACCGGTATGGCCTCCTCCGAGGACGT	<i>Age</i> I
mRFP-rev3	TTTTGTACAAGGCGCCGGTGGAGTGGCGGC	<i>Bsr</i> G I
AD-ApaEco	AATTGGCC	

#### *Agarose gel electrophoresis of DNA*

DNA was analysed on gels containing 0.6-1.0% agarose in TAE buffer and SYBR Green (1:10000 dilution, S-11494, Life technologies). TAE buffer contains 40 mM Tris acetate and 1 mM EDTA (pH 8.2-8.4; Sigma). Gels were run in TAE buffer at 5 V/cm. DNA samples were loaded with DNA Gel loading Dyes (6x) (R0611, Life technologies) and marked by GeneRuler 1 kb DNA Ladder (SM0312, Life technologies)

#### *DNA purification*

Bands containing DNA fragments were excised from agarose gels and purified using silica beads according to the supplier's protocol (Jetsorb; Genomed). Briefly, DNA gel slices were melted in high salt buffer (300 µL per 100 mg agarose) containing 5-10 µL bead suspension at 50°C for 15 min. During this process, DNA was bound to silica beads. Then DNA was washed, dried, eluted with 20 µL TE buffer, and stored at -20°C.

#### *DNA digestions*

0.3-1.5 µg DNA (plasmids DNA or PCR products) was digested with 10 U of the restriction enzymes, in the appropriate digestion buffer, under the conditions suggested by the enzyme suppliers (Fermentas, New England Biolabs). For subcloning of restriction fragments, the reaction products were purified by gel extraction prior to ligation.

#### *DNA fragments ligation*

Ligation was carried out in 10 µL reaction system containing: 1 µL 10x Ligase buffer, 1 U T4 DNA Ligase, and 1:1 ~1:5 molar ratio of vector : insert DNA. For the construction of FU

-dendra-SP plasmid, 1  $\mu$ L an additional adapter primer (1 pM) was added to the ligation system. The reaction was incubated for 30 min at room temperature or overnight at 16°C before transformation.

### *Transformation*

Frozen chemically competent bacteria DH5 $\alpha$  (-80 °C) were thawed and incubated with 1-10  $\mu$ L ligation reactions on ice for 30 min. Then the cells were heat shocked for 30 seconds in a 42°C water bath and placed on ice 2 min. 250  $\mu$ L pre-warmed LB medium was added to the transformed cells, which were then incubated (1 h, 37°C, 225 rpm) and plated into LB agar medium with antibiotics (e.g. Kanamycin) over night.

### *Positive cloning identification*

On the following day of transformation, several single colonies were picked up and grew in LB medium with antibiotics overnight. DNA of these colonies were purified using a plasmid purification kit according to the manufacturer's protocol (QIAprep Spin Miniprep Kit). Purified DNA was identified firstly by digestion using restriction enzymes, and then was sequenced (Eurofins Genomics). Finally, the plasmids DNA with corrected sequences were prepared in a large scale (QIAprep Spin Maxprep Kit) for experiments and stored at -20°C.

## **1.3 Cell culture**

All research using animals was carried out according to the European Community Council directive of 24 November 1986 (86/609/EEC), the guidelines of the French Ministry of Agriculture and the Direction départementale des services vétérinaires de Paris (Ecole Normale Supérieure, Animalerie des Rongeurs, license B 75-05-20). Primary cultures of dissociated hippocampal neurons were prepared from Sprague Dawley rats at embryonic day 18-20 as described [Renner et al. 2011]. The general dissection process are introduced: i) The brain vertical side was placed up in the dissection medium (10% HBSS and 0.02 M HEPES in water). The tissue needs to remain submerged at all times. ii) Using a dissecting microscope, hold the hindbrain region and make a small incision to separate the two hemispheres. iii) Hold the hemisphere carefully and remove the meningeal tissue. Then the hippocampus tissue was transferred to dissection medium containing 0.25% (w/v) trypsin and were incubated 10 min at 37°C. Finally, neurons were plated at a density of  $2.5 \times 10^4$  cells/cm<sup>2</sup> onto 18 mm diameter glass coverslips precoated with 80  $\mu$ g/ml poly-D,L-ornithine (Sigma), and maintained at 37°C in a 5% CO<sub>2</sub> humidified incubator in Neurobasal medium supplemented with 2% B27 supplement, 2

mM L-glutamine, and 5 U/mL penicillin and 5 µg/mL streptomycin (all from Invitrogen). Neurons were maintained in the incubator until used for experiments at DIV 20-23.

#### **1.4 Transfection and infection (lentiviral production)**

Neurons were transfected at days *in vitro* (DIV) 9-12 with Lipofectamine 2000 reagent (Invitrogen). Firstly, per well, 0.5 µg plasmid DNA and 2 µL Lipofectamine were incubated in 50 µL Neurobasal medium (NBM) respectively for 10 min. Then, mix NBM-DNA and Nbc-lipofectamine medium for 15 min. Take out the original NBM of neuron and keep it at 36°C, while put 500 µL fresh NBM per well. Neurons were incubated with the mix solution DNA-lipofectamine (100 µL) 30 min in the incubator. Finally, rinse the cells 3 times with NBM, and put back the original medium. For double transfections, 0.25 µg of each construct was used.

For super-resolution experiments, neurons were infected at DIV 1 with lentivirions driving the expression of dendra-SP (construct FU-dendra-SP). Lentiviral particles were produced for infection as previously described [Waites et al. 2009]. HEK cells were plated on 10 cm dishes coating with 10 µg/mL poly-L-lysine (P1524, Sigma) in PBS, and were maintained to confluence in DMEM medium containing 10% fetal bovine serum. Then the DMEM medium was replaced with Neurobasal medium containing 2 mM L-glutamine and 2% B27 on the day of transfection. Cells were cotransfected with pFUGW-dendra-SP construct (5 µg) together with two packaging plasmids pCMVΔ R8.9 (7.5 µg) and VSVg (5 µg) in 1.5 ml Opti-MEM medium (Invitrogen), using 60 µL Lipofectamine 2000 (Invitrogen) per 10 cm plate. HEK cells were then incubated at 32°C, 5% CO<sub>2</sub>. The medium was exchanged and discarded after 24 hours and the virus was collected with culture medium after ~48 h, passed through a 0.45-µm filter to remove cell debris, and stored as aliquots at -80°C.

#### **1.5 Drug treatments**

Latrunculin A (latA), 4-aminopyridine (4AP), dihydroxyphenylglycine (DHPG) and 2-methyl-6-(phenylethynyl)-pyridine (MPEP) were obtained from Tocris Bioscience (Avonmouth, UK) and used at a concentration of 5 µM, 50 µM, 10 µM and 50 µM, respectively. For immunocytochemistry and super-resolution STORM/PALM imaging, drugs were added directly to the culture medium (for 5-60 min) prior to fixation. To test the reversibility of the 4AP and latA treatments, cells were treated for 30 min with 4AP (50 µM) or Latrunculin A (5 µM), and the medium with the drugs was then replaced with culture medium without drug for 30 min or 2 hours, respectively.

In the SPT experiments, cells were pre-incubated for 20 min with 4AP in culture medium, labelled with antibody-coupled quantum dots (QDs) for 5 min (see below) and then imaged in MEM recording medium (see below) for up to 20 min in the presence of 4AP. Latrunculin A was added to the medium at the beginning of the SPT recording session that lasted for up to 20 min. SPT experiments were also done after 4AP washout using the following protocol: cells were incubated for 30 min with 4AP in culture medium, and then the diffusion was measured by SPT in MEM recording medium without 4AP.

### **1.6 Live imaging analysis of SP cluster modification**

Neurons cotransfected with TMD-pHluorin and mRFP-SP were used to study the dynamic modification of SP clusters in living cells under latrunculin A (5  $\mu$ M) incubation during time lapse (0, 5, 10, 20, 30 min). The inverted Nikon Eclipse Ti microscope (for STORM/PALM, see below) was used to observe this modification. The density and intensity of SP clusters after latrunculin A application were measured and the morphology of neurons visualized by TMD-pHluorin.

### **1.7 Immunocytochemistry**

Cells were fixed at room temperature for 10 min in paraformaldehyde (PFA, 4% w/v) in PBS, and permeabilized for 4 min with Triton X-100 (0.25% v/v in PBS). Cells were then incubated for 30 min in blocking solution (PBS containing 0.25% w/v gelatin, Sigma) and for 1 hour with guinea pig anti-synaptopodin antibody (1:500, cat.no. 163004, Synaptic Systems) diluted in 0.125% gelatin-PBS. Alexa Fluor 488 (A488)-conjugated donkey anti-guinea pig antibody (1:1000, Jackson ImmunoResearch Laboratories) was used as secondary antibody. Incubation for 45 min with Alexa Fluor 647 (A647)-phalloidin (0.2  $\mu$ M, A22287, Invitrogen) was used to label actin filaments. For double staining of synaptopodin with mGluR5 or  $\alpha$ -actinin2, fixed cells were incubated with primary antibodies (anti-mGluR5, 1:1000, cat.no. NA75-116, NeuroMab;  $\alpha$ -actinin2, 1:500, cat.no. A7811, Sigma) for 48 hours at 4°C or 1 hour at room temperature. A488 donkey anti-guinea pig and Dylight 549 goat anti-mouse were chosen as secondary antibodies (1:1000, Jackson ImmunoResearch Laboratories).

Acquisition of fluorescence images was done on a spinning disk confocal microscope (LeicaDM5000B, Leica Microsystems, with a Yokogawa CSU10 spinning disk head), equipped with a CCD camera (CoolSnap, Princeton Instruments) and controlled by Metamorph software (Molecular Devices). Images were taken with a Photometrics 63x immersion objective, and exposure times were kept constant and were such as to capture the full intensity range in each

channel. For quantification, images were filtered by wavelet segmentation using an interface implemented in Metamorph [Racine et al. 2007] to generate binary masks of SP. The integrated intensity of SP and phalloidin was then measured in SP regions of the mask using homemade software (ImAnalysis, [Hennekinne et al. 2013]) in Matlab (MathWorks). Quantification of SP cluster densities was done on portions of dendrites (length > 10  $\mu\text{m}$ ) with clearly protruding spines.

### **1.8 Statistical analysis**

All experiments were performed in three or more independent cultures. Data obtained by immunocytochemistry and STORM/PALM were compared using the Mann-Whitney U-test (MW). Diffusion data (SPT) were analysed using the Kolmogorov–Smirnov test (KS). Data values and statistical analyses are summarised in Annexes tables 1-5. Data are generally given as mean  $\pm$  standard deviation (SD) or standard error of the mean (SEM), or as median, 25% and 75% of the population. The methods of SPT and STORM/PALM are introduced in below section [Single molecule imaging].

## 2 Single molecule imaging

The spatial resolution of microscope is determined by the size of point spread function (PSF), which represents the 3D intensity profile of the image of a point object. Two points closer than the FWHM of the PSF will appear as a single object, making them undistinguishable from each other [Huang et al. 2010]. In conventional fluorescence microscopy, the resolution limit, about 200-300 nm in the lateral direction and 500-700 nm in the axial direction, constrains the ability to observe small subcellular structures and molecules [Huang et al. 2010]. In response to this dilemma, recent advances in single molecule imaging techniques allowed to overcome the diffraction barrier, providing super-resolution images (in the nanometer range). The achievement of imaging in super-resolution benefits from the detection and localization of single fluorescence emitters. In my study, two kinds of single molecule imaging techniques were used: single particle tracking (SPT) using quantum dots (QDs) and photoactivated localization microscopy (PALM) and stochastic optical reconstruction microscopy (STORM) based on photo-switchable fluorophores.

### 2.1 Single particle tracking using quantum dots

SPT is a powerful technique to analyze the lateral diffusion of the lipid and protein components of biological membranes. The common procedures to study lateral diffusion include: i) labelling of the molecules of interest ii) recording of QDs positions over time and construction of trajectories from these positions; iii) localization of the trajectories with cellular compartments and iv) diffusion analysis [Alcor et al. 2009] (Fig. 2.1).

#### Labeling of molecules using quantum dots

##### *The properties of QDs*

Quantum dots (QDs) are particularly suited for SPT thanks to their photophysical properties. The small size ensure QDs to enter small space without perturbing the normal diffusion of proteins. The high photostability allows to acquire long enough trajectories of QDs-labeled molecules (tens of minutes to hours) [Alivisatos, P 2004; Bannai et al. 2006]. QDs are composed by cadmium selenide (CdSe) nanocrystal semiconductors, covered by a zinc sulphide (ZnS shell). This crystal is hydrophobic and thus it has to be encapsulated to ensure its biocompatibility, after which it reaches a hydrodynamic size of 15-25 nm. With respect to usual organic dyes, QDs have very high brightness owing to their extinction coefficient. This

provides a high signal to noise ratio (SNR), even under standard epifluorescence microscopes and allows the precise localization of individual QDs below diffraction limit (pointing accuracy~10 nm). QDs also presents a particular property: blinking between "on" and "off" states randomly. This feature is favorable to the identification of individual QDs, but it complicates data processing because trajectories of labeled molecules must be reconstructed manually (see below) [Triller and Choquet 2008, Pinaud et al. 2010]. Nowadays, commercial QDs coupled with biotin, streptavidin or IgG are commonly used to label antibody of membrane proteins or lipids and used in SPT.

### *Molecule labeling*

To track membrane protein diffusion, quantum dots (QDs) were attached to their extracellular fluorophore tags, as reported previously [Renner et al. 2009]. Briefly, 50 nM goat anti-rabbit F(ab')<sub>2</sub>-tagged QDs emitting at 655 nm (Q11422MP, Invitrogen) were incubated first with polyclonal rabbit anti-GFP antibody (1:10 dilution; cat.no. 132002, Synaptic Systems) for 30 min in PBS, and then blocked for 15 min with casein (1x) in a final volume of 10 µl. Transfected neurons were incubated with the pre-coupled QDs (1:6000-1:10000 final dilution) for 5 min at 37°C in MEM recording medium (phenol red-free minimal essential medium, supplemented with 33 mM glucose (Sigma), 20 mM HEPES, 2 mM glutamine, 1 mM sodium pyruvate, and 2% B27, all from Invitrogen) and rinsed in recording medium.

### **Recording of QDs positions**

Neurons were imaged for up to 30 min in MEM recording medium in an open chamber mounted onto an inverted microscope (IX71, Olympus, Tokyo, Japan) equipped with an oil-immersion objective (Olympus, 63x, NA 1.45). Fluorescence was detected using a xenon lamp, appropriate emission filters (GFP: excitation wavelength 485 nm with a bandwidth of 20 nm, emission 535/30; RFP: ex 560/25, em 605/15; QD: ex 460/60, em 655/15; all from Semrock) and a charge-coupled device (CCD) camera (Cascade 512B, Roper Scientific). QD trajectories were recorded with an exposure time of 12 ms over 5000 image frames (1 min streamed recording) with Metamorph software (Molecular Devices).

### **Construction of trajectories**

Tracking and analysis were done as described [Renner et al. 2010] using the homemade software SPTTrack\_v4 in Matlab (MathWorks). The common approach to analyze the motion of spots is localization and reconstruction of individual trajectories from raw data captured by

microscope camera. First, fluorescent spots centers are usually located by Gaussian fitting of the point spread function intensity profile, with a spatial accuracy of 5-10 nm. This is applied successively to each frame of the sequence [Courty et al. 2006; Pinaud et al. 2010]. After localization, trajectories are constructed automatically by connecting the centers of fluorescent spots across adjacent frames within the entire image series. In the case of QDs blinking, firstly, two parameters are considered to connect two nearby QDs trajectories using automatic program: trajectories continuously move in more than 10 frames and the distance between them is less than 2 pixels. Then a manual association step was performed to connect trajectories those corresponding to the same QDs as long as possible.

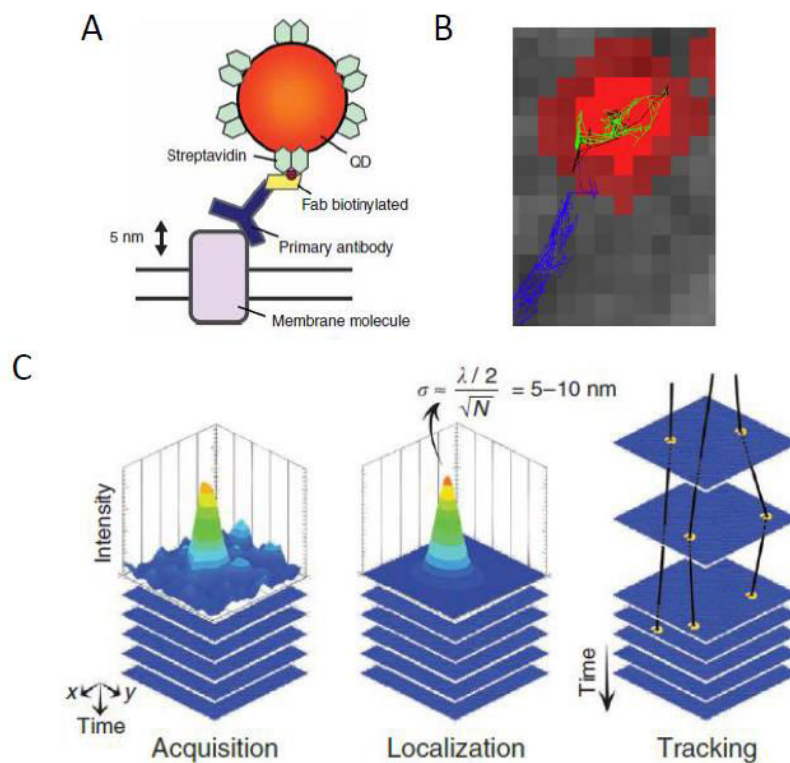


**Figure 2.1 Processing and analysis of SPT data.**

**A.** Scheme of molecule special labelled with QDs. The membrane proteins are recognized by primer antibodies (blue) which couple with secondary antibodies with biotin (yellow). The QDs (orange) functionalized with streptavidin (green) then link to the complex of molecule/antibodies. From [Bannai et al. \[2006\]](#). **B.** Example of localization of QD trajectory with cellular of compartment. QDs move in (green) and out (blue) of synapse (synaptic boutons stained by FM 4-64, red). From [Triller and Choquet \[2008\]](#). **C.** Processes of trajectories construction. Each QD is firstly acquired by microscope camera and then be localized by using Gaussian fitting of the intensity profile. Finally, trajectories are formed by linking the fluorescent spots. The localization accuracy ( $\sigma$ ) is determined by the emission wavelength ( $\lambda$ ) and the total number of detected photons ( $N$ ). From [Pinaud et al. \[2010\]](#).

### Localization of trajectories within mRFP-SP cluster in the spine neck

After the reconstruction of QDs trajectories, it is allowed to obtain the position dependence on the time for each trajectory. QDs trajectories in synaptopodin-negative (SP-) or SP-expressing spines (SP+) were identified based on the presence of mRFP-SP clusters. To distinguish between SP-free and SP-containing areas of SP+ spines, trajectories were classified according to their co-localization with binary mRFP-SP images. mRFP-SP images were filtered by wavelet segmentation using an interface implemented in Metamorph [Racine et al. 2007] to generate binary masks of SP.

### One-dimensional diffusion analysis

Only trajectories with at least 15 consecutive frames were considered. The mean square displacement (MSD) was calculated using  $MSD(ndt) = (N-n)^{-1} \sum_{i=1}^{N-n} [(x_{i+n} - x_i)^2 + (y_{i+n} - y_i)^2] dt$ , where  $x_i$  and  $y_i$  are the coordinates in frame  $i$ ,  $N$  is the total number of steps in the trajectory,  $dt$  is the time between two successive frames and  $ndt$  is the time interval over which displacement is averaged [Saxton and Jacobson 1997]. For a simple two-dimensional Brownian motion, the  $MSD(ndt)$  plot is linear with a slope of  $4D$ , where  $D$  is the diffusion constant.

However, measurements are more complicated when the membrane exhibits a high curvature (ex: axons, dendrites, spines). In curved membranes, 2D SPT trajectories on a flat surface are the projections of the real displacements in the 3D membrane. Due to the effect of the shape of membrane on recovery half-time of fluorescence, the diffusion constants measured by FRAP can differ by a factor of  $\sim 2$  with the real ones [Sbalzarini et al. 2006]. The bias in diffusion measurements that appears in 2D SPT in the particular membrane geometry of neurites was evaluated by Renner et al [Renner et al. 2011] (Fig. 2.2). They found that the diffusion coefficient calculated with projected trajectories is underestimated by 25 to 50% than the real  $D$  in the case of 2D-SPT over the tubular surface. And this underestimation is mainly determined by the radius of the tubular surface. Moreover, they proved that the one-dimensional MSD calculated only the displacement in the direction of cylinder axis could provide accurate estimates, avoiding the effect from geometry [Renner et al. 2011]. I made use of this method in order to analysis molecules diffusion in spine necks and dendrites. One-dimensional MSD can be calculated taking into account the displacement in parallel with the axis of spine necks and dendrites. The one-dimensional diffusion coefficient  $D_{1D}$  is calculated by using

$$MSD_{1D}(t) = 2D_{1D}t + b.$$

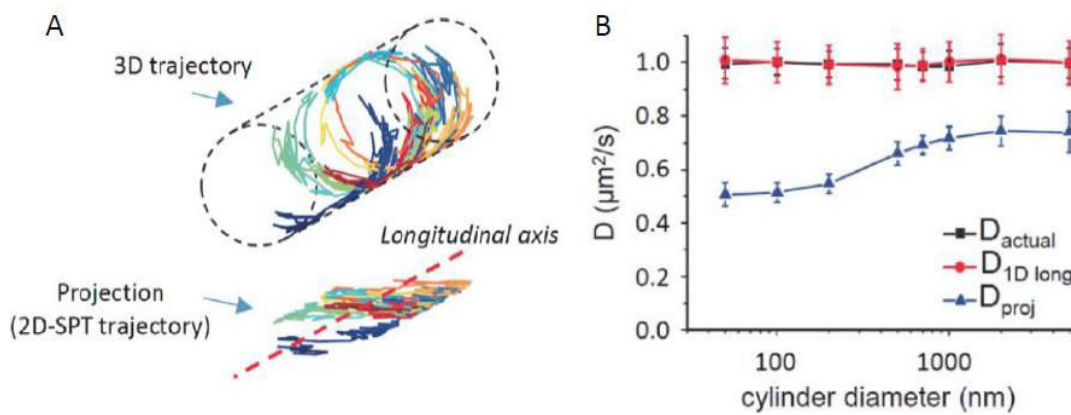


**Figure 2.2 Effect of geometry on diffusion measurements on cylindrical structures.**

**A.** Example of simulated cylindrical trajectory (top) and its 2D projection (bottom). Dotted red line: cylinder axis. Color indicates time (start: blue, end: red). **B.** Effect of cylinder diameter on values of  $D$  calculated on the projected trajectory ( $D_{proj}$ , 25-50% lower than the real value  $D_{actual}$ ) or  $D$  calculated from the components of displacements parallel to the axis indicated by the dotted line in (D) ( $D_{1Dlong}$ ) (mean  $\pm$  SD). From [Renner et al. \[2011\]](#).

## 2.2 Super-resolution STORM/PALM imaging

The principle of STORM/PALM is based on the acquisition of images with stochastic on/off switching of single fluorophores. By controlling their emission properties, a different subset of fluorophores in the sample are activated at any given time, allowing subsets of fluorophores to be imaged without spatial overlap that can then be localized with high precision. Repeating the activation and imaging process thousands of times for different subsets of fluorophores in the sample allows reconstructing a super-resolution image (Fig. 2.3) [[Huang et al. 2009](#)]. Using this approach, a lateral image resolution as high as  $\sim 20$  nm has been achieved [[Rust et al. 2006](#)].

### Molecules labeling

#### *The properties of fluorescent probes*

In PALM/STORM, the probes must be switched on and off. This means these probes must switch between a fluorescent state and a "dark" state that does not emit light in this wavelength range. Second, the number of photons detected for each fluorophore should be high enough to clearly distinguish from the surrounding background. Third, the dark state emission should be minimal. Last, a low spontaneous activation rate is also required. All switchable fluorophores can be spontaneously activated by thermal energy even in the absence of specific exposure to the activation light source, and thus prevent the single-molecule detection [[Huang et al. 2010](#); [Bates et al. 2013](#)].

The achievement of super resolution imaging by PALM and STORM are depended on different types of fluorophores. PALM chooses photo-switchable or photo-convertible fluorescent proteins (ex. Dendra2 or mEos2), whereas STORM exploits the photo-switchable properties of organic fluorophores/dyes (ex. Cy5 or Alexa647). Fluorescent proteins for PALM make it easier to label intracellular proteins in living cells, while dyes for STORM are more flexible for labeling different molecular species.

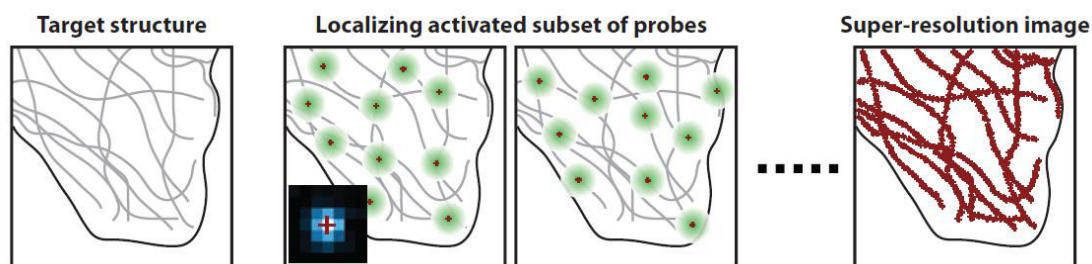


**Figure 2.3** The principle of STORM/PALM imaging.

A sparse set of fluorophores is activated at any given time and imaged without spatial overlap (large green circle). The position of each activated fluorophore is determined by Gaussian fitting to find the centroid of the spot (small red cross). After repeating the activation and imaging process for many times, the positions of a sufficient number of fluorophores are determined and a super-resolution image is then reconstructed. From [Huang et al. \[2009\]](#).

### *Sample labeling*

In my study, STORM and PALM were combined to study the distribution of F-actin filaments and dendra-SP respectively in the spine neck. Hippocampal neurons were infected with dendra-SP at DIV1, and were stained with A647-phalloidin to label F-actin.

### **The acquisition of fluorophore detection**

Dual-colour single-molecule imaging was carried out sequentially, as described previously [[Izeddin et al. 2011](#)] on an inverted Nikon Eclipse Ti microscope with a 100x oil-immersion objective (NA 1.49), an additional 1.5x lens, and an Andor iXon EMCCD camera (image pixel size, 107 nm). First, low-resolution conventional fluorescence images of the non-converted form of dendra-SP and of A647-phalloidin were taken with a mercury lamp and specific filters (dendra: ex 560/25, em 607/36; A647: ex 650/13, em 684/24; Semrock). Then, we reversibly switched A647 fluorophores between the dark and the fluorescent state in reducing buffer conditions (10% glucose in PBS containing with 50 mM  $\beta$ -mercaptoethylamine (cysteamine), 0.5 mg/ml glucose oxidase and 40  $\mu$ g/ml catalase from Sigma, and degassed with  $N_2$ ) [[Heilemann et al.](#)

2008] under continuous 532 nm and 633 nm laser illumination (em 684/24). Subsequently, dendra fluorophores were converted and imaged by PALM, using 405 nm and 561 nm lasers (em 607/36). Generally movies of 20000 frames were acquired at frame rates of 50 ms (A647) and 100 ms (Dendra). The z position was maintained during acquisition by a Nikon perfect focus system. Both laser intensities of the imaging lasers (633 nm and 561 nm) were set with the AOTF (acousto-optictunable filter) to 100% of 300 mW output power. To obtain a more or less constant number of fluorophore detections, the intensities of the activation lasers (532 nm and 405 nm) were increased continuously during the recordings.

### Localization and reconstruction of fluorophore detection

The localization and reconstruction of single fluorophore was done by fitting the point spread function of spatially separated fluorophores with a 2D Gaussian distribution [Izeddin et al. 2011], similar with QDs as shown the middle image in Fig. 2.1C.

### Drift correction

The image shift could result from the mechanical drift in the microscopy, such as thermal expansion or vibration of the sample stage. In this case, the relative position of fluorophores localized at different time points are not accurate. The following methods were used to correct the lateral and axial drift in the sample during acquisition in dual-color PALM/STORM imaging:

1) Stage and color shift correction (Fig. 2.4A): a) TetraSpeck beads (100 nm, T-7279, Invitrogen) were introduced into the sample. Since they can bind to the glass substrate and do not significantly bleach over the acquisition. The tracking of their trajectories over time can be used to correct the drift of sample [Rust et al. 2006; Betzig et al. 2006]. b) The drift also was corrected computationally using imaging correlation. The sample drift during time window may be determined by calculating the correlation function between the images generated from consecutive time slices. After the calculation of drift for all time slices, the drift is then subtracted from each localization to generate the drift-corrected image [Bates et al. 2013]. 2) Correction for multiple detections (Fig. 2.4B): when a fluorophore appears in more than one frames, all its consecutive detections have to be considered as coming from a single molecule. As all these detections happen within a circle that corresponds to the localization accuracy, I considered all the consecutive detections in within a circle of 30 nm (equal to localization accuracy) as one single molecule. The position of this molecule was the average position of all the mentioned detections.

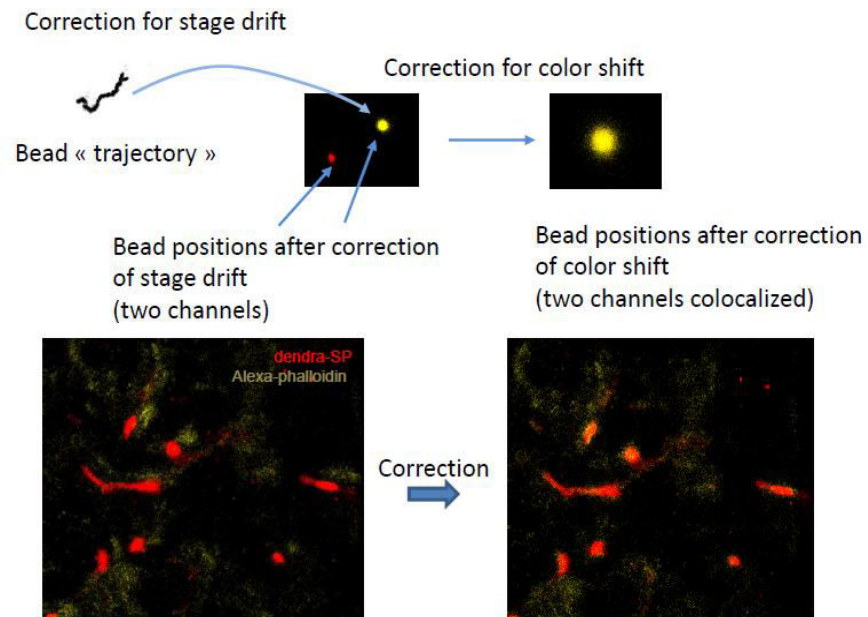
Applied both correction approaches, I was able to investigate the distribution and

colocalization of molecules with super-resolution using PALM and STORM.

**Measurement of the width of SP and F-actin domain in spine neck**

STORM and PALM images were rendered by superimposing the coordinates of single-molecule detections, which were represented by 2D Gaussian curves of unitary intensity and with a width representing the localization accuracy ( $\sigma = 10$  nm). The full width at half maximum (FWHM) of SP clusters and F-actin profiles across the spine neck in dual-colour rendered images was measured by Image J.

### A Drift correction 1: stage and color shifts



### B Drift correction 2: multiple detections

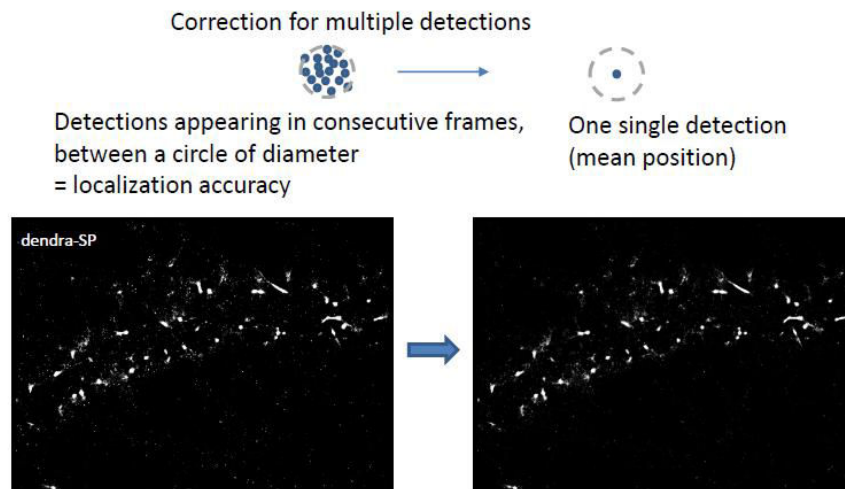


**Figure 2.4** The steps of drift correction in dual-color PALM/STORM imaging.

**A.** Stage and color shift correction through fluorescence beads and computing imaging correlation. **B.** Multiple detections correction. Detections are appearing in consecutive frames in a defined region could be considered as one single detection done by a home made program (Matlab).



## **III Results**



## 1 Spine neck as a diffusion barrier to confine molecules diffusion

A barrier along the neck decreasing the lateral diffusion of membrane molecules could have important consequences for the trapping of receptors at synapses. On one hand, retaining receptors in the area surrounding the synapse could increase their probability to be stabilized by binding to scaffold proteins in the postsynaptic density. On the other hand, the neck barrier could isolate the population of receptors in the spine head from that of the dendrite shaft. Thus, I have investigated two structural elements of spine neck, actin and synaptopodin (SP) that could create a diffusion barrier at spine necks, using single molecule tracking and super-resolution microscopy.

In order to analyze the mechanisms responsible for a reduction of lateral diffusion, I have analyzed the mobility of three membrane proteins with different topological properties (Fig. 1.1A): 1) GFP-GPI, a glycosylphosphatidylinositol (GPI)-anchored protein, embedded in the out leaflet of the plasma membrane; 2) TMD-pHluorin contains one transmembrane segment and a short intracellular sequence (36 amino acids); 3) pHluorin-mGluR5 encompasses an extracellular glutamate-binding domain followed by seven transmembrane segments and a large cytoplasmic tail of approximate 352 amino acid residues tagged with an extracellular pHluorin. The pHluorin (super-ecliptic pHluorin) tag, a pH sensitive GFP, is almost invisible at pH < 6.0 but the fluorescence intensity increases with pH up to a maximum of 8.5 [Ashby et al, 2004], allowing to record greater fluorescence of fluorophores attached to membrane proteins when exposed on the cell exterior (pH≈7.4) than inside acidic vesicles(pH≈5.6). Thus all three constructs contain a extracellular fluorophore tag to which quantum dots (QDs) were attached via specific antibodies, and their diffusion was compared in different of dendritic spines and dendrites / neurites. Dendritic spines are 3D structures with different diameters. To avoid errors coming from the projection of 3D into 2D, diffusion was calculated only with trajectories parallel to the cylinder axis (white lines in Fig. 1.1B), named as longitudinal component diffusion coefficient  $D_{1Dlong}$  [Renner et al. 2011]. For detailed information about the analysis of diffusion in tubular membranes, please see Methods section.

### 1.1 The dendrite diameter influences the diffusion of molecules

As predicted by Saffman and Delbrück [Saffman and Delbrück 1975] and demonstrated by the group of Patricia Bassereau [Domanov et al. 2011], the diffusion of membrane proteins in

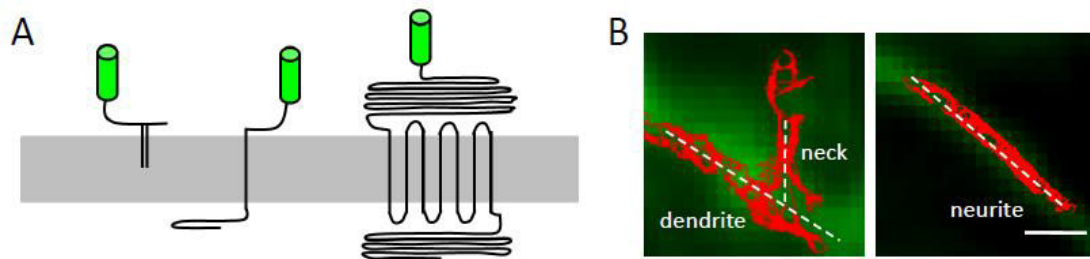


**Figure 1.1 Different constructs used for the diffusion study.**

**A.** Three different transmembrane or membrane-associated constructs were used to investigate diffusion barrier properties at spine neck: a GPI-anchored GFP (GFP-GPI), a TMD-pHluorin with a single transmembrane domain (TMD) and a short intracellular sequence, and pHluorin-mGluR5, containing seven TMDs and a cytoplasmic domain of 352 amino acid residues. All constructs have an extracellular fluorophore used for antibody coupling with quantum dots (QD). **B.** Regions of QDs trajectories analysis. White dot line: axis of cylindrical tubes; Green: pHluorin-mGluR5. Due to the curvature of membrane, only trajectories parallel to the axis of cylindrical tubes (spine necks, dendrites, neurites) were taken into account to calculate the diffusion of molecules. Scar bar: 1  $\mu\text{m}$  in B.

cylindrical membranes is dependent upon the cylinder radius. This effect was particularly strong in the case of very thin cylinders (radius < 50 nm) and it was observed in relatively thin neurites (radius < 200 nm, [Domanov et al. 2011]). Dendrites are relatively wide (radius of ~100-0.5  $\mu\text{m}$ ), thus I wondered if the effect of "size" of the membrane could be observed in this case. To this aim, I compared the mobility of the three membrane proteins (probes) mentioned above, with respect to the dendrite widths, in mature cultured hippocampal neurons (DIV 20-23). I have analyzed trajectories that happen only on dendritic shafts, without entering dendritic spines (Fig. 1.1B).

I observed a progressive decrease of the lateral mobility as the dendrites width was reduced (Fig. 1.2), with an important scattering of data, that can be attributed to inhomogeneities in dendritic membrane or variations from tubular shape. For example, compared to diffusion in wider dendrites ( $R \approx 1 \mu\text{m}$ ), the mobility of GFP-GPI decreased in thinner dendrites ( $R \approx 200 \text{ nm}$ ), with up to 4-fold overall slowing down (Fig. 1.2A). A similar trend was observed for the diffusion of the other proteins, even if the correlation curve between diffusion coefficient of TMD-pHluorin and pHluorin-mGluR5 and tube width were less obvious than that of GFP-GPI in mature dendrites than in immature neurites [Domanov et al. 2011]. This result could be attributed to the following factors: 1) the width of dendrites was larger than the of tubes studied by Domanov et al; 2) compared to the artificial tube, mature dendrites are complex containing for example cytoskeleton that may affect lateral diffusion.

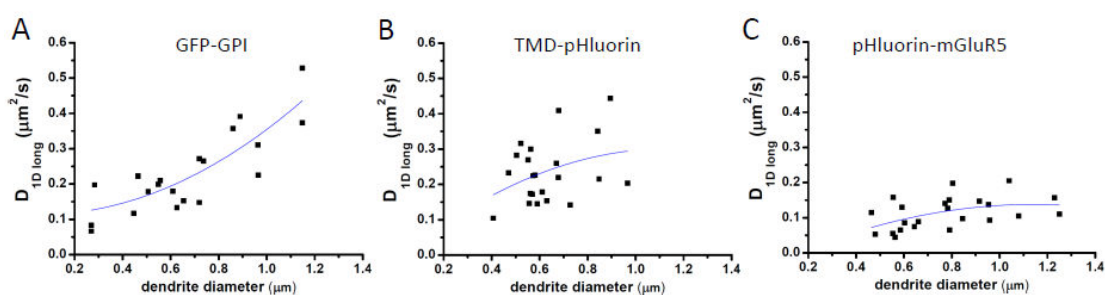


**Figure 1.2 Effect of the diameter of dendrite on membrane proteins diffusion.**

Diffusion mobility of GFP-GPI (A), TMD-pHluorin (B) and pHluorin-mGluR5 (C) in mature dendrites or neurites (DIV 20-23). All molecules showed a reduction trend in diffusion in dendrites with small radius. Each point represents a mean diffusion coefficient obtained from 4 to 36 individual trajectories.

## 1.2 The role of spine neck as a diffusion barrier

Since spine necks are thinner (~100-170nm, [Bethge et al. 2013]) than dendrites, lateral diffusion should be reduced in spine necks with respect to dendrites. However, as mentioned above, the presence of multiple factors in biological membranes that affect diffusion such as actin cytoskeleton [Kusumi et al. 2012] may overcome the effects of membrane size. Therefore I compared the lateral diffusion of the different probes in spine necks with respect to dendritic shafts. The topological differences between the probes lie in the number of transmembrane domain and the length of cytoplasmic tail. By comparing the diffusion coefficient of the probes in spine necks and dendrites, I investigated whether the spine neck geometry alone restricted the molecules' access to spines or whether other barriers existed.

I observed a general decrease in mobility in the spine neck compared to that of the dendrite for two molecules with transmembrane domains (TMD-pHluorin, pHluorin-mGluR5), but not GFP-GPI, (Fig. 1.3). GPI-anchored protein displayed a fast and highly variable mobility, and its diffusion coefficient is no significant different in spine neck ( $0.27 \pm 0.005 \mu\text{m}^2/\text{s}$ ) and in dendrite ( $0.25 \pm 0.006 \mu\text{m}^2/\text{s}$ ) ( $p=0.095$ , Kolmogorov-Smirnov test,  $n_{\text{neck}} = 981$ ,  $n_{\text{dendrite}} = 1504$  trajectories). TMD-pHluorin diffusion exhibited slower mobility in both spine necks ( $0.21 \pm 0.01 \mu\text{m}^2/\text{s}$ ) and in dendrites ( $0.25 \pm 0.005 \mu\text{m}^2/\text{s}$ ) ( $p < 0.001$ , KS test,  $n_{\text{neck}} = 183$ ,  $n_{\text{dendrite}} = 970$  trajectories). The pHluorin-mGluR5 construct, which was much slower than that of the other two constructs. Also, the speed of diffusion in dendrites ( $0.13 \pm 0.003 \mu\text{m}^2/\text{s}$ ) diffused also was greater in dendrites than in spine necks ( $0.09 \pm 0.004 \mu\text{m}^2/\text{s}$ ) ( $p < 0.001$ , KS test,  $n_{\text{neck}} = 317$ ,  $n_{\text{dendrite}} = 1295$  trajectories).

These results suggest that the difference in diameter between spine necks and dendrites is not sufficient to explain the slow down of certain molecules in spine necks. Diffusion may be reduced by other means, for example, by the presence of barriers provided by actin cytoskeleton.

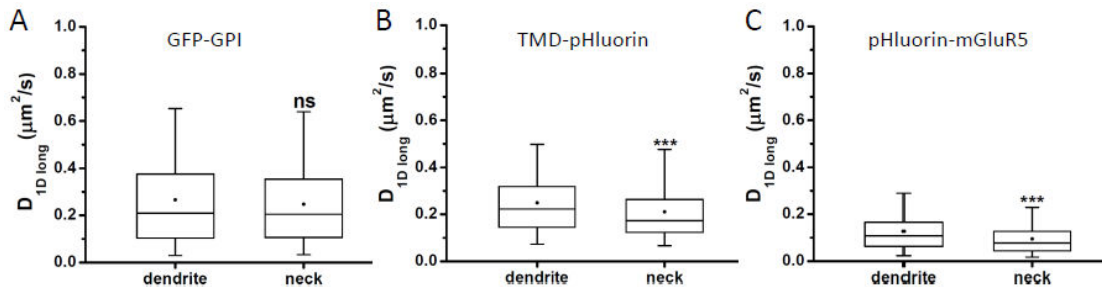


**Figure 1.3 Effects of spine neck and dendritic shaft on membrane proteins diffusion.**

The diffusion of GFP-GPI (A), TMD-pHluorin (B) and pHluorin-mGluR5 (C) in spine necks and dendrites were compared. Only diffusion coefficients of TMD-pHluorin and pHluorin-mGluR5 were significantly slower in spines necks than in dendritic shafts. The diffusion coefficient was calculated on the longitudinal component of displacements along axis of cylindrical tubes ( $D_{1D \text{ long}}$ ; boxes indicate 5, 25, 50, 75 and 95% of all trajectories; dots: mean value; \*\*\*  $p < 0.001$ , KS test;  $n \geq 183$  trajectories, 3-5 cultures).

## 2 The role of synaptopodin in molecule diffusion

### 2.1 The distribution of synaptopodin in dendritic spines

#### 2.1.1 Synaptopodin is present in a majority of spine necks

Synaptopodin (SP) is one of the few known proteins to be located in the spine neck. I hypothesized that the presence of SP may exert an influence on the diffusion of membrane proteins across the spine neck via actin cytoskeleton. Therefore, I first characterized the sub-cellular localization of SP using conventional fluorescence microscopy and super resolution microscopy imaging.

Endogenous SP was labeled with a specific antibody against the murine protein. For visualization of the cell morphology, I made use of another membrane probe, a chimera containing a single transmembrane domain (TMD) fused at its C-terminus with an extracellular pHluorin tag. Quantification of the endogenous SP distribution (Fig. 2.1A) revealed that  $86.9 \pm 1.0\%$  of spines contain SP. Native SP is mainly clustered in the neck of  $68.9 \pm 1.5\%$  of the identified spines, and less frequently in the spine head ( $14.8 \pm 1.1\%$ ) or in the dendrite at the spine base ( $3.2 \pm 0.6\%$ ) ( $n=3$  cultures, 35 cells, 56 segments, 998 spines) (Fig. 2.1B). The quantification was done in two dimensional (2D) images that are the projection of the three dimensional (3D) structure of dendritic spines. Spines that are vertical to the focal plane were quantified, leading to an certain underestimation of the total number of spines. This bias could also produce a little deviation in the localization of SP and of the percentage of spines containing SP.

An mRFP-tagged version of SP protein was designed and co-transfected with TMD-pHluorin into neurons, the latter construct used for displaying neuronal morphology. The distribution of the recombinant SP protein in spines was essentially the same as the endogenous one, with  $67 \pm 1.5\%$  of spine necks,  $16.2 \pm 1.2\%$  of spine heads and  $3.4 \pm 0.6\%$  of spine bases containing SP ( $n=4$  cultures, 38 cells, 68 regions, 965 spines) (Fig. 2.1C,D). To examine whether the mRFP-SP goes the same position as endogenous SP in spines, neurons were co-transfected with TMD-pHluorin and an mRFP-tagged SP, and stained with anti-SP antibody. Results demonstrated that most of mRFP-SP clusters (red) completely overlap with total SP (green) (Fig. 2.2).

All data considered, we conclude that SP is present in a majority (about 87%) of mature spines in cultured hippocampal neurons with a preferential location in the neck of the spine. Thus recombinant mRFP-SP does reflect precisely the distribution of endogenous SP and can be used to investigate the relevant function of SP.

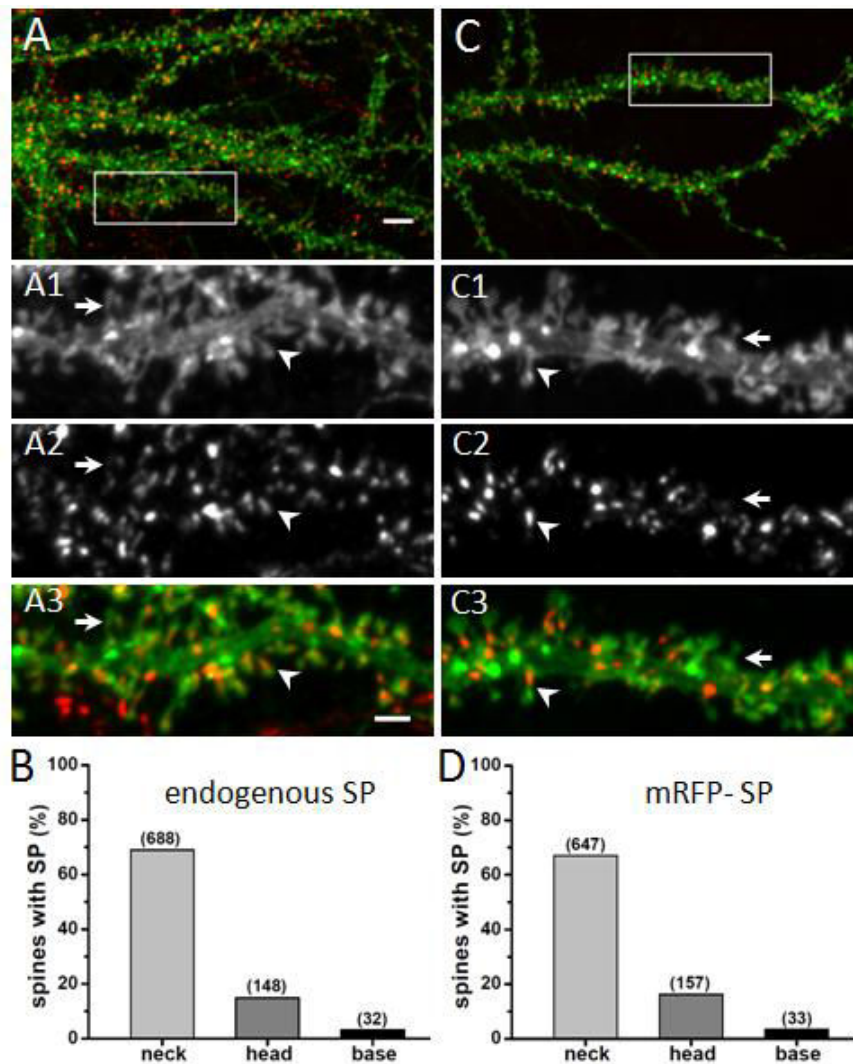


**Figure 2.1 Distribution of SP in dendritic spines of hippocampal cultured neurons.**

**A.** Localization of endogenous SP in dissociated cultured hippocampal neurons transfected with TMD-pHluorin (green) for the visualization of neuron morphology and immunolabelled for SP (red). Higher magnifications of the selected area (white box) are shown in A<sub>1</sub> (TMD-pHluorin), A<sub>2</sub> (SP) and A<sub>3</sub> (merged image). The arrowhead indicates a SP cluster located in a spine neck, while the arrow points to a spine devoid of SP. Scale bars: 5  $\mu$ m in A, 2  $\mu$ m in A1-3. **B.** Data quantification shows that  $87.0 \pm 1.1\%$  (mean  $\pm$  SD) of spines overall are positive for SP. A more refined analysis indicates a preferential distribution in the spine neck compared to head or spine base compartments (neck,  $68.9 \pm 1.5\%$ ; head,  $14.8 \pm 1.1\%$ ; base,  $3.2 \pm 0.6\%$ ;  $n = 998$  spines from 3 independent experiments). **C.** Recombinant mRFP-SP distribution in hippocampal neurons. Neurons were co-transfected with TMD-pHluorin (green) and mRFP-SP (red). Zoomed images of the selected area (white box) are shown in C<sub>1</sub> (TMD-pHluorin), C<sub>2</sub> (SP) and C<sub>3</sub> (merged image). **D.** Quantitative analysis indicates that  $86.7\% \pm 1.1\%$  (mean  $\pm$  SD) of all spines contain mRFP-SP clusters. The distribution within the neck, head and base of the spine is similar to that observed for endogenous SP (neck,  $67.0 \pm 1.5\%$ ; head,  $16.2 \pm 1.2\%$ ; base,  $3.4 \pm 0.6\%$ ;  $n = 965$  spines from 4 experiments).

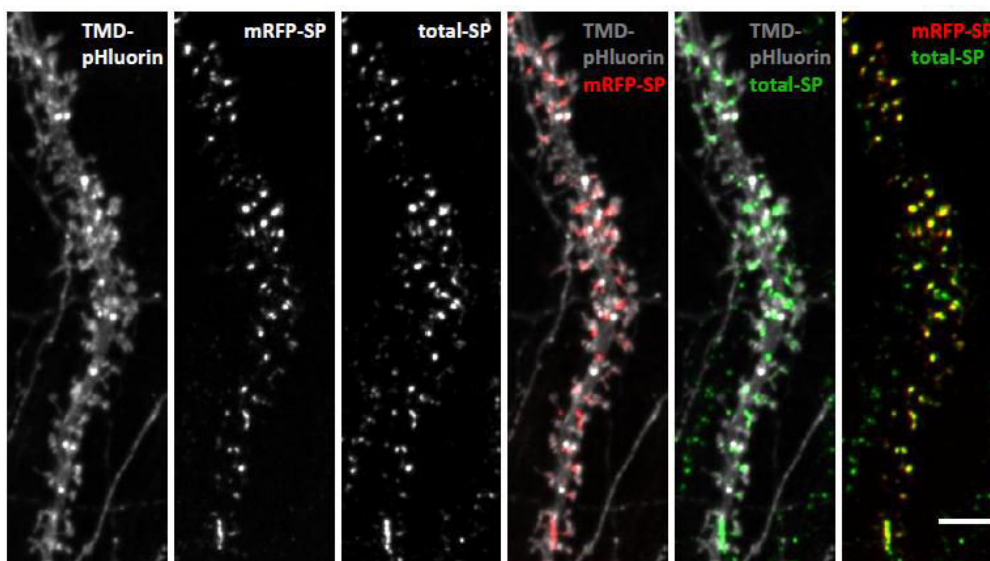


**Figure 2.2 Respective distribution of mRFP-SP and endogenous SP.**

Neurons were co-transfected TMD-pHluorin and mRFP-SP at DIV 9, and stained with anti-SP antibody at DIV 21. SP antibody detected both of mRFP-SP and endogenous-SP, named total-SP. From left to right panel: individual TMD-pHluorin, mRFP-SP, total-SP and then merged images of TMD-pHluorin (grey) and mRFP-SP (red), TMD-pHluorin (grey) and total-SP (green), mRFP-SP (red) and total-SP (green). The last image showed that the colocalization of mRFP-SP clusters and total SP, and revealed that only few clusters of endogenous SP (green) do not contain mRFP-SP. Scar bar: 5  $\mu$ m

### 2.1.2 Synaptopodin occupies part of the inner volume of the spine neck

To further characterize the sub-cellular distribution of SP, I performed super-resolution imaging of SP in dendritic spines. Though multi-colour STORM has been developed to investigate the relative organizations between different molecules, multi-colour STORM imaging requires photo-switchable probes (dyes) with distinct emission wavelengths, which make the photo-activation of fluorophores more complicated. In this case, to gain two colour images with high resolution efficiently, complementary tools STORM (using dyes) and PALM (using fluorescent proteins) were chosen to study the nano-localization of SP in spine neck.

Hippocampal neurons were infected at DIV 1 with a lentivirus driving the expression of SP tagged with the photo-convertible fluorophore Dendra2. The fluorophore Dendra2 is photoconvertible irreversibly at low UV laser intensity and is therefore well suited for PALM imaging. Also, it displays less blinking than the Eos fluorophore, which enables high sampling of the structure of interest [Durisic et al. 2014; Lee et al. 2012]. Neurons were fixed at three weeks in culture and labelled with Alexa647-phalloidin. Phalloidin, a toxin found in death cap

mushroom, can stabilize F-actin and prevent the depolymerization of actin fibers [Cooper 1973]. Because of its selective binding to the polymerized F-actin, pHluorin with fluorescent tags are used to visualize F-actin. Images in conventional optical microscopy displayed the colocalization of SP and F-actin (Fig. 2.3A, Fig. 4.1A). Intensity of F-actin in spines was measured with a binary mask of SP clusters. This showed that SP immunoreactivity positively correlated with that of F-actin in spines under basal condition (Fig. 4.1B;  $R^2=0.687$ ;  $n=500$  SP clusters from 2 neurons).

The photoactivation of dyes in STORM specific works in the blinking-inducing buffer which requires oxygen removal [Dempsey et al. 2011]. Thus, STORM was performed prior to PALM in different channels, as described in the methods section. The pointing accuracy, estimated as the standard deviation of single fluorophore detections in sparsely labelled areas, was  $\sigma_x=12.2 \pm 2.2$  nm and  $\sigma_y=12.9 \pm 2.2$  nm (for Dendra2, mean  $\pm$  SD,  $n = 27$ ). Dual-colour super-resolution images were then generated by rendering the Alexa647 and Dendra2 detections resulting in images of SP and F-actin in dendrites with a spatial resolution of approximately 30 nm ( $=2.35 \times$  standard deviation for a Gaussian distribution with  $\sigma$ ) [Huang et al. 2010]. The resulting images showed the precise distribution of SP in the spine neck, where it co-localized with F-actin (Fig. 2.3B).

Intensity profiles across the spine neck in rendered images revealed that the width of the SP domain was noticeably smaller than the region occupied by F-actin (Fig. 2.3C). This suggests that the distribution of SP is limited to the inner part of the neck, whereas F-actin is present throughout the entire volume of the neck. Quantification of the full width at half maximum (FWHM) showed that the mean width of the F-actin domain was  $105 \pm 4$  nm (Fig. 2.3D), in line with previous measurements of the inner spine neck diameter [Izeddin et al. 2011]. SP occupied a significantly smaller region of the neck with a width of  $66 \pm 3$  nm ( $p < 0.001$ , MW test,  $n_{1,2} = 34$  spines). The difference of  $40 \pm 4$  nm in the width of the two domains means that there is a gap of approximately 20 nm between the SP domain and the inner layer of the plasma membrane (indicated by the F-actin domain). As regards the length of SP clusters, some SP regions covered the whole length of the spine neck and even sometimes entered into spine heads, while some SP only occupied half or less of the length of the spine neck.

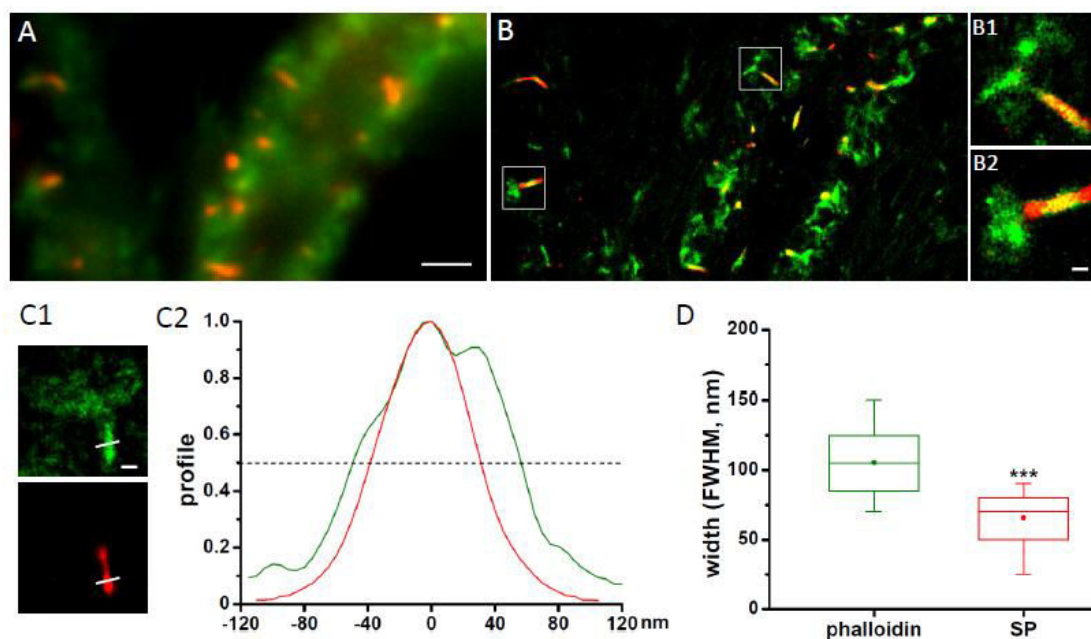


**Figure 2.3 SP distribution within the spine neck.**

**A.** Conventional fluorescence microscopy of hippocampal neurons expressing dendra-SP (red). F-actin filaments were labelled with A647-phalloidin (green). **B.** Super-resolution STORM/PALM imaging of the same dendritic segment. Single dendra and A647 fluorophore detections were rendered with a 2D Gaussian distribution with  $\sigma = 10$  nm and represented in false colors (red and green, respectively). B<sub>1</sub> and B<sub>2</sub> are high magnifications of individual spines (white boxes in B), where SP is clearly visible along the spine neck, while phalloidin stains both neck and spine head. **C.** Analysis of the width of the SP and phalloidin domains in the spine neck. The full width at half maximum (FWHM) was used as a measure of the width of phalloidin (green) and SP (red) detections in rendered STORM/PALM images. Measurements from an individual spine are shown in C1 and C2. **D.** Quantification of the FWHM of phalloidin and SP domains in spine necks. The box indicates the median, 5, 25, 75 and 95% of the spine population, the mean width is shown as a dot (n = 33 spines, 5 cultures). Scale bars: 2  $\mu$ m in A, 200 nm in B2 and C1.

To try to measure the distance between SP domain and the plasma membrane in spine neck, I made use of TMD-pHluorin construct and Dendra-SP co-expressed in hippocampal neurons. STORM imaging of TMD-pHluorin, using Alexa 647-coupled antibodies, allowed me to distinguish clearly the edges of plasma membranes and therefore the morphology of dendritic spines (Fig. 2.4A). Quantification of the FWHM showed that the mean width of the spine neck was  $194.5 \pm 8.5$  nm (mean  $\pm$  SEM, n=18 spines) (Fig. 2.4B,C). An detection of Dendra-SP by PALM is depicted in Fig. 2.4D, which demonstrated a clear gap about 60 nm between the SP domain and the plasma membrane (indicated by staining of Alexa 647-coupled GFP antibodies). The neck width measured with this technique is bigger than that measured in slices by

two-photon excitation STED microscopy (100-170 nm) [Bethge et al. 2013]. In addition to the huge variability of spine morphology, the difference includes the width of plasma membrane (5-10 nm) and the size of the A647-tagged primary GFP antibodies used for labeling membrane (~5 nm) in each sides.

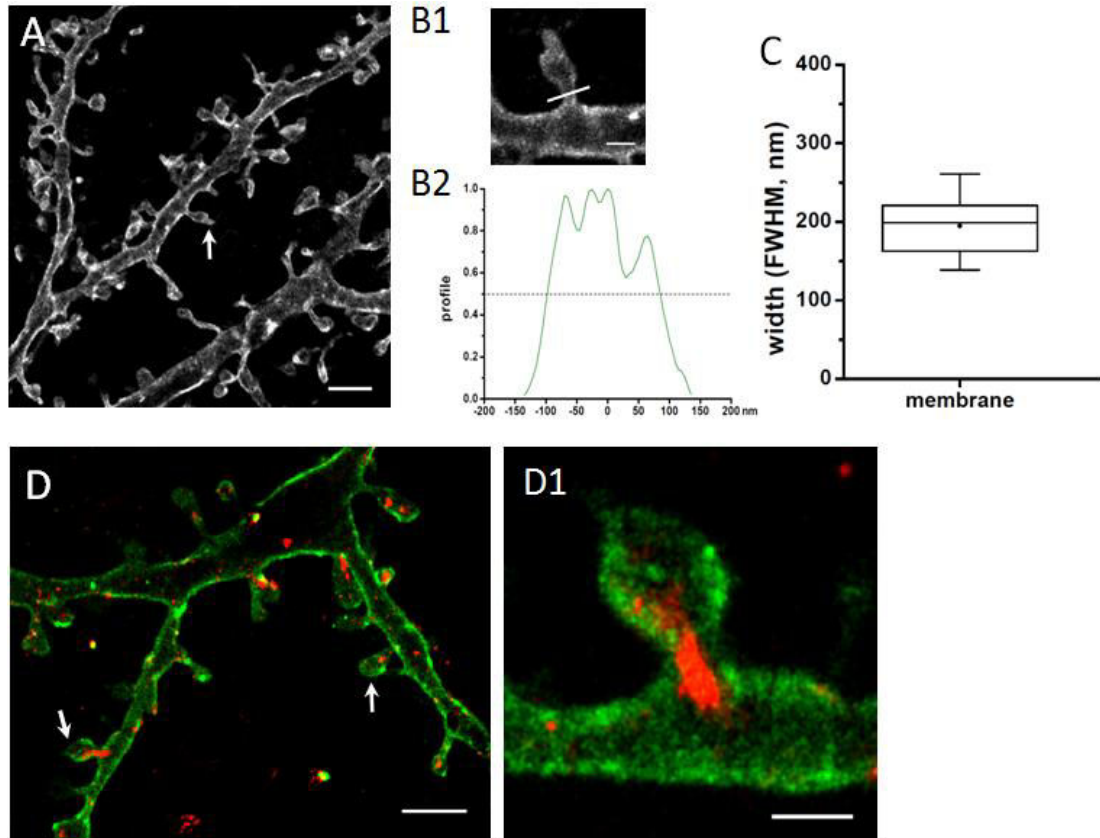


**Figure 2.4 The plasma membrane at spine neck revealed by super resolution imaging.**

Neurons were co-transfected with dendra-SP and TMD-pHluorin constructs at DIV 9, then stained by anti-GFP antibody coupling. **A.** STORM imaging of TMD-pHluorin displayed detailed information about the morphology of dendritic spines. **B.** High magnification image of an individual spine (arrow in A), where the edge of the plasma membrane of the spine neck is clearly defined. White line across the spine neck is used to measure the FWHM profile. **C.** Quantification of the FWHM of plasma membrane at spine necks (n=18 spines, 2 neurons). **D.** Dual-color STORM/PALM imaging exhibited the localization of SP in dendritic spines. Arrows indicate spines profiles with SP clusters in the neck region. D1 is the high magnification of an individual spine (in D). Scar bar: 2  $\mu\text{m}$  in A and D; 500 nm in B1 and D1.

## 2.2 Synaptopodin affects the diffusion of membrane proteins in the spine neck

Next, I compared the diffusion of three probes in spines containing SP (SP+) or not (SP-), as judged by the presence or absence of mRFP-SP clusters that was co-expressed together with the membrane constructs (Fig. 2.5A). I also distinguished sub-regions of the neck where SP was present or not (*SP area* versus *no SP area* in SP+ spines).

First, I observed that a GPI-anchored GFP protein displayed a fast and highly variable diffusion in the neck of spines, independent of the presence of SP. There was no obvious difference in  $D_{1Dlong}$  of GFP-GPI in SP+ spines and in SP-spines ( $0.256 \pm 0.009 \mu\text{m}^2/\text{s}$ ), nor in the SP area ( $0.247 \pm 0.013 \mu\text{m}^2/\text{s}$ ) and no SP area ( $0.232 \pm 0.011 \mu\text{m}^2/\text{s}$ ) of the SP+ spine necks ( $p=0.063$ , KS test,  $n_{in\ SP}=258$ ,  $n_{no\ SP}=260$ ,  $n_{SP-}=463$  trajectories) (Fig. 2.5B).

The diffusion of TMD-pHluorin was neither significantly different between the SP areas ( $0.168 \pm 0.012 \mu\text{m}^2/\text{s}$ ) and no SP area ( $0.203 \pm 0.018 \mu\text{m}^2/\text{s}$ ) in SP+ spines ( $p=0.551$ , KS test,  $n_{in\ SP}=58$ ,  $n_{no\ SP}=57$  trajectories) (Fig. 2.5C), meaning that the presence of SP is not correlated with a reduction of mobility of these membrane proteins. However, the speed of diffusion in SP-spines ( $0.270 \pm 0.021 \mu\text{m}^2/\text{s}$ ,  $n_{SP-}=68$  trajectories) was significantly faster than that in SP+ spines ( $p < 0.01$ , KS test). This difference may be attributed to a role of SP on the internal organization or maturation of the spine, that would have an indirect effect on diffusion mobility of membrane proteins. It has been shown that SP clusters are prone to localize in mushroom spines with big heads [Vlachos et al. 2009], which are functionally strong in response to neuronal activation and have a higher density of receptors [Bourne and Harris 2008]. My results suggest that the presence of SP makes a barrier to restrict the diffusion of receptors and thus promotes the trapping of receptors at synapse.

In the case of pHluorin-tagged mGluR5, I observed a significant reduction of mobility in sub-regions of spine necks where SP was present ( $0.070 \pm 0.005 \mu\text{m}^2/\text{s}$ ) in comparison to where it was absent ( $0.096 \pm 0.005 \mu\text{m}^2/\text{s}$ ) ( $p < 0.001$ ,  $n_{in\ SP}=123$ ,  $n_{no\ SP}=105$  trajectories) (Fig. 2.5D). There were also significant differences between the in SP- spines ( $0.122 \pm 0.008 \mu\text{m}^2/\text{s}$ ,  $n_{SP-}=89$  trajectories) and no SP area in SP+ spines ( $p < 0.05$ , KS test). As pHluorin-mGluR5 (but not the other probes) contains a large intracellular domain, these data confirm the hypothesis of enhanced intracellular barriers to diffusion in SP(+) spine necks.

The presence of synaptopodin in spine necks further hinders the diffusion of membrane proteins with transmembrane domains, particularly for proteins such as mGluR5 with long cytoplasmic tail. Thus I hypothesized that actin filaments could mediate the limitation of

synaptopodin on mGluR5 diffusion, since actin has been shown to modulate the diffusion of receptors in and out of synapse by interacting with receptors or their scaffolds.

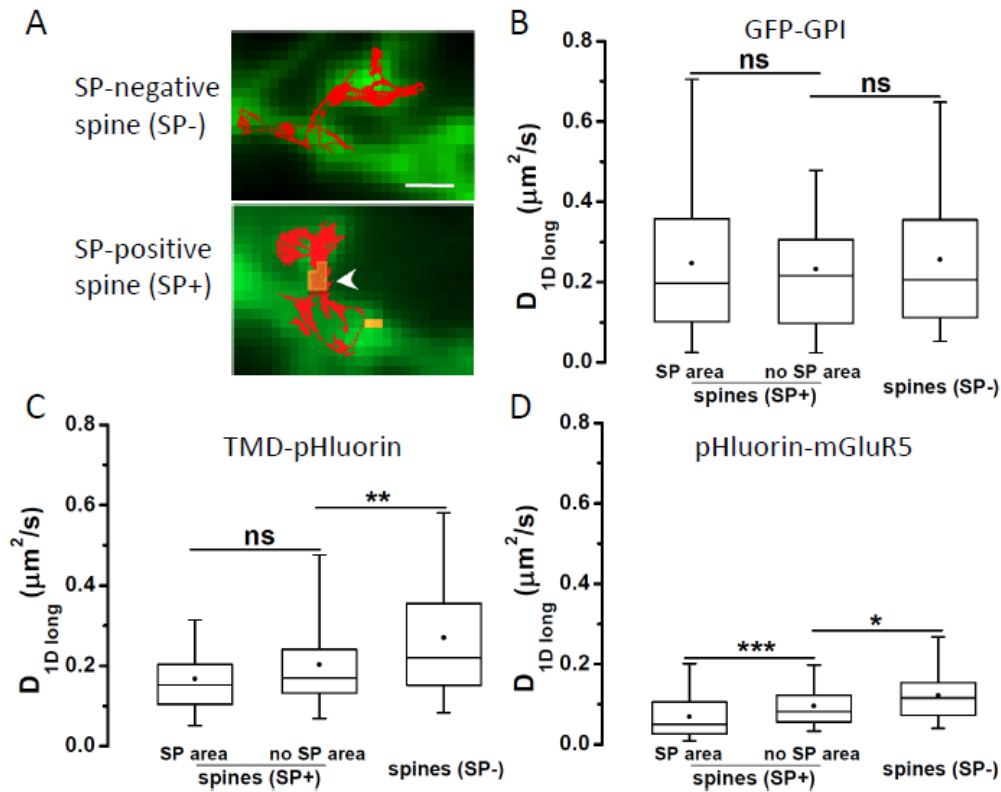


**Figure 2.5 Role of SP on membrane protein diffusion in the spine neck.**

**A.** QD trajectories (red) were recorded in SP-negative (top panel) and SP-positive spines (bottom panel). pHluorin-mGluR5 in green; SP cluster in yellow (white arrowhead). **B-D.** Quantification of QD diffusion in spines necks for GFP-GPI (B), TMD-pHluorin (C) and pHluorin-mGluR5 (D). Trajectories were analyzed either in spines negative for SP (SP-) or positive for SP (SP+). For the latter, traces on top of SP clusters (SP area) or in areas devoid of SP (no SP area) were considered separately. The diffusion coefficient was calculated on the longitudinal component of displacements along the spine neck axis ( $D_{1Dlong}$ ; boxes indicate 5, 25, 50, 75 and 95% of all trajectories; dots: mean value; ns: not significantly different, \*  $p < 0.05$ , \*\*  $p < 0.01$ , \*\*\*  $p < 0.001$ , KS test;  $n \geq 54$  trajectories, 3-5 cultures). Scale bar: 1  $\mu\text{m}$  in A.

### 3 Actin filaments are involved in the effect of SP presence on diffusion

#### 3.1 Actin depolymerization abolishes the slowing down of mGluR5 diffusion in SP-positive spines

In order to assess the importance of actin cytoskeleton on the slow down mGluR5 diffusion observed in SP presence, I challenged neurons with latrunculin A (latA, 5  $\mu$ M) that causes the rapid depolymerization of F-actin. LatA sequesters G-actin and thus causes the disruption of actin filaments [Bae et al. 2012].

As expected, the changes in F-actin polymerization in response to latrunculinA treatment were paralleled by an enhanced diffusion of mGluR5 in the spine neck. Within 5-10 minutes of latA application (Fig. 3.1B), to an extent that  $D_{1Dlong}$  values became indistinguishable between those in SP regions ( $0.115 \pm 0.005 \mu\text{m}^2/\text{s}$ ) and SP-free regions ( $0.110 \pm 0.004 \mu\text{m}^2/\text{s}$ ) in the SP+ spines ( $p=0.094$ , KS test,  $n_{in\ SP}=211$ ,  $n_{no\ SP}=396$  trajectories); The diffusion of mGluR5 was still significantly constricted in SP+ spines, compared to in SP- spines ( $0.140 \pm 0.005 \mu\text{m}^2/\text{s}$ ) ( $p<0.001$ , KS test,  $n_{SP-}=439$  trajectories). After longer latA treatment (15-20 min), a further increase in mGluR5 mobility was recorded in SP+ spines (SP area:  $0.129 \pm 0.008 \mu\text{m}^2/\text{s}$ ; no SP area:  $0.133 \pm 0.007 \mu\text{m}^2/\text{s}$ ;  $p=0.309$ ; KS test,  $n_{in\ SP}=92$ ,  $n_{no\ SP}=262$  trajectories), to an extent that after 15-20 minutes the speed of diffusion was as fast as in SP- spines ( $0.137 \pm 0.005 \mu\text{m}^2/\text{s}$ ) ( $p=0.375$ ; KS test,  $n_{SP-}=359$  trajectories) (Fig. 3.1C).

Compared to control condition, this increase of diffusion was most pronounced in SP region of SP+ spines (latA 5-10 min/15-20 min exposure versus control:  $p<0.001$ , KS test; Fig. 3.1D). Therefore, the presence of SP restricting the diffusion of mGluR5 is mediated by actin filaments. The diffusion of mGluR5 in SP- spines was not significantly altered by latA treatment (latA 5-10 min exposure versus control:  $p=0.07$ , KS test; Fig. 3.1F). This suggest that in SP-spines there is no enough F-actin to make the difference between latA-treated and untreated neurons. Therefore, the presence of SP restricts the diffusion of mGluR5 is mediated by actin filaments.

#### 3.2 Modulation of synaptopodin by actin depolymerization

Another important point is to know if actin filaments are needed for the stabilization of synaptopodin. Hippocampal neurons were treated with 5  $\mu$ M latrunculin for 5 minutes and were stained endogenous-SP and F-actin (Fig. 3.3A,B). Results showed that the intensity of phalloidin labelling in regions of endogenous SP was reduced to approximately 35% of the

initial value (Fig. 3.3C). The drastic disruption of the F-actin cytoskeleton had clear consequences for the distribution of SP. To our surprise, two different effects were observed in the SP clusters after disruption of F-actin, one on the SP cluster intensity and one on SP cluster number. The first effect occurred in the first 5 min of latA incubation and increased with longer treatment. After one hour, the total SP fluorescence increased gradually by 70% (Fig. 3.3C); meanwhile, the number of SP cluster decreased from  $3.64 \pm 0.68$  to  $2.68 \pm 0.66$  (mean  $\pm$  SD) per  $\mu\text{m}$  in dendrite ( $p < 0.001$ , MW test, 3 cultures,  $n \geq 100$  cells) (Fig. 3.3D), suggesting that the stabilization of SP in spine neck requires actin filaments. It is known that F-actin can recover after latA washout. Consistent with F-actin, SP clustering was also reversible, as shown in immunostaining (Fig. 3.2).

To investigate this phenomenon in detail, neurons were co-transfected with TMD-pHluorin and mRFP-SP. Living images were taken to record the modification of SP clusters under latA incubation with time (Fig. 3.3E). Up to 30 min of latA incubation, the density of dendritic spines was not altered by disruption of F-actin; however, the morphology of spines was modified. As expected [Honkura et al. 2008], the bulbous head of some spines were replaced with irregular ones. Remarkably, latA not only caused the disappearance of some small SP clusters already after 5 min treatment, but also increased the size and the total fluorescence intensity of some stable SP clusters. These effects were aggravated by longer latA treatment.

The extent of the changes of the spine cytoskeleton become apparent in dual-colour STORM/PALM images that show near complete loss of microfilaments in the spine head and dendrites (Fig. 3.4A, compare Fig. 2.3B). However, part of phalloidin labelling was retained in the spine neck, as judged by the co-localization with SP, and the inner diameter of the spine neck is not changed, measuring  $100 \pm 4$  nm (FWHM;  $p = 0.37$ , MW test,  $n_{\text{ctr}} = 34$ ,  $n_{\text{lat}} = 33$ ). The width of the SP domain however increased significantly ( $p < 0.001$ ) from  $66 \pm 3$  nm to  $84 \pm 3$  nm within 5 minutes of latA treatment (Fig. 3.4B). This is consistent with the observation of the increased size of SP cluster in live imaging. This means that the distance between SP and the inner edge of the plasma membrane is reduced to about 8 nm, instead of 20 nm in the control situation.

Taken together, these data suggest that small (and unstable) SP clusters are stabilized by actin filaments. LatA treatment frees SP molecules from these clusters, molecules that are recruited to large (and stable) SP clusters. Usually, mushroom spines are prone to contain big and stable SP clusters that can resist longer time in response to latA treatment, while relatively thin spines comprise smaller SP clusters that are prone to collapse.

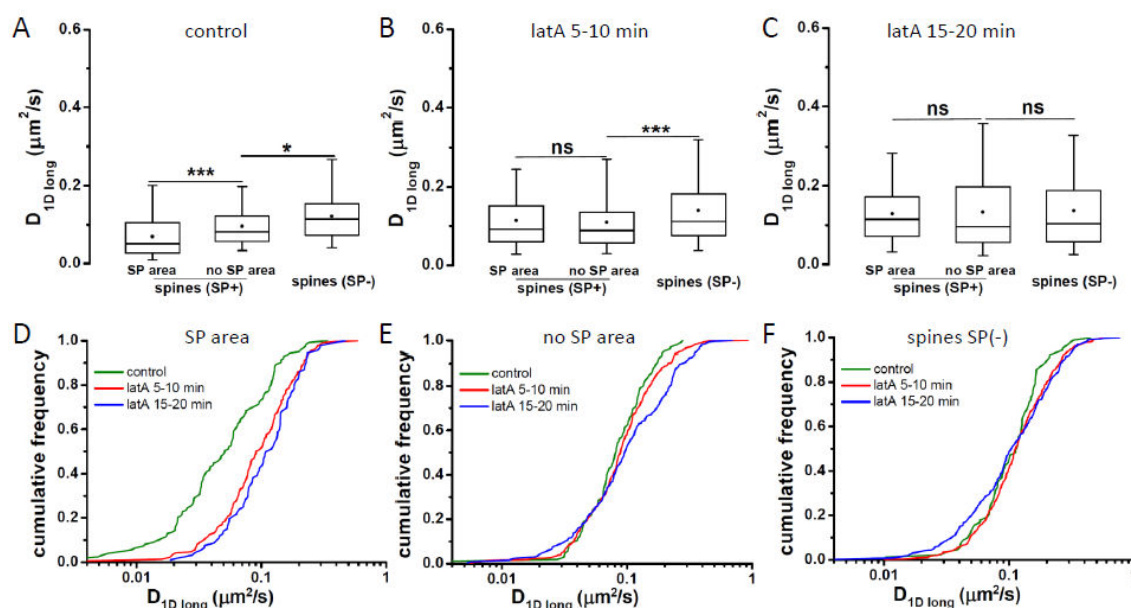


**Figure 3.1 Effect of actin depolymerization on mGluR5 diffusion**

**A.** Same control as in Fig. 2.5D. **B,C.** Diffusion coefficients  $D_{1Dlong}$  of pHluorin-mGluR5 in the necks of SP+ spines and SP- spines during latA exposure for 5-10 min (B) and 15-20 min (C).  $D_{1Dlong}$ ; boxes indicate 5, 25, 50, 75 and 95% of all trajectories; dots: mean value; ns: not significantly different, \*\*\*  $p < 0.001$ .  $n \geq 92$  trajectories from 3-5 cultures. **D-F.** Cumulative distribution of pHluorin-mGluR5 diffusion coefficients tracked in SP area (D), outside of SP clusters (E) in SP+ spines, and in SP-spines (F) in control (green lines) and latA treatment 5-10 min (red lines) and 15-20 min (blue lines). **D.** Diffusion coefficients within SP domains of the spine neck increased during 5  $\mu\text{M}$  latrunculin A application. **E.** The mobility of mGluR5 increased in the region of no SP cluster after longer latA incubation (15-20min,  $p < 0.01$ ). **F.** No significant changes of diffusion occur during latA treatment (5-10min) in SP-negative spines ( $p = 0.07$  at 5-10 min). KS test.

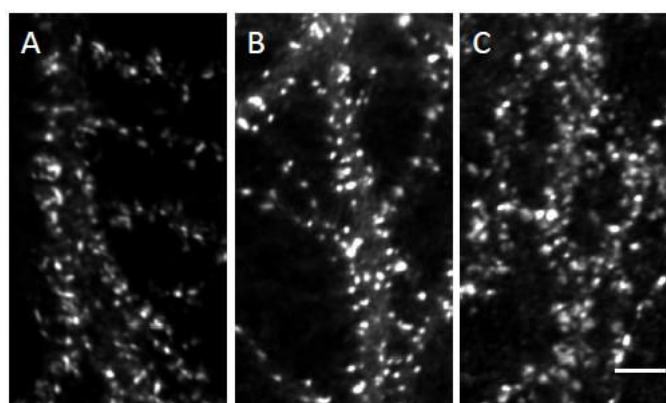


**Figure 3.2 Synaptopodin recovered after latA washout.**

Immunoreactivity of endogenous SP in control (A), lat A treatment (B, 5  $\mu\text{M}$ , 30 min) and lat A washout neurons (C, 5  $\mu\text{M}$ , 30 min, then washout, wait 2 hours). Scale bar: 5  $\mu\text{m}$ .

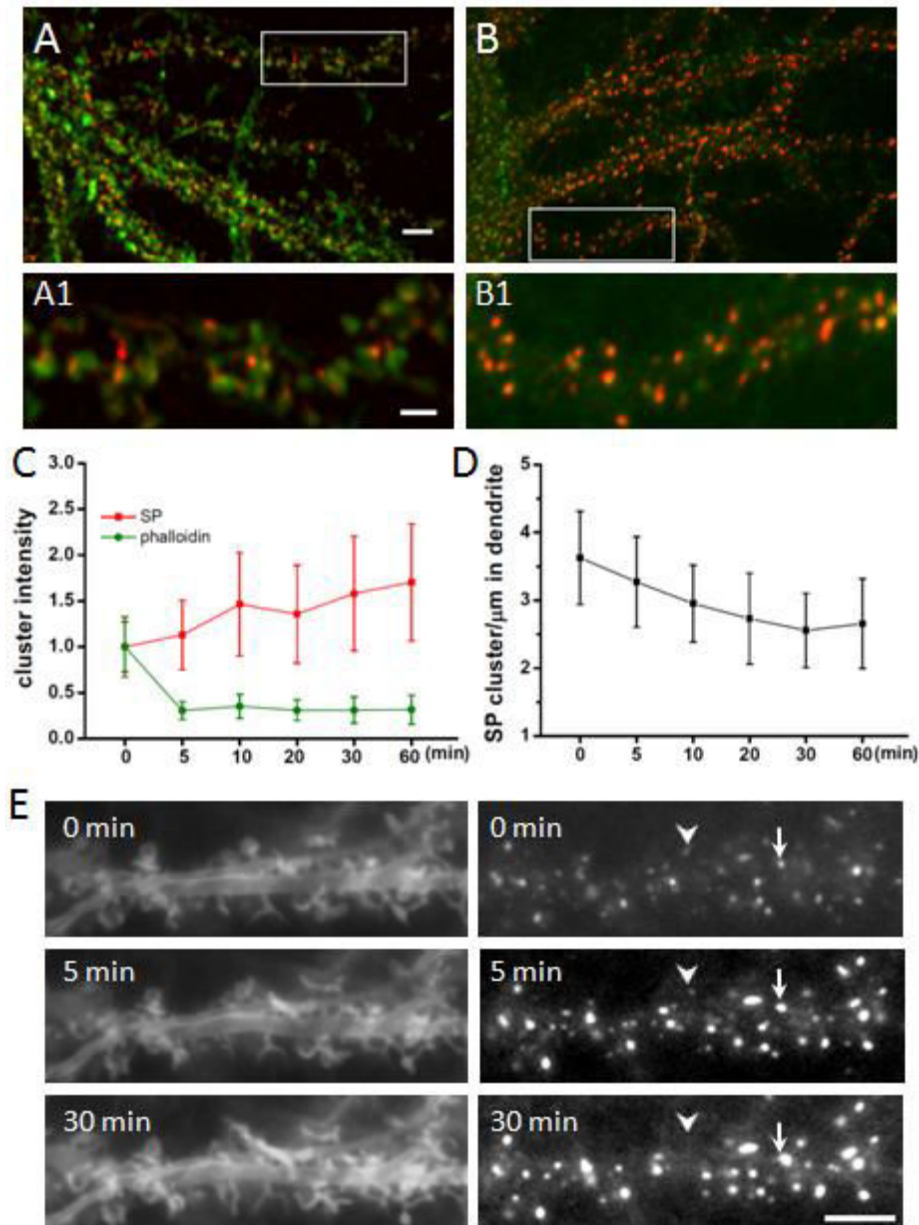


**Figure 3.3 Effects of actin depolymerization on SP distribution**

**A,B.** Immunoreactivity of endogenous SP (red) and A647-phalloidin (green) in control neurons (A) and after latrunculin A treatment (5  $\mu$ M, 5 min) (B). Boxes in (A,B) indicate regions of higher magnification shown in the bottom panels. **C.** Quantification of the total fluorescence intensity of SP clusters and phalloidin label in SP clusters during latA incubation at different time points ( $n \geq 100$  cells, 3 cultures, normalized mean fluorescence  $\pm$  SD,  $p \leq 0.001$  from 5-60 min, MW test). **D.** The effect of latA incubation on the density of SP clusters. ( $n \geq 100$  cells, 3 cultures, mean  $\pm$  SD,  $p < 0.001$  from 5-60 min, MW test). **E.** Live images after latA treatment showed the progressive loss of some faint clusters (arrowhead) and the concomitant increase in size and intensity of other clusters (arrow). Neurons were co-transfected with TMD-pHluorin (left panel) and mRFP-SP (right panel). Images from top to bottom: 0 min, 5 min and 30 min latA incubation. Scale bars: 5  $\mu$ m in A,E; 2  $\mu$ m in A1.

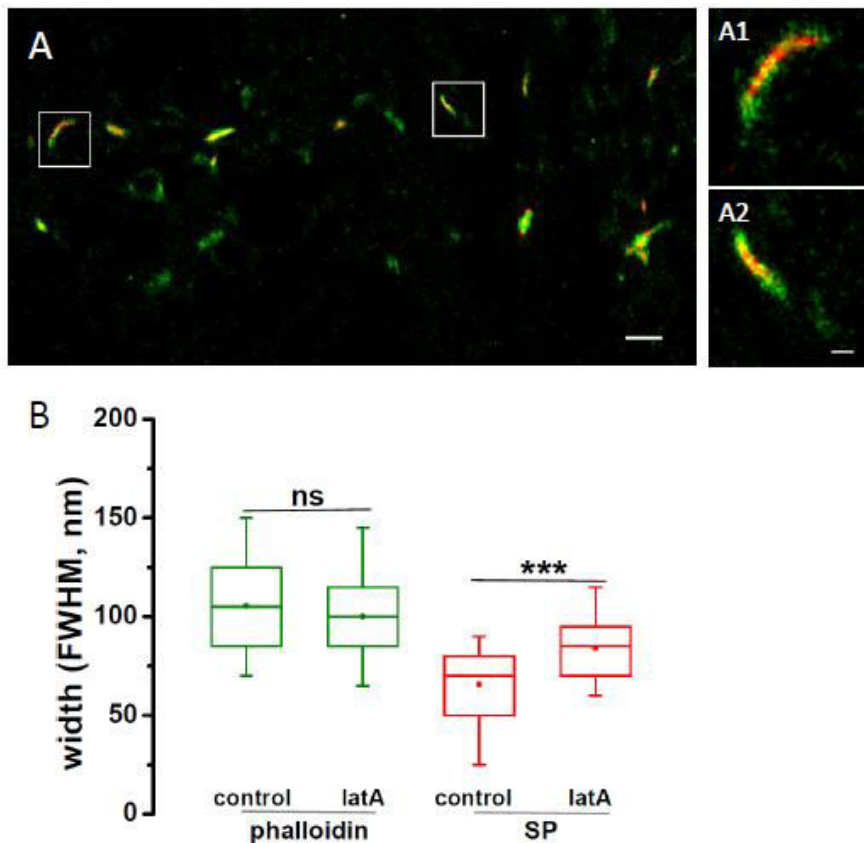


**Figure 3.4 Effect of actin depolymerization on SP structure revealed by STORM/PALM.**

**A.** Super-resolution imaging of dendra-SP (red) and A647-phalloidin (green) in spines after 5 min latrunculin A application. A1 and A2 is the zoomed images, which demonstrated the loss actin filament in the spine head after latA incubation. **B.** Quantification of the FWHM of SP domains in spine necks under latA condition (5 μM, 5 min). Compared with control, actin depolymerization by latA treatment induced a significant expansion of the SP domain, but not affected the F-actin domain in spine neck (ns: not significantly different, \*\*\*  $p < 0.001$ , MW test,  $n_{ctr} = 34$ ,  $n_{lat} = 33$ ). Scale bars: 1 μm in A, 200 nm in A2.

## 4 Neuronal activity increases diffusion of mGluR5 in the spine neck

### 4.1 Neuronal activity regulates the amount of synaptopodin

Actin is a major structural component in dendritic spines and that mediates the remodeling of spine morphology under basal conditions and also in response to neuronal activity. LTP induction by tetanic stimulus shifts F-actin/G-actin equilibrium toward polymerization, related with enlargement of spine [Okamoto et al. 2004; Matsuzaki 2004]. By contrast, LTD induction by low-frequency stimuli results in a shift in the F-actin/G-actin toward depolymerization, concomitant with collapse of spines [Okamoto et al. 2004]. Application of 4-aminopyridine (4AP) is also known to induce activity-dependent depolymerization of F-actin [Ouyang et al. 2007]. 4AP is a voltage-dependent potassium channel blocker. I speculated that the increase of neuronal activity by 4AP, depolymerizing actin filaments, may affect the clustering of SP and the diffusion of mGluR5 in spine necks.

Hippocampal neurons were treated with 50  $\mu$ M 4AP to increase the network activity [Buckle and Haas 1982]. After application of 4AP for 30 minutes, primary hippocampal neurons were double stained with anti-SP antibody and Alexa647-phalloidin (Fig. 4.1A). As previously, a positive correlation between SP and phalloidin immunoreactivity was observed in presence of 4AP (Fig. 4.1C,  $R^2=0.585$ ). Most interestingly, the slope of the related curve are similar in control and 4AP condition (control: 0.67; 4AP: 0.69), which suggests SP and F-actin undergo similar modification in response to neuronal activity. 4AP incubation had no effect on the number of SP-positive spines per 1  $\mu$ m stretch of dendrite (Fig. 4.1D) (control:  $3.51 \pm 0.84$  spines /  $\mu$ m dendrite, mean  $\pm$  SD; 4AP:  $3.56 \pm 0.74$ ;  $p = 0.44$ , MW test,  $n_{ctr} = 142$ ,  $n_{4AP} = 144$  regions), but reduced the amount of phalloidin-labelling significantly (Fig. 4.1E;  $p < 0.001$ , MW test,  $n_{ctr} = 151$ ,  $n_{4AP} = 149$ ). SP intensity levels decreased in parallel with F-actin (Fig. 4.1F). This suggests that after the increase of synaptic activity, all SP clusters (stable or instable) are reduced concomitantly with actin depolymerization.

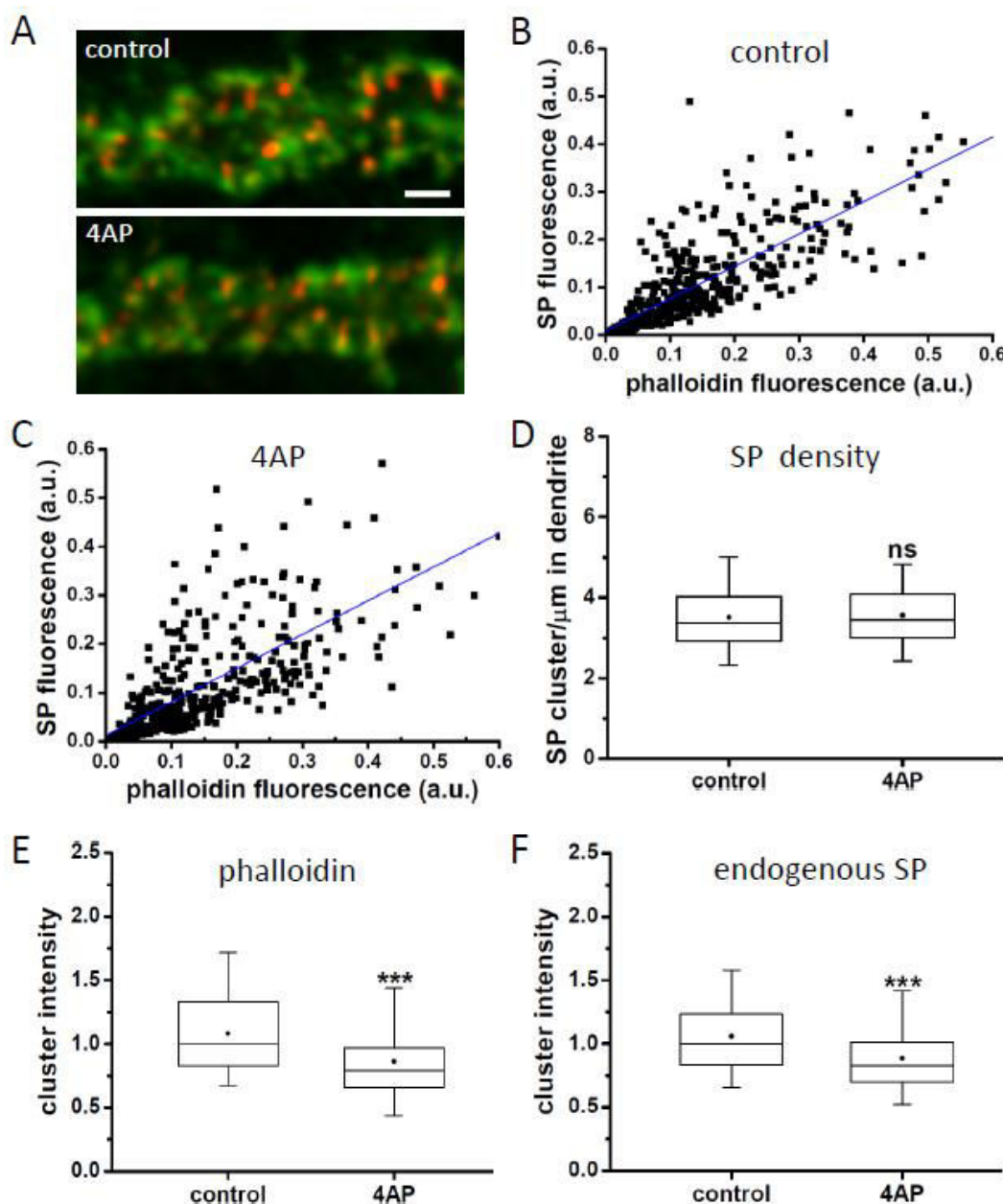


**Figure 4.1 Immunocytochemistry showed the effect of neuronal activity on SP amount**

**A.** Immunocytochemistry of endogenous SP (red) and A647-phalloidin staining (green) in hippocampal neurons under control condition (top panel) or after 30 minutes of 50  $\mu$ M 4AP incubation (bottom panel). **B,C.** SP immunoreactivity positively correlated with phalloidin intensity under basal condition (B) and (C) 4AP situation ( $n=500$  clusters from 2 neurons). a.u., arbitrary unit. **D.** The density of SP clusters in dendrite in control and 4AP conditions ( $n \geq 142$  spines from 3 cultures). **E,F.** Normalized total fluorescence intensity of phalloidin (E) and SP levels (F) in control and 4AP treatment, quantified within SP-positive clusters. Boxes indicate 5, 25, 50, 75 and 95% of all clusters; dots: mean value; ns: not significantly different, \*\*\*  $p < 0.001$ , Mann-Whitney U test. Scale bar: 2  $\mu$ m in A.

Interestingly, super-resolution imaging revealed a normal morphological distribution of F-actin and the SP domains in the spine neck under 4AP condition (Fig. 4.2B). Compared to control, the widths of F-actin ( $104 \pm 5$  nm) and SP domains ( $76 \pm 5$  nm) in the spine neck were not significantly altered after 4AP treatment (phalloidin domain:  $p = 0.65$ ; SP domain:  $p = 0.1$ , MW test,  $n_{ctr} = 34$ ,  $n_{4AP} = 29$ ) (Fig. 4.2C). This means that in contrast to latrunculin treatment, the internal organization of the spine neck is preserved under these conditions, even though the levels of both protein components were reduced.

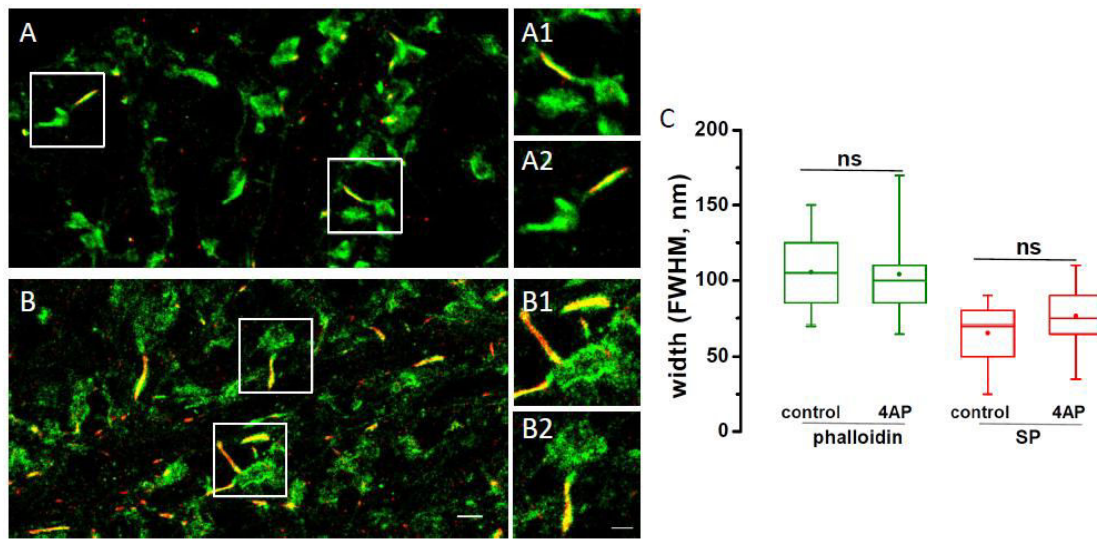


**Figure 4.2 STORM/PALM imaging revealed the effect of neuronal activity on SP distribution.**

**A,B.** Hippocampal neurons expressing dendra-SP (red) were stained with A647-phalloidin (green) to label F-actin filaments in control (A) and 4AP situation (B). A1, A2, B1 and B2 are zoomed images. Super-resolution STORM/PALM imaged represented single dendra and A647 fluorophore detections in false colours (red and green, respectively). **C.** Measurements of rendered super-resolution images showed the widths of the SP and F-actin domains in the spine neck were not influenced by 4AP incubation ( $n_{ctr}=34$ ,  $n_{4ap}=30$  spines,). Scale bars: 1  $\mu$ m in B, 500 nm in B2.

## 4.2 Neuronal activity regulates the diffusion of mGluR5.

Compared to control condition, a strong increase in  $D_{1Dlong}$  values was recorded in both SP+ spines and SP-spines under 4AP treatment (Fig. 4.4A,B,  $D_{in SP}=0.082 \pm 0.005 \mu\text{m}^2/\text{s}$ ,  $D_{no SP}=0.116 \pm 0.007 \mu\text{m}^2/\text{s}$ ,  $D_{Sp}=0.160 \pm 0.007 \mu\text{m}^2/\text{s}$ ;  $n= 135, 293, 247$  trajectories, respectively). This increase was observed in all analysed neck regions, independent of the presence or absence of SP. This suggests that the depolymerization of actin filaments had a general influence on the diffusion of mGluR5.

I then investigated the reversibility of these changes. Neurons were pre-incubated with

4AP for 30 min and rinsed before recording. In this condition, the fluorescence of Alexa647-phalloidin and SP clusters were partially recovered (Fig. 4.3). In SP+ spines, the diffusion coefficient of mGluR5 in the SP area was similar ( $0.081 \pm 0.007 \mu\text{m}^2/\text{s}$ ) to that of no SP cluster region ( $0.091 \pm 0.009 \mu\text{m}^2/\text{s}$ ) ( $p=0.613$ , KS test,  $n_{\text{in SP}}=65$ ,  $n_{\text{no SP}}=85$  trajectories). However, the significant difference of mGluR5 mobility was also preserved between in SP+ spines and in SP- spines ( $0.143 \pm 0.008 \mu\text{m}^2/\text{s}$ ) ( $p<0.001$ , KS test,  $n_{\text{sp.}}=294$  trajectories) (Fig. 4.4C). The cumulative frequency of the diffusion of mGluR5 in control condition and 4AP washout situation was compared (Fig. 4.4D). In 4AP washout treatment, the increase in  $D_{1\text{Dlong}}$  values was only observed in SP area. Comparing the data of Fig. 4.4B with Fig. 4.4D, the extent of acceleration of diffusion in 4AP washout is lower than that of in 4AP, with respect to control condition (control versus 4AP washout:  $p<0.05$ ; control versus 4AP:  $p<0.001$ ; KS test). This correlated with the partial recovery of SP cluster detected by immunoreactivity. The diffusion in SP- spines in control and 4AP washout conditions were quite similar ( $p=0.239$ , KS test), but both of them displayed slower speed of diffusion than in 4AP ( $p<0.01$ , KS test). This also suggests the reversibility of F-actin in SP- spines.

Taken together, our observations indicate that both mGluR5 diffusion and SP localization are reversibly regulated in response to enhanced synaptic activity and/or associated changes of spines cytoskeleton.

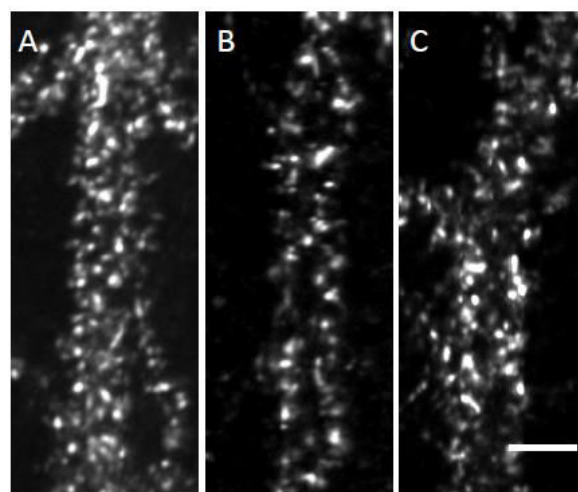


**Figure 4.3 The reversibility of synaptopodin occurred after 4AP washout.**

Immunoreactivity of endogenous SP in control (A), 4AP treatment (B, 50  $\mu\text{M}$ , 30 min) and 4AP washout neurons (C, 50  $\mu\text{M}$ , 30 min, then washout, wait 30 min). Scale bar: 5  $\mu\text{m}$ .

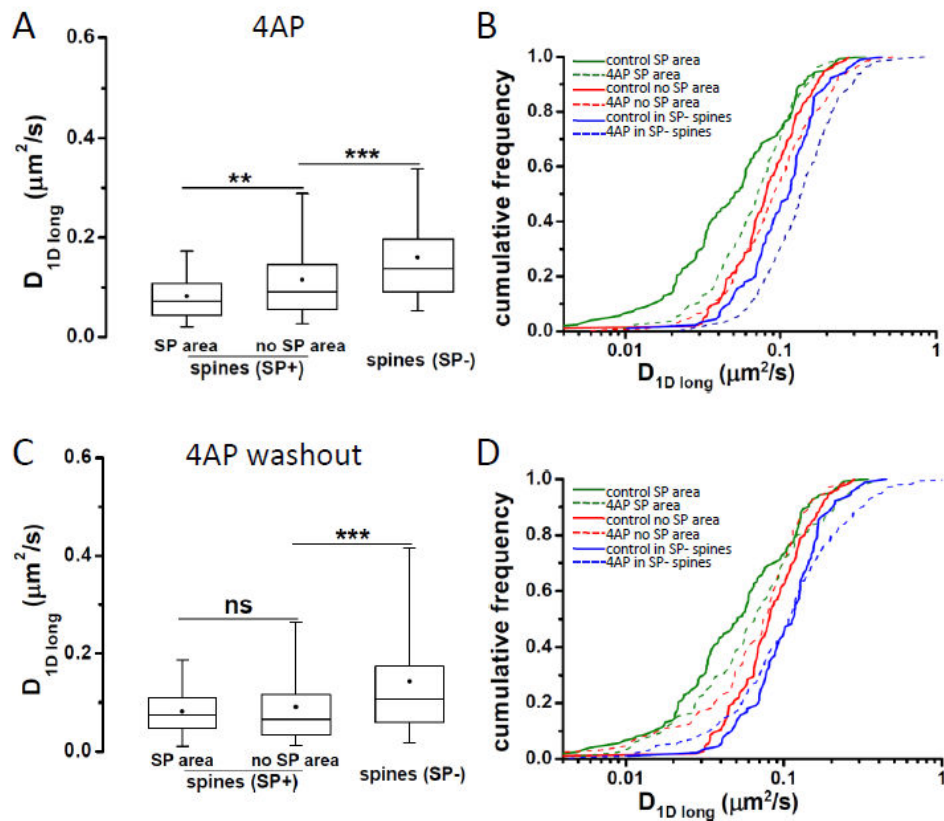


**Figure 4.4 Effect of neuronal activity on mGluR5 diffusion.**

**A.** Diffusion coefficients of pHluorin-mGluR5 in SP- and SP+ spine necks after 4AP incubation ( $n \geq 135$  trajectories from 3-5 cultures). **B.** Cumulative distribution of pHluorin-mGluR5 diffusion coefficients tracked in SP- (blue) and in SP+ spines, either on top (green) or outside of SP clusters (red) in control (solid lines) and after 4AP treatment (dashed lines). **C,D.** The effect of 4AP washout on the diffusion mobility of mGluR5. **C,** diffusion coefficient of pHluorin-mGluR5 ( $n \geq 65$  trajectories from 3-5 cultures). **D.** The cumulative distribution of mGluR5 after 4AP washout. Compared to A,B, there is no 4AP in the MEM recording medium in C,D.  $D_{1D \text{ long}}$ ; boxes indicate 5, 25, 50, 75 and 95% of all trajectories; dots: mean value; ns: not significantly different, \*\*  $p < 0.01$ , \*\*\*  $p < 0.001$ , KS test.

### 4.3 Neuronal activity regulates the amount of $\alpha$ -actinin2.

After application of 4AP for 30 minutes, primary hippocampal neurons were double stained with anti-SP antibody and  $\alpha$ -actinin2 (Fig. 4.5A). In parallel with the SP level (Fig. 4.1F), the amount of  $\alpha$ -actinin2 was significantly reduced after 4AP incubation (Fig. 4.5B;  $p < 0.001$ , MW test,  $n_{\text{ctr}} = 90$ ,  $n_{4\text{AP}} = 92$ ). Furthermore, a positive correlation between SP and  $\alpha$ -actinin2 immunoreactivity was observed in the control and 4AP conditions (Fig. 4.5C,D; control:  $R^2 = 0.872$ , 4AP:  $R^2 = 0.846$ ). These results suggest that after the increase of synaptic activity, all SP clusters (stable or instable) were reduced concomitantly with their binding protein  $\alpha$ -actinin2.

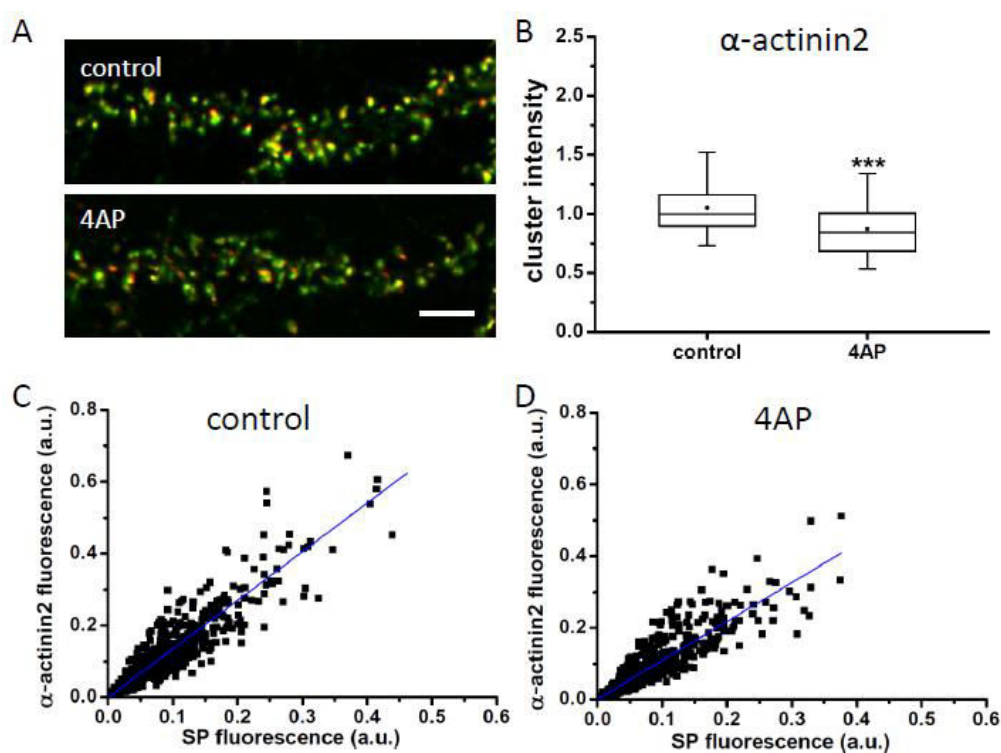


**Figure 4.5** Immunocytochemistry showed the effect of neuronal activity on  $\alpha$ -actinin2 amount.

**A.** Immunocytochemistry of endogenous SP (red) and  $\alpha$ -actinin2 staining (green) in hippocampal neurons under control conditions (top panel) or after 30 minutes of 50  $\mu\text{M}$  4AP incubation (bottom panel). **B.** Normalized total fluorescence intensity of  $\alpha$ -actinin2 in control and 4AP treatment, quantified within SP-positive clusters. **C,D.** SP immunoreactivity positively correlated with  $\alpha$ -actinin2 intensity under basal conditions (C) and (D) 4AP situation ( $n = 1000$  clusters from 4 neurons). ns: not significantly different, \*\*\*  $p < 0.001$ , Mann-Whitney U test. a.u., arbitrary unit. Scale bar: 5  $\mu\text{m}$  in A.

## 5 The relationship between synaptopodin and mGluR5

As shown by my results, the presence of SP strongly impeded the diffusion mobility of mGluR5 under control condition. This was reflected by the lower diffusion coefficient of mGluR5 in SP area compared to SP free regions in SP(+) spines. Therefore, synaptopodin could potentially exert a scaffolding effect on mGluR5, inducing its enrichment in the spine neck.

To address this question, hippocampal neurons were double stained with anti-SP and anti-mGluR5 antibodies. Preliminary immunostained imaging revealed that about 40% of mGluR5 clusters co-localized with SP clusters in spines (Fig. 5.1A). Interestingly, SP intensity is positively correlated with mGluR5 staining (Fig. 5.1B,  $R^2=0.84$ ;  $n=3000$  spines from 8 neurons), indicating that spines with larger SP clusters also contain more mGluR5 clusters. It has been shown that mGluR5 in the postsynaptic membrane is enriched at the edge of the postsynaptic density in a perisynaptic fashion [Lujan et al. 1996]. However, though it has been rarely reported that mGluR5 can express in the spine neck, my results suggest that a partial of SP and mGluR5 co-localize in neck regions. Super resolution imaging would be required to further analyze the distribution of mGluR5 in the spine neck.

It has been reported that the lateral diffusion of mGluR5 in the plasma membrane was regulated by its activity. The presence of DHPG (10  $\mu$ M) induced the increase of mGluR5 diffusion during both diffusive and confined events [Serge et al. 2002]. Interestingly, the amount of SP can also be regulated by the activity of mGluR5 receptor itself. After incubation with the agonist DHPG (10  $\mu$ M) for 30 min or 60 min, the total fluorescence intensity of SP clusters was reduced about 25% compared to that of control condition (Fig. 5.1C). The antagonist MPEP (50  $\mu$ M) had no effect on the total intensity of SP clusters.

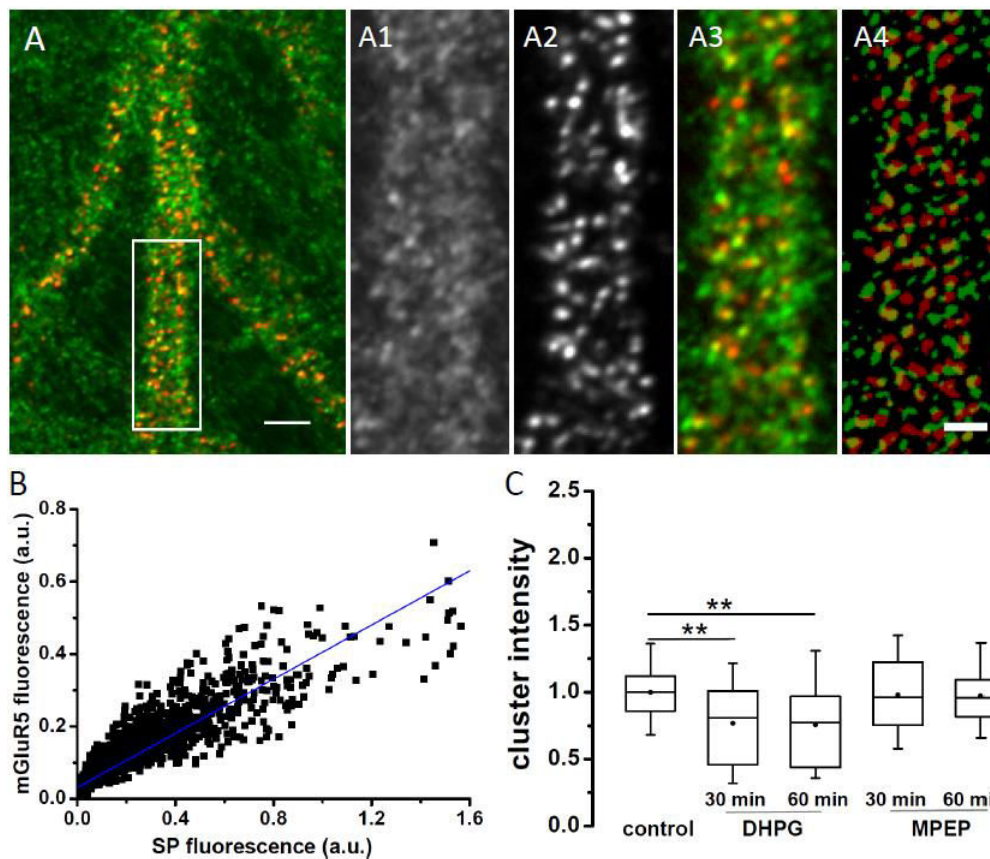


**Figure 5.1 The relationship between synaptopodin cluster and mGluR5 receptor in spines.**

**A.** Immunocytochemistry showed a partial co-localization between synaptopodin and mGluR5 clusters. Neurons were stained with anti-mGluR5 antibody (A1, green in A3) and anti-SP antibody (A2, red in A3). A4 is the merged MIA of mGluR5 (green) and SP (red) masks. **B.** Synaptopodin immunoreactivity positively correlated with mGluR5 intensity in regions defined by SP clusters mask. **C.** Neurons were stained with anti-SP antibody after regents incubation (DHPG, 10  $\mu$ M; MPEP, 50  $\mu$ M). The agonist DHPG induced the decrease of SP intensity. ns: not significantly different, \*\*\*  $p < 0.001$ , Manny whitney U test, a.u., arbitrary unit. Scale bar: 5  $\mu$ m in A; 2  $\mu$ m in A4.



## **IV Discussion**



The neck of dendritic spine acts as a diffusion barrier that separates the site of synaptic transmission in the spine head from dendrite [Adrian et al. 2014]. The thin spine neck limits the recruitment of soluble synaptic components as well as their escape from the spine head, which has consequences for synaptic plasticity [Majewska et al. 2000]. It was suggested that a diffusion barrier also exists for membrane molecules [Ashby et al. 2006] and this is particularly relevant for the dynamic exchange of membrane proteins such as neurotransmitter receptors at synapses. I have therefore investigated the presence and the mechanisms behind such a lateral diffusion barrier.

### **1 The role of the spine neck geometry for membrane protein diffusion**

Between dendrites and spine necks there is a change of membrane radii. It has been demonstrated that in tubular membranes with radii ranging from 10-200 nm the diffusion is reduced in thinner tubes. This can be explained by a hydrodynamic effect due to the finite size of the membrane [Domanov et al. 2011]. Thus I first investigated this effect on the lateral diffusion of various membrane constructs on dendrites and spine necks in dissociated hippocampal neurons.

I made use of three different probes that are inserted into the membrane by different means: 1) a construct associated with the outer leaflet of the plasma membrane (GFP-GPI); 2) a construct with one transmembrane domain only (TMD-pHluorin) with a short intracellular sequence; and 3) a large membrane molecule, the metabotropic glutamate receptor mGluR5 coupled to pHluorin. The mGluR5 receptor contains seven transmembrane domains and furthermore forms a disulfide-bridged homodimer via its globular extracellular ligand-binding domains [Pin, 2009]. These three probes have allowed me to distinguish between different mechanisms that may affect diffusion: membrane geometry (which should affect them all) or different sources of diffusion barriers such as lipid rafts, actin cytoskeleton, pickets [Kusumi et al. 2012]. These barriers would affect differentially GFP-GPI (which is slowed down in lipid rafts), TMD-pHluorin (which would be affected by pickets but not by actin cytoskeleton) and mGluR5-pHluorin (which would reveal the importance of F-actin and/or specific interactions). For example, the intracellular septin-7 complex at the base of the spine neck forms a barrier at the entrance of spine that is important for AMPARs diffusion and therefore entry in or exit from the spine domain [Ewers et al. 2014].

In all cases, GFP-GPI displayed the fastest speed of diffusion, followed by TMD-pHluorin. As expected the diffusion was the slowest for mGluR5-pHluorin. This is in agreement with the notion that molecule diffusion rate depend on its size [Saffman and Delbrück 1975].

All the molecules had a tendency to decrease diffusion with the reduction of dendrites diameter. More specifically, compared to the wider dendrites, the diffusion on spine necks was slower for membrane proteins with transmembrane domains (TMD-pHluorin and mGluR5 constructs), but not GFP-GPI, even though the projection errors were accounted for by considering only the longitudinal component of the diffusion ( $D_{1Dlong}$ ). The fact that there was no significant change for GFP-GPI implies that the sole reduction of membrane diameter is not sufficient to create a diffusion barrier in spine necks. Thus, differences in mobility could be linked to the presence of obstacles and barriers to diffusion. These barriers could either be non-specific (such as actin cytoskeleton) or target particular molecules by specific interactions (such as scaffolding molecules).

## 2 Synaptopodin and mGluR5 diffusion

Synaptopodin (SP) is one of few proteins preferentially located in the spine neck, and as such it is ideally placed to regulate the exchange of synaptic components. It has been shown with EM analysis that SP-immunoreactivity is physical associated with the spine apparatus (SA), an organelle containing stacks of SER and electron-dense plates [Deller et al. 2000b; Spacek and Harris 1997]. Indeed, SP is a marker and an essential component of SA, since SA is absent in SP-deficient mice [Deller et al. 2003]. In vitro, Vlachos [2009] showed that about 30% of spines in hippocampal neurons contain a clearly discernable SP cluster; in vivo, Orth [2005] found that 36% of all spines contain SP in outer and middle molecular layers of the dentate gyrus. I found that the percentage of spines with SP is higher than that reported in the above mentioned studies. However, my results are in line with a study by Spacek et al. [1997], who published that more than 80% of the large mushroom spines typically contain a SA, and thus very likely contain SP.

I have compared the diffusion properties of membrane proteins in the neck of spines expressing SP or not. In agreement with the above considerations, I did not find any SP-dependent differences in the diffusion of GFP-GPI construct associated with the outer membrane layer. The same was true for TMD-pHluorin with its short intracellular sequence. However, the diffusion of mGluR5 was slower in regions of the spine neck expressing SP than in SP-free areas. These results indicate that SP contributes or highlights the presence of a barrier to lateral diffusion in the spine neck. This observation is consistent with the work of Ewers et al [2014] which described that proteins assembled in base of spine neck can impede the diffusion of receptors from entering the spine neck. It shows that Septin7 localized at the base of spine neck restricts the diffusion of AMPARs and therefore contributes to the

biochemical compartmentalization of spine neck. The final consequences of the restricted diffusion of receptor would be their enhanced clustering at synapses, associated with synaptic plasticity.

However, which is the connexion between the presence of SP and a barrier to diffusion at the level of the plasma membrane? Is the barrier due to direct molecular interactions or to spatial constraints that are related to the structural organization of spine neck?

Group I mGluR types are mainly found in the perisynaptic region in the postsynaptic membrane, regulating the activity of their ionotropic glutamate receptors [Baude et al. 1993; Luján et al. 1997]. However, they are not exclusively located around synapses. mGluR5 physically binds and assembles via the intracellular C-terminal domains with functionally related proteins such as scaffolds, enzymes and cytoskeletal anchor proteins [Enz 2012]. In the results section, a partial colocalization of SP and mGluR5 was detected in spine necks and a positive correlation existed between their fluorescence intensity.

So what could be the evidence that a direct interaction exists between SP and mGluR5? In the results section, the distance between the SP and the plasma membrane was about 20 nm in control condition. Since mGluR5 has a long and flexible intracellular region of 352 amino acid residues, it could easily contact the SP domain [Enz 2012]. However, latA rapidly increased the width of the SP domain but not altered the width of spine neck, which caused the distance of SP and the plasma membrane was reduced from 20 nm to 8 nm. The increased size and fluorescence intensity of SP domain was correlated with an acceleration of mGluR5 diffusion following latA induction. The data mean the two proteins have not been facilitated under these conditions, arguing against a direct interaction.

Indirect interactions of SP and mGluR5 could be possible via the long intracellular segment of mGluR5, which contains Homer and actinin binding sites [Serge et al. 2003; Kalinowska et al. 2015]. Homer family are scaffold proteins that interact with mGluR5 controlling its targeting to synapses [Serge et al. 2002]. However, although the long form of SP contains a PRRPF motif for Homer binding, the neuronal SP-short isoform does not bear it [Asanuma et al. 2005]. In the results section, I showed the colocalization of SP and  $\alpha$ -actinin2 in dendritic spines and the positive correlation between their fluorescence intensity.  $\alpha$ -actinin is composed of two calponin homology (CH) domains which bind actin filaments, a central rod domain containing Spectrin repeats, and two C-terminal EF hand motifs that confer  $\text{Ca}^{2+}$  affinity [Kremerskothen et al. 2002]. The Spectrin repeats form a platform for protein-protein interactions. For instance,  $\alpha$ -actinin2 binds by its central rod domains to the cytoplasmic tail of NMDAR subunits, and thus link receptors to the submembrane actin cytoskeleton [Wyszynski et al. 1997]. The

Spectrin repeats are sufficient and necessary for the binding of SP to  $\alpha$ -actinin2 [Asanuma et al. 2005; Kremerskothen et al. 2005].  $\alpha$ -actinin4 is enriched at excitatory synapses where it colocalizes with group 1 mGluRs also through the Spectrin repeats direct binding to the cytoplasmic tail of receptors [Kalinowska et al. 2015]. As  $\alpha$ -actinin2 and  $\alpha$ -actinin4 are highly conserved in evolution, there is a very probable that both actinins interact with mGluR5 and SP in the same way. Yet again, such an indirect interaction between SP and mGluR5 would create a positive correlation between SP clustering and mGluR5 confinement, which is contrary to my observation.

If an interaction of SP and mGluR5 exists, it is probably labile and/or dependent on actin filaments integrity. Arguably the most important and regular structural element of the spine neck is the F-actin cytoskeleton that is responsible for maintaining the shape of the spine and inducing rapid morphological changes. For example, long-term potentiation (LTP) is generally accompanied by an increase in the spine head volume, which requires the re-modelling of the actin cytoskeleton [Matsuzaki 2004; Okamoto et al. 2004]. The organization of F-actin in the neck is noticeably different from that of the spine head. Whereas the latter consists of a complex and highly dynamic network of branched F-actin, the spine neck has both branched as well as linear actin filaments that are arranged more or less in parallel [Hotulainen and Hoogenraad 2010]. Consequently, the neck can undergo substantial variation in length [V; Araya et al. 2014], while changes in width have been seen less frequently [Honkura et al. 2008; Tønnesen et al. 2014]. In my experiments the width of the spine necks was remarkably constant as judged by the profile of the F-actin domain in super-resolution STORM data, irrespective of the pharmacological treatments used.

Given the high concentration of F-actin in the spine, it is not surprising that filaments below the plasma membrane obstruct the space and reduce the movement of membrane proteins [Kusumi et al. 2005]. As expected, the changes in F-actin polymerization in response to latA were paralleled by an enhanced diffusion rate of mGluR5 in the spine neck. However, this increase was most pronounced in SP regions of SP+ spines, to an extent that  $D_{1Dlong}$  values became indistinguishable from those in SP-free regions of the same spines within 5-10 minutes of latA application. Longer latA treatment (15-20 minutes) led to a further increase in mGluR5 mobility in SP+ spines that became as fast as in SP- spines. The temporal profile suggests that the accelerated diffusion of mGluR5 is related to the F-actin depolymerization. Interestingly, in SP-negative spines, the mGluR5 diffusion was not significantly altered by latA treatment. This suggests that in SP-negative spine there is not sufficient F-actin to make the differences in the rate of molecule diffusion between latA-treated and untreated neurons. This data shows that

F-actin is involved in the slow down of the diffusion of mGluR5 in the spines containing SP.

### 3 Synaptopodin and actin cytoskeleton

SP contains an actin/actinin binding domain and strategically occupies a precise sub-domain of the spine neck. This indicates the position of SP in the spine neck could affect by the polymerization state of actin, and/or conversely, be affected by it. Indeed, I have always observed a positive correlation between the intensity of SP associated fluorescence and phalloidin-labeled actin filaments. Depolymerization of F-actin by latrunculin A, which targets the more dynamic filaments at short times of treatment, caused the re-distribution of SP clusters. Small SP clusters disappeared and the newly free SP molecules were probably recruited into large and more stable SP clusters, expanding their size. This indicates that the stability of SP is also influenced by the polymerization state of actin, in particular in thin spines.

In turn, SP helps the stabilization of F-actin. Firstly, compared to SP-negative spines, spines endowed with SP are more resistant to the disruption effect of latA, as denoted by less changes in their morphology, disappearance or elongation [Vlachos et al. 2009]. In line with this study, latA incubation induced the formation of large SP clusters that retained more F-actin to maintain the morphology of spines, with respect to small SP clusters. Secondly, SP may influence the dynamic equilibrium of actin. The stable F-actin pool with relatively slow turnover is present near the spine neck [Honkura et al. 2008], where the spine apparatus (SA) and SP are localized. This indicates SA/SP may partially participates in the localization and size of stable F-actin pool. The presence of SP is more prevalent in spines with large head volumes, even if SP could be found in different types of spines (stubby, thin, mushroom) [Vlachos et al. 2009]. Lastly, the presence of SP facilitates the expansion of spines after NMDA-dependent activation [Korkotian et al. 2014].

Combining these reports with my results, I can assume that the presence of SP in the spine neck facilitates a dense local F-actin network, which in turn creates a diffusion barrier particularly in the mushroom spines. Receptors could then be retained at the level of the spine head, and therefore re-captured by their scaffolding molecules at the PSD [Triller and Choquet 2008]. Interestingly, it has been proposed that in large mushroom spine there is a local synthesis of AMPAR [Matsuo et al. 2008]. These receptors would then remain in the spine head, being internally recycled [Malinow and Malenka 2002] and re-captured in synapses despite their high lateral mobility [Tardin et al. 2003]. Activity-dependent postsynaptic local translation within dendritic spines can be achieved through the recruitment of polyribosomes [Ostroff et al. 2002] and several mRNA into spines [Grooms et al. 2006]. All these processes involved in the

trafficking of receptor are important to regulate the trapping of receptors at synapses in response to neuronal activity.

The fact that SP "prefers" mushroom spines, which contain larger (potentiated) synapses and more receptors suggest a potential role of SP during plasticity mechanisms such as helping retaining receptors in the spine head, facilitating the acquisition of this particular status of isolated compartment. Both actin cytoskeleton and SP have been related to plasticity mechanisms. Activity-dependent changes in the actin cytoskeleton and its related proteins play a critical role in synaptic efficiency [Cingolani and Goda 2008]. For instance, L-LTP can promote the polymerization of F-actin and upregulate the expression of SP [Yamazaki et al. 2001; Fukazawa et al. 2003; Vlachos et al. 2009].

I found that changes in neuronal activity had an effect on SP clusters and mGluR5 diffusion in the spine neck. Activity-dependent depolymerization of F-actin induced by 4AP treatment decreased the amount of SP simultaneously, but not influenced the size of SP domain in the spine neck. Actually, a strong increase in the rate of mGluR5 diffusion was observed in all analyzed neck regions, independently of the presence or absence of SP. However, the fact that spines containing SP restricts the mobility of mGluR5 were also preserved in 4AP treatment. The increase of mGluR5 diffusion across the spine neck would mean less concentration of receptors in the neck, close to the internal calcium store. This may temper the increase of internal  $Ca^{2+}$  concentration due to synaptic activation and the excitotoxicity which can result from it [Szydłowska and Tymianski 2010]. Taken together, our observations indicate that changes in mGluR5 diffusion and SP clustering are associated with changes of the spine cytoskeleton and are regulated by enhanced synaptic activity.

SP is tightly associated with SA that is a specialized organelle formed by endoplasmic reticulum, implicated to regulate the calcium kinetics in dendritic spines [Fifková et al. 1983]. Since the internal calcium concentration alters the polymerization and dynamics of actin cytoskeleton [Oertner and Matus 2005], it could be the link between SP and actin polymerization. As a matter of facts, SP is linked to the release of calcium from the SA. An SP-dependent accumulation of GluR1 in spine head is mediated by the release of calcium from intracellular stores via ryanodine receptors (RyR) [Vlachos et al. 2009].

In conclusion, my findings lend support to a model whereby synaptopodin acts as an organizer of the spine neck in mature spines (Fig. 1). Firstly, the presence of SP correlates with the reduction of mGluR5 diffusion in the spine neck as a consequence of the local organization of the spine cytoskeleton. LatA application induced the re-distribution and recruitment of SP

clusters which was accompanied by an acceleration of mGluR5 diffusion especially in SP-positive spines. Thus F-actin and SP are inversely related, and mGluR5 diffusion increases with SP levels. This result points to a specific role of synaptopodin in the organization of the spine neck cytoskeleton. Secondly, SP occupies a different and precise sub-domain of the spine neck, suggesting that SP does not interact with the totality of actin filaments in the neck. Rather, SP appears to be associated with a pool of F-actin that is activity-dependent, as seen in the correlated reduction of F-actin and SP levels in the presence of 4AP. In contrast, the latrunculin A sensitive dynamic pool of F-actin [Honkura et al. 2008] had an inverse effect on the SP domain, obstructing the accumulation of SP within the spine neck. These observations can be reconciled if we assume that the presence of SP in the spine neck creates a dense local F-actin network that blocks the recruitment of further SP molecules. This may be the result of the increased crowding in the spine necks containing synaptopodin and a spine apparatus. Synaptopodin would thus exert an indirect effect via F-actin on the diffusion of membrane proteins in the spine neck.

#### 4 Perspectives

My work revealed that in spine necks containing synaptopodin there is a diffusion barrier for mGluR5, a membrane receptor with a large intracellular domain. The consequence of this restriction would be the facilitation of receptor trapping at synapses. In order to verify this conclusion, the next step would be to investigate the mobility of other membrane proteins across the spine neck such as AMPARs, which enter and exit synapses and regulate the strength of synaptic transmission and plasticity [Triller and Choquet 2008]. The importance of this diffusion barrier should be verified using a SP knockout mouse.

The expression of mGluR5 in intracellular membranes (e.g. endoplasmic reticulum) can induce  $Ca^{2+}$  response and mediate synaptic plasticity in hippocampal neurons [Purgert et al. 2014]. The majority (78%) of ER-containing spines are also positive for spine apparatus. ER-containing spines control the potential for mGluR-mediated synaptic depression [Holbro et al. 2009]. It would be interesting to study the localization of mGluR5 and SP associated with spine apparatus in the spine neck using super resolution imaging techniques (PALM/STORM). By combining super-resolution microscopy with calcium imaging, the function of mGluR6 could then be related to its sub-spine distribution. Furthermore, sptPALM, a new developed technique that combines PALM with SPT, can resolve the dynamic of intracellular membrane proteins, using genetically encoded fluorescent proteins [Manley et al. 2008]. The diffusion processes of mGluR5 on the cell surface as well as in the intracellular membrane may thus

provide new insights into the role of synaptopodin and the spine apparatus in the regulation of mGluR5 dynamics and function.

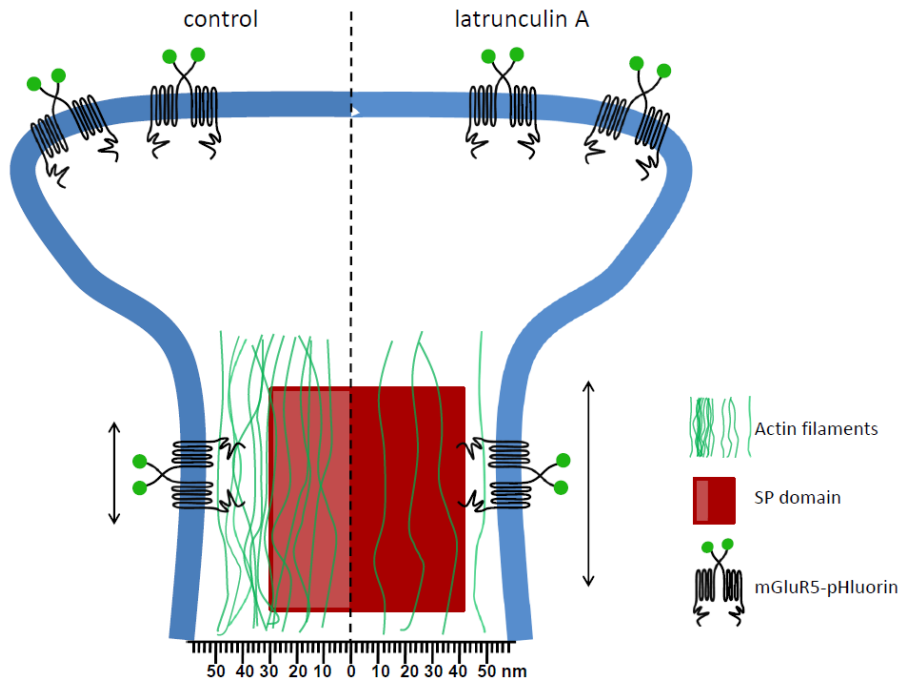


**Figure 1. Schematic illustration showing the organization of spines containing synaptopodin.**

SP restricts the diffusion (shown as arrows) of mGluR5 receptors (illustrated as dimers) via the actin cytoskeleton in dendritic spines. In control condition (left part of the mushroom spine), the width of the SP domain (pink box) in the neck is around 60 nm (= 2 x 30 nm) and that of the F-actin domain (dense green lines, not drawn to scale) is 100 nm. The presence of SP has an effect on the diffusion of mGluR5 in the spine neck, and thus contributes to the compartmentalization of receptors at synapses. During latA treatment (right part of the mushroom spine), the disruption of F-actin (loose green lines) increases the width of the SP domain (red box) to 84 nm. This is accompanied by the acceleration of mGluR5 diffusion in the spine neck.

## References



- Adesnik, Hillel, Roger a. Nicoll, and Pamela M. England. 2005. "Photoinactivation of Native AMPA Receptors Reveals Their Real-Time Trafficking." *Neuron* 48:977–85.
- Adrian, Max et al. 2014. "Barriers in the Brain: Resolving Dendritic Spine Morphology and Compartmentalization." *Frontiers in Neuroanatomy* 8(December):1–12.
- Alcor, Damien, Géraldine Gouzer, and Antoine Triller. 2009. "Single-Particle Tracking Methods for the Study of Membrane Receptors Dynamics." *European Journal of Neuroscience* 30(June):987–97.
- Alivisatos, Paul. 2004. "The Use of Nanocrystals in Biological Detection." *Nature biotechnology* 22(1):47–52.
- Araya, Roberto, Jiang Jiang, Kenneth B. Eisenthal, and Rafael Yuste. 2006. "The Spine Neck Filters Membrane Potentials." *Proceedings of the National Academy of Sciences of the United States of America* 103:17961–66.
- Araya, Roberto, Tim P. Vogels, and Rafael Yuste. 2014. "Activity-Dependent Dendritic Spine Neck Changes Are Correlated with Synaptic Strength." *Proceedings of the National Academy of Sciences of the United States of America* 111:2895–2904.
- Arellano, Jon I., Ruth Benavides-Piccione, Javier Defelipe, and Rafael Yuste. 2007. "Ultrastructure of Dendritic Spines: Correlation between Synaptic and Spine Morphologies." *Frontiers in neuroscience* 1(1):131–43.
- Asanuma, Katsuhiko et al. 2005. "Synaptopodin Regulates the Actin-Bundling Activity of A-Actinin in an Isoform-Specific Manner." 115(5).
- Ashby, Michael C. et al. 2004. "Removal of AMPA Receptors (AMPA) from Synapses Is Preceded by Transient Endocytosis of Extrasynaptic AMPARs." *The Journal of neuroscience : the official journal of the Society for Neuroscience* 24(22):5172–76.
- Ashby, Michael C., Kyoko Ibaraki, and Jeremy M. Henley. 2004. "It's Green Outside: Tracking Cell Surface Proteins with pH-Sensitive GFP." *Trends in Neurosciences* 27(5):257–61.
- Ashby, Michael C., Susie R. Maier, Atsushi Nishimune, and Jeremy M. Henley. 2006. "Lateral Diffusion Drives Constitutive Exchange of AMPA Receptors at Dendritic Spines and Is Regulated by Spine Morphology." *The Journal of neuroscience : the official journal of the Society for Neuroscience* 26(26):7046–55.
- Bae, Jeomil, Bong Hwan Sung, In Ha Cho, and Woo Keun Song. 2012. "F-Actin-Dependent Regulation of NESH Dynamics in Rat Hippocampal Neurons." *PLoS ONE* 7(4):4–15.
- Bannai, Hiroko et al. 2006. "Imaging the lateral diffusion of membrane molecules with quantum dots." *Nature Protocols* 1:2628-34.
- Bannai, Hiroko et al. 2009. "Activity-Dependent Tuning of Inhibitory Neurotransmission Based on GABAAR Diffusion Dynamics." *Neuron* 62:670–82.
- Bates, Mark, Sara a. Jones, and Xiaowei Zhuang. 2013. "Stochastic Optical Reconstruction Microscopy (STORM): A Method for Superresolution Fluorescence Imaging." *Cold Spring Harbor Protocols* 8:498–520.
- Bats, Cecile, Laurent Groc, and Daniel Choquet. 2007. "The Interaction between Stargazin and PSD-95 Regulates AMPA Receptor Surface Trafficking." *Neuron* 53:719–34.
- Baude, Agnes et al. 1993. "The Metabotropic Glutamate Receptor (mGluR1 $\alpha$ ) Is Concentrated at Perisynaptic Membrane of Neuronal Subpopulations as Detected by Immunogold Reaction." *Neuron* 11:771–87.
- Bellot, Alba et al. 2014. "The Structure and Function of Actin Cytoskeleton in Mature Glutamatergic Dendritic Spines." *Brain research* 1573:1–16.

- Bennett, Max R. 1999. "The Early History of the Synapse: From Plato to Sherrington." *Brain Research Bulletin* 50(2):95–118.
- Bennett, Vann, and Jane Healy. 2009. "Membrane Domains Based on Ankyrin and Spectrin Associated with Cell-Cell Interactions." *Cold Spring Harbor perspectives in biology* 1.
- Berg, Howard C. 1983. "Random Walks in Biology." Princeton: Princeton University Press.
- Berning, S., K. I. Willig, H. Steffens, P. Dibaj, and S. W. Hell. 2012. "Nanoscopy in a Living Mouse Brain." *Science* 335(February):551–551.
- Bethge, Philipp, Ronan Chéreau, Elena Avignone, Giovanni Marsicano, and U. Valentin Nägerl. 2013. "Two-Photon Excitation STED Microscopy in Two Colors in Acute Brain Slices." *Biophysical Journal* 104(February):778–85.
- Betzig, Eric et al. 2006. "Imaging Intracellular Fluorescent Proteins at Nanometer Resolution." *Science (New York, N.Y.)* 313(September):1642–45.
- Blanpied, Thomas a., Derek B. Scott, and Michael D. Ehlers. 2002. "Dynamics and Regulation of Clathrin Coats at Specialized Endocytic Zones of Dendrites and Spines." *Neuron* 36:435–49.
- Bliss, T. V, and G. L. Collingridge. 1993. "A Synaptic Model of Memory: Long-Term Potentiation in the Hippocampus." *Nature* 361:31–39.
- Blom, Hans et al. 2013. "Spatial Distribution of DARPP-32 in Dendritic Spines." *PLoS ONE* 8(9):1–9.
- Bloodgood, Brenda L., and Bernardo L. Sabatini. 2005. "Neuronal Activity Regulates Diffusion across the Neck of Dendritic Spines." *Science (New York, N.Y.)* 310:866–69.
- Boeckers, T. M. 2006. "The Postsynaptic Density." *Cell and Tissue Research* 326:409–22.
- Bogdanov, Yury et al. 2006. "Synaptic GABAA Receptors Are Directly Recruited from Their Extrasynaptic Counterparts." *The EMBO journal* 25(18):4381–89.
- Borgdorff, Aren J., and Daniel Choquet. 2002. "Regulation of AMPA Receptor Lateral Movements." *Nature* 417(1999):649–53.
- Bourne, Jennifer, and Kristen M. Harris. 2007. "Do Thin Spines Learn to Be Mushroom Spines That Remember?" *Current Opinion in Neurobiology* 17:381–86.
- Bourne, Jennifer N., and Kristen M. Harris. 2008. "Balancing Structure and Function at Hippocampal Dendritic Spines." *Annual review of neuroscience* 31:47–67.
- Brakeman, P. R. et al. 1997. "Homer: A Protein That Selectively Binds Metabotropic Glutamate Receptors." *Nature* 386:284–88.
- Buckle, B. Y. P. J., and H. L. Haas. 1982. "Universitdtsklinik, 8091." 109–22.
- Calamai, Martino et al. 2009. "Gephyrin Oligomerization Controls GlyR Mobility and Synaptic Clustering." *The Journal of neuroscience : the official journal of the Society for Neuroscience* 29(24):7639–48.
- Capani, Francisco, Maryann E. Martone, Thomas J. Deerinck, and Mark H. Ellisman. 2001. "Selective Localization of High Concentrations of F-Actin in Subpopulations of Dendritic Spines in Rat Central Nervous System : A Three- Dimensional Electron Microscopic Study." 170(February):156 – 70.
- Carrasco, Silvia, and Tobias Meyer. 2011. "STIM Proteins and the Endoplasmic Reticulum-Plasma Membrane Junctions." *Annual review of biochemistry* 80:973–1000.
- Charrier, Cécile et al. 2010. "A Crosstalk between  $\beta 1$  and  $\beta 3$  Integrins Controls Glycine Receptor and Gephyrin Trafficking at Synapses." *Nature neuroscience* 13(11):1388–95.

- Charrier, Cécile, Marie-Virginie Ehrensperger, Maxime Dahan, Sabine Lévi, and Antoine Triller. 2006. "Cytoskeleton Regulation of Glycine Receptor Number at Synapses and Diffusion in the Plasma Membrane." *The Journal of neuroscience : the official journal of the Society for Neuroscience* 26(33):8502–11.
- Chazeau, Anaël et al. 2014. "Nanoscale segregation of actin nucleation and elongation factors determines dendritic spine protrusion." *The EMBO Journal* 33: 2745–64.
- Chen, L. et al. 2000. "Stargazin Regulates Synaptic Targeting of AMPA Receptors by Two Distinct Mechanisms." *Nature* 408(December):936–43.
- Choquet, Daniel, and Antoine Triller. 2013. "The Dynamic Synapse." *Neuron* 80(3):691–703.
- Cingolani, Lorenzo a, and Yukiko Goda. 2008. "Actin in Action: The Interplay between the Actin Cytoskeleton and Synaptic Efficacy." *Nature reviews. Neuroscience* 9(May):344–56.
- Clapp, Peter, Sanjiv V Bhawe, and Paula L. Hoffman. 2008. "How Adaptation of the Brain to Alcohol Leads to Dependence: A Pharmacological Perspective." *Alcohol research & health : the journal of the National Institute on Alcohol Abuse and Alcoholism* 31:310–39.
- Cohen, R. S., S. K. Chung, and D. W. Pfaff. 1985. "Immunocytochemical Localization of Actin in Dendritic Spines of the Cerebral Cortex Using Colloidal Gold as a Probe." *Cellular and molecular neurobiology* 5(3):271–84.
- Courty, Sébastien et al. 2006. "Tracking Individual Proteins in Living Cells Using Single Quantum Dot Imaging." *Methods in enzymology* 414(06):211–28.
- Coussen, Françoise et al. 2002. "Recruitment of the Kainate Receptor Subunit Glutamate Receptor 6 by Cadherin/catenin Complexes." *The Journal of neuroscience : the official journal of the Society for Neuroscience* 22(15):6426–36.
- Cowan, W. M., and E. R. Kandel. 2001. "Kandel's Brief History of Synapse and Synaptic Transmission." *Synapse*:1–87.
- Dahan, Maxime et al. 2003. "Diffusion Dynamics of Glycine Receptors Revealed by Single-Quantum Dot Tracking." *Science (New York, N.Y.)* 302(2000):442–45.
- Dani, Adish, Bo Huang, Joseph Bergan, Catherine Dulac, and Xiaowei Zhuang. 2010. "Superresolution Imaging of Chemical Synapses in the Brain." *Neuron* 68(5):843–56.
- Deller, T., T. Merten, S. U. Roth, P. Mundel, and M. Frotscher. 2000b. "Actin-Associated Protein Synaptopodin in the Rat Hippocampal Formation: Localization in the Spine Neck and Close Association with the Spine Apparatus of Principal Neurons." *The Journal of comparative neurology* 418(2):164–81.
- Deller, T., P. Mundel, and M. Frotscher. 2000a. "Potential Role of Synaptopodin in Spine Motility by Coupling Actin to the Spine Apparatus." *Hippocampus* 10(5):569–81.
- Deller, Thomas et al. 2002. "Laminar Distribution of Synaptopodin in Normal and Reeler Mouse Brain Depends on the Position of Spine-Bearing Neurons." *Journal of Comparative Neurology* 453(January):33–44.
- Deller, Thomas et al. 2003. "Synaptopodin-Deficient Mice Lack a Spine Apparatus and Show Deficits in Synaptic Plasticity." *Proceedings of the National Academy of Sciences of the United States of America* 100(18):10494–99.
- Dempsey, Graham T., Joshua C. Vaughan, Kok Hao Chen, Mark Bates, and Xiaowei Zhuang. 2011. "Evaluation of Fluorophores for Optimal Performance in Localization-Based Super-Resolution Imaging." *Nature Methods* 8(12):1027–36.
- Denk, Winfried et al. 1990. "Two-Photon Laser Scanning Fluorescence Microscopy." (April):73–76.

- Dityatev, Alexander, Melitta Schachner, and Peter Sonderegger. 2010. "The Dual Role of the Extracellular Matrix in Synaptic Plasticity and Homeostasis." *Nature reviews. Neuroscience* 11:735–46.
- Domanov, Yegor a et al. 2011. "Mobility in Geometrically Confined Membranes." *Proceedings of the National Academy of Sciences of the United States of America* 108(31):12605–10.
- Dong, H. et al. 1997. "GRIP: A Synaptic PDZ Domain-Containing Protein That Interacts with AMPA Receptors." *Nature* 386:279–84.
- Dupuis, Julien P. et al. 2014. "Surface Dynamics of GluN2B-NMDA Receptors Controls Plasticity of Maturing Glutamate Synapses." *EMBO Journal* 33(8):842–61.
- Durisc, Nela, Lara Laparra-Cuervo, Angel Sandoval-Álvarez, Joseph Steven Borbely, and Melike Lakadamyali. 2014. "Single-Molecule Evaluation of Fluorescent Protein Photoactivation Efficiency Using an in Vivo Nanotemplate." *Nature methods* 11(2):156–62.
- Ehrensperger, Marie-Virginie, Cyril Hanus, Christian Vannier, Antoine Triller, and Maxime Dahan. 2007. "Multiple Association States between Glycine Receptors and Gephyrin Identified by SPT Analysis." *Biophysical journal* 92(May):3706–18.
- Elias, G. M., L. a B. Elias, P. F. Apostolides, a R. Kriegstein, and R. a Nicoll. 2008. "Differential Trafficking of AMPA and NMDA Receptors by SAP102 and PSD-95 Underlies Synapse Development." *Proceedings of the National Academy of Sciences of the United States of America* 105(52):20953–58.
- Elias, Guillermo M., and Roger a. Nicoll. 2007. "Synaptic Trafficking of Glutamate Receptors by MAGUK Scaffolding Proteins." *Trends in Cell Biology* 17(7):343–52.
- Engelman, Donald M. 2005. "Membranes Are More Mosaic than Fluid." *Nature* 438(December):578–80.
- Enz, Ralf. 2012. "Structure of Metabotropic Glutamate Receptor C-Terminal Domains in Contact with Interacting Proteins." *Frontiers in Molecular Neuroscience* 5(April):1–11.
- Ewers, Helge et al. 2014. "A Septin-Dependent Diffusion Barrier at Dendritic Spine Necks." *PLoS ONE* 9:e113916.
- Fiala, J. C., M. Feinberg, V. Popov, and K. M. Harris. 1998. "Synaptogenesis via Dendritic Filopodia in Developing Hippocampal Area CA1." *The Journal of neuroscience: the official journal of the Society for Neuroscience* 18(21):8900–8911.
- Fifková, E., J. a Markham, and R. J. Delay. 1983. "Calcium in the Spine Apparatus of Dendritic Spines in the Dentate Molecular Layer." *Brain research* 266:163–68.
- Fischer, Maria, Stefanie Kaech, Darko Knutti, and Andrew Matus. 1998. "Rapid Actin-Based Plasticity in Dendritic Spines." *Neuron* 20:847–54.
- Frischknecht, Renato et al. 2009. "Brain Extracellular Matrix Affects AMPA Receptor Lateral Mobility and Short-Term Synaptic Plasticity." *Neuroforum* 15(7):94–95.
- Frost, Nicholas a., Hari Shroff, Huihui Kong, Eric Betzig, and Thomas a. Blanpied. 2010. "Single-Molecule Discrimination of Discrete Perisynaptic and Distributed Sites of Actin Filament Assembly within Dendritic Spines." *Neuron* 67(1):86–99.
- Fujiwara, Takahiro, Ken Ritchie, Hideji Murakoshi, Ken Jacobson, and Akihiro Kusumi. 2002. "Phospholipids Undergo Hop Diffusion in Compartmentalized Cell Membrane." *Journal of Cell Biology* 157:1071–81.
- Fukazawa, Yugo et al. 2003. "Hippocampal LTP Is Accompanied by Enhanced F-Actin Content within the Dendritic Spine That Is Essential for Late LTP Maintenance in Vivo." *Neuron* 38:447–60.
- Gerrit Van Meer, and Kai Simons. 1994. "Lipid Polarity and Sorting in Epithelial Cells." *Current Topics in Membranes* 40:539–63

- Gerrow, K., and a. Triller. 2014. "GABAA Receptor Subunit Composition and Competition at Synapses Are Tuned by GABAB Receptor Activity." *Molecular and Cellular Neuroscience* 60:97–107.
- Gerrow, Kimberly, and Antoine Triller. 2010. "Synaptic Stability and Plasticity in a Floating World." *Current Opinion in Neurobiology* 20(5):631–39.
- Gouzer, Géraldine, Christian G. Specht, Laure Allain, Toru Shinoe, and Antoine Triller. 2014. "Benzodiazepine-Dependent Stabilization of GABAA Receptors at Synapses." *Molecular and Cellular Neuroscience* 63:101–13.
- Gray, E. G. 1959. "Axo-Somatic and Axo-Dendritic Synapses of the Cerebral Cortex." *Journal of anatomy* 93:420–33.
- Gray, Noah W., Robby M. Weimer, Ingrid Bureau, and Karel Svoboda. 2006. "Rapid Redistribution of Synaptic PSD-95 in the Neocortex in Vivo." *PLoS Biology* 4(11):2065–75.
- Grazi, E., P. Cuneo, E. Magri, and C. Schwienbacher. 1992. "Preferential Binding of A-Actinin to Actin Bundles." *FEBS Letters* 314(3):348–50.
- Greengard, Paul, Patrick B. Allen, and Angus C. Nairn. 1999. "Beyond the Dopamine Receptor: The DARPP-32/protein Phosphatase-1 Cascade." *Neuron* 23:435–47.
- Grienberger, Christine, and Arthur Konnerth. 2012. "Imaging Calcium in Neurons." *Neuron* 73(5):862–85.
- Groc, L. et al. 2006. "NMDA Receptor Surface Trafficking Depends on NR2A/NR2B Subunits." 103(49).
- Groc, Laurent et al. 2004. "Differential Activity-Dependent Regulation of the Lateral Mobilities of AMPA and NMDA Receptors." *Nature neuroscience* 7(7):695–96.
- Groc, Laurent, Daniel Choquet, et al. 2007. "NMDA Receptor Surface Trafficking and Synaptic Subunit Composition Are Developmentally Regulated by the Extracellular Matrix Protein Reelin." *The Journal of neuroscience : the official journal of the Society for Neuroscience* 27(38):10165–75.
- Groc, Laurent, Mathieu Lafourcade, et al. 2007. "Surface Trafficking of Neurotransmitter Receptor: Comparison between Single-Molecule/quantum Dot Strategies." *The Journal of neuroscience : the official journal of the Society for Neuroscience* 27(46):12433–37.
- Grooms, Sonja Y. et al. 2006. "Activity Bidirectionally Regulates AMPA Receptor mRNA Abundance in Dendrites of Hippocampal Neurons." *The Journal of neuroscience : the official journal of the Society for Neuroscience* 26(32):8339–51.
- Grunditz, Asa, Niklaus Holbro, Lei Tian, Yi Zuo, and Thomas G. Oertner. 2008. "Spine Neck Plasticity Controls Postsynaptic Calcium Signals through Electrical Compartmentalization." *The Journal of neuroscience : the official journal of the Society for Neuroscience* 28(50):13457–66.
- Harris, K. M., and S. B. Kater. 1994. "Dendritic Spines: Cellular Specializations Imparting Both Stability and Flexibility to Synaptic Function." *Annual review of neuroscience* 17:341–71.
- Harris, K. M., and J. K. Stevens. 1989. "Dendritic Spines of CA 1 Pyramidal Cells in the Rat Hippocampus: Serial Electron Microscopy with Reference to Their Biophysical Characteristics." *The Journal of neuroscience : the official journal of the Society for Neuroscience* 9(August):2982–97.
- Harris, Kristen M., and Richard J. Weinberg. 2012. "Ultrastructure of Synapses in the Mammalian Brain." *Cold Spring Harbor Perspectives in Biology* 4:7.
- Heilemann, Mike et al. 2008. "Subdiffraction-Resolution Fluorescence Imaging with Conventional Fluorescent Probes." *Angewandte Chemie - International Edition* 47:6172–76.
- Hell, Stefan W. 2003. "Toward Fluorescence Nanoscopy." *Nature biotechnology* 21(11):1347–55.
- Hennekinne, Laetitia, Sabrina Colasse, Antoine Triller, and Marianne Renner. 2013. "Differential Control of Thrombospondin over Synaptic Glycine and AMPA Receptors in Spinal Cord Neurons." *The Journal of neuroscience : the official journal of the Society for Neuroscience* 33(28):11432–39.

- Henriques, Ricardo, and Musa M. Mhlanga. 2009. "PALM and STORM: What Hides beyond the Rayleigh Limit?" *Biotechnology Journal* 4:846–57.
- Hering, H., and M. Sheng. 2001. "Dendritic Spines: Structure, Dynamics and Regulation." *Nature reviews. Neuroscience* 2(12):880–88.
- Hoe, Hyang Sook, Ji Yun Lee, and Daniel T. S. Pak. 2009. "Combinatorial Morphogenesis of Dendritic Spines and Filopodia by SPAR and  $\alpha$ -actinin2." *Biochemical and Biophysical Research Communications* 384(1):55–60.
- Holbro, Niklaus, Asa Grunditz, and Thomas G Oertner. 2009. "Differential Distribution of Endoplasmic Reticulum Controls Metabotropic Signaling and Plasticity at Hippocampal Synapses." *Proceedings of the National Academy of Sciences of the United States of America* 106(35): 15055–60.
- Holtmaat, Anthony, Linda Wilbrecht, Graham W. Knott, Egbert Welker, and Karel Svoboda. 2006. "Experience-Dependent and Cell-Type-Specific Spine Growth in the Neocortex." *Nature* 441(June):979–83.
- Honkura, Naoki, Masanori Matsuzaki, Jun Noguchi, Graham C. R. Ellis-Davies, and Haruo Kasai. 2008. "The Subspine Organization of Actin Fibers Regulates the Structure and Plasticity of Dendritic Spines." *Neuron* 57:719–29.
- Hönscher, Carina, and Christian Ungermann. 2014. "A Close-up View of Membrane Contact Sites between the Endoplasmic Reticulum and the Endolysosomal System: From Yeast to Man." *Critical reviews in biochemistry and molecular biology* 9238(3):1–7.
- Hotulainen, Pirta, and Casper C. Hoogenraad. 2010. "Actin in Dendritic Spines: Connecting Dynamics to Function." *The Journal of cell biology* 189(4):619–29.
- Howard, Mackenzie a, Guillermo M. Elias, Laura a B. Elias, Wojciech Swat, and Roger a Nicoll. 2010. "The Role of SAP97 in Synaptic Glutamate Receptor Dynamics." *Proceedings of the National Academy of Sciences of the United States of America* 107(8):3805–10.
- Huang, Bo, Hazen Babcock, and Xiaowei Zhuang. 2010. "Breaking the Diffraction Barrier: Super-Resolution Imaging of Cells." *Cell* 143(7):1047–58.
- Huang, Bo, Mark Bates, and Xiaowei Zhuang. 2009. "Super-Resolution Fluorescence Microscopy." *Annual review of biochemistry* 78:993–1016.
- Huganir, Richard L., and Roger a. Nicoll. 2013. "AMPA Receptors and Synaptic Plasticity: The Last 25 Years." *Neuron* 80(3):704–17.
- Iino, R., I. Koyama, and a Kusumi. 2001. "Single Molecule Imaging of Green Fluorescent Proteins in Living Cells: E-Cadherin Forms Oligomers on the Free Cell Surface." *Biophysical journal* 80(March):2667–77.
- Irie, M. et al. 1997. "Binding of Neuroligins to PSD-95." *Science (New York, N.Y.)* 277(September):1511–15.
- Izeddin, Ignacio et al. 2011. "Super-Resolution Dynamic Imaging of Dendritic Spines Using a Low-Affinity Photoconvertible Actin Probe." *PloS one* 6(1):e15611.
- Jacob, Tija C. et al. 2005. "Gephyrin Regulates the Cell Surface Dynamics of Synaptic GABA<sub>A</sub> Receptors." *The Journal of neuroscience : the official journal of the Society for Neuroscience* 25(45):10469–78.
- Jedlicka, Peter, Andreas Vlachos, Stephan W. Schwarzacher, and Thomas Deller. 2008. "A Role for the Spine Apparatus in LTP and Spatial Learning." *Behavioural Brain Research* 192:12–19.
- Jones, Sara a, Sang-Hee Shim, Jiang He, and Xiaowei Zhuang. 2011. "Fast, Three-Dimensional Super-Resolution Imaging of Live Cells." *Nature methods* 8(6):499–508.
- Kalinowska, Magdalena et al. 2015. "Actinin-4 Governs Dendritic Spine Dynamics and Promotes Their Remodeling by Metabotropic Glutamate Receptors." *Journal of Biological Chemistry* jbc.M115.640136.

- Kelly, P. T., T. L. McGuinness, and P. Greengard. 1984. "Evidence That the Major Postsynaptic Density Protein Is a Component of a Ca<sup>2+</sup>/calmodulin-Dependent Protein Kinase." *Proceedings of the National Academy of Sciences of the United States of America* 81(February):945–49.
- Kennedy, Matthew J., and Michael D. Ehlers. 2006. "Organelles and Trafficking Machinery for Postsynaptic Plasticity." *Annual review of neuroscience* 29:325–62.
- Khosravani, Houman, Christophe Altier, Gerald W. Zamponi, and Michael a. Colicos. 2005. "The Arg473Cys-Neuroigin-1 Mutation Modulates NMDA Mediated Synaptic Transmission and Receptor Distribution in Hippocampal Neurons." *FEBS Letters* 579:6587–94.
- Kneussel, M. et al. 1999. "Loss of Postsynaptic GABA(A) Receptor Clustering in Gephyrin-Deficient Mice." *The Journal of neuroscience: the official journal of the Society for Neuroscience* 19(21):9289–97.
- Korkotian, Eduard, Michael Frotscher, and Menahem Segal. 2014. "Synaptopodin Regulates Spine Plasticity: Mediation by Calcium Stores." *The Journal of neuroscience: the official journal of the Society for Neuroscience* 34(35):11641–51.
- Korkotian, Eduard, David Holcman, and Menahem Segal. 2004. "Dynamic Regulation of Spine-Dendrite Coupling in Cultured Hippocampal Neurons." *European Journal of Neuroscience* 20:2649–63.
- Kornau, H. C., L. T. Schenker, M. B. Kennedy, and P. H. Seeburg. 1995. "Domain Interaction between NMDA Receptor Subunits and the Postsynaptic Density Protein PSD-95." *Science (New York, N.Y.)* 269:1737–40.
- Korobova, F., and Svitkina, T. 2010. "Molecular architecture of synaptic actin cytoskeleton in hippocampal neurons reveals a mechanism of dendritic spine morphogenesis." *Molecular Biology of the Cell* 21: 165-76.
- Kremerskothen, J. et al. 2002. "Brain-Specific Splicing of  $\alpha$ -Actinin 1 mRNA." *Biochemical and Biophysical Research Communications* 295:678–81.
- Kremerskothen, Joachim, Christian Plaas, Stefan Kindler, Michael Frotscher, and Angelika Barnekow. 2005. "Synaptopodin, a Molecule Involved in the Formation of the Dendritic Spine Apparatus, Is a Dual Actin/ $\alpha$ -Actinin Binding Protein." *Journal of neurochemistry* 92(3):597–606.
- Kuriu, Toshihiko, Akihiro Inoue, Haruhiko Bito, Kenji Sobue, and Shigeo Okabe. 2006. "Differential Control of Postsynaptic Density Scaffolds via Actin-Dependent and -Independent Mechanisms." *The Journal of neuroscience: the official journal of the Society for Neuroscience* 26(29):7693–7706.
- Kusters, Remy, Lukas C. Kapitein, Casper C. Hoogenraad, and Cornelis Storm. 2013. "Shape-Induced Asymmetric Diffusion in Dendritic Spines Allows Efficient Synaptic AMPA Receptor Trapping." *Biophysical Journal* 105(12):2743–50.
- Kusumi, Akihiro et al. 2005. "Paradigm Shift of the Plasma Membrane Concept from the Two-Dimensional Continuum Fluid to the Partitioned Fluid: High-Speed Single-Molecule Tracking of Membrane Molecules." *Annual review of biophysics and biomolecular structure* 34:351–78.
- Kusumi, Akihiro et al. 2012. "Dynamic Organizing Principles of the Plasma Membrane That Regulate Signal Transduction: Commemorating the Fortieth Anniversary of Singer and Nicolson's Fluid-Mosaic Model." *Annual Review of Cell and Developmental Biology* 28:215–50.
- Ladépêche, Laurent, Julien Pierre Dupuis, and Laurent Groc. 2014. "Surface Trafficking of NMDA Receptors: Gathering from a Partner to Another." *Seminars in Cell and Developmental Biology* 27:3–13.
- Lee, Sang-Hyuk, Jae Yen Shin, Antony Lee, and Carlos Bustamante. 2012. "Counting Single Photoactivatable Fluorescent Molecules by Photoactivated Localization Microscopy (PALM)." *Proceedings of the National Academy of Sciences of the United States of America* 109(43):17436–41.
- Lévi, Sabine et al. 2008. "Homeostatic Regulation of Synaptic GlyR Numbers Driven by Lateral Diffusion." *Neuron* 59(Div):261–73.

- Lévi, Sabine, Maxime Dahan, Antoine Triller, and Sabine Le. 2012. "Labeling Neuronal Membrane Receptors with Quantum Dots Protocol Labeling Neuronal Membrane Receptors with Quantum Dots." 296–301.
- Li, Zheng, Ken Ichi Okamoto, Yasunori Hayashi, and Morgan Sheng. 2004. "The Importance of Dendritic Mitochondria in the Morphogenesis and Plasticity of Spines and Synapses." *Cell* 119:873–87.
- Lois, Carlos, Elizabeth J. Hong, Shirley Pease, Eric J. Brown, and David Baltimore. 2002. "Germline Transmission and Tissue-Specific Expression of Transgenes Delivered by Lentiviral Vectors." *Science (New York, N.Y.)* 295(February):868–72.
- López-Muñoz, Francisco, and Cecilio Alamo. 2009. "Historical Evolution of the Neurotransmission Concept." *Journal of Neural Transmission* 116:515–33.
- Lu, Jiuyi et al. 2007. "Postsynaptic Positioning of Endocytic Zones and AMPA Receptor Cycling by Physical Coupling of Dynamin-3 to Homer." *Neuron* 55:874–89.
- Lujan, R., Z. Nusser, J. D. Roberts, R. Shigemoto, and P. Somogyi. 1996. "Perisynaptic Location of Metabotropic Glutamate Receptors mGluR1 and mGluR5 on Dendrites and Dendritic Spines in the Rat Hippocampus." *The European journal of neuroscience* 8:1488–1500.
- Luján, Rafael, J. David B. Roberts, Ryuichi Shigemoto, Hitoshi Ohishi, and Peter Somogyi. 1997. "Differential Plasma Membrane Distribution of Metabotropic Glutamate Receptors mGluR1 $\alpha$ , mGluR2 and mGluR5, Relative to Neurotransmitter Release Sites." *Journal of Chemical Neuroanatomy* 13:219–41.
- Maiti, Panchanan, Jayeeta Manna, and Michael P. McDonald. 2015. "Merging Advanced Technologies with Classical Methods to Uncover Dendritic Spine Dynamics: A Hot Spot of Synaptic Plasticity." *Neuroscience Research* 1–13.
- Majewska, a, a Tashiro, and R. Yuste. 2000. "Regulation of Spine Calcium Dynamics by Rapid Spine Motility." *The Journal of neuroscience: the official journal of the Society for Neuroscience* 20(22):8262–68.
- Malinow, Roberto, and Robert C. Malenka. 2002. "AMPA Receptor Trafficking and Synaptic Plasticity." *Annual review of neuroscience* 25:103–26.
- Matsuo, Naoki, Leon Reijmers, and Mark Mayford. 2008. "Spine-Type-Specific Recruitment of Newly Synthesized AMPA Receptors with Learning." *Science (New York, N.Y.)* 319(February):1104–7.
- Matsuzaki Masanori, Honkura Naoki, Graham C.R. Ellis-Davies and Kasai Haruo. 2004. "Structural Basis of Long-Term Potentiation in Single Dendritic Spines." *Nature* 429(June):761–66.
- Matus, a. 2000. "Actin-Based Plasticity in Dendritic Spines." *Science (New York, N.Y.)* 290(October):754–58.
- Meier, J., C. Vannier, a Sergé, a Triller, and D. Choquet. 2001. "Fast and Reversible Trapping of Surface Glycine Receptors by Gephyrin." *Nature neuroscience* 4:253–60.
- Manley, Suliana et al. 2008. "High-Density mapping of single-molecule trajectories with photoactivated localization microscopy." *Nature Methods* 2:155–57.
- Mockett, Bruce G. et al. 2011. "Calcium/calmodulin-Dependent Protein Kinase II Mediates Group I Metabotropic Glutamate Receptor-Dependent Protein Synthesis and Long-Term Depression in Rat Hippocampus." *The Journal of neuroscience: the official journal of the Society for Neuroscience* 31(20):7380–91.
- Mondin, M. et al. 2011. "Neurexin-Neuroigin Adhesions Capture Surface-Diffusing AMPA Receptors through PSD-95 Scaffolds." *Journal of Neuroscience* 31(38):13500–515.
- Moss, S. J., and T. G. Smart. 2001. "Constructing Inhibitory Synapses." *Nature reviews. Neuroscience* 2(April):240–50.

- Muir, James et al. 2010. "NMDA Receptors Regulate GABAA Receptor Lateral Mobility and Clustering at Inhibitory Synapses through Serine 327 on the  $\gamma 2$  Subunit." *Proceedings of the National Academy of Sciences of the United States of America* 107:16679–84.
- Mukherjee, J. et al. 2011. "The Residence Time of GABAARs at Inhibitory Synapses Is Determined by Direct Binding of the Receptor 1 Subunit to Gephyrin." *Journal of Neuroscience* 31(41):14677–87.
- Mundel, P. et al. 1997. "Synaptopodin: An Actin-Associated Protein in Telencephalic Dendrites and Renal Podocytes." *The Journal of cell biology* 139(1):193–204.
- Mysore, Shreesh P., Chin-Yin Tai, and Erin M. Schuman. 2007. "Effects of N-Cadherin Disruption on Spine Morphological Dynamics." *Frontiers in cellular neuroscience* 1(December):1.
- Nägerl, U. Valentin, Katrin I. Willig, Birka Hein, Stefan W. Hell, and Tobias Bonhoeffer. 2008. "Live-Cell Imaging of Dendritic Spines by STED Microscopy." *Proceedings of the National Academy of Sciences of the United States of America* 105:18982–87.
- Nakagawa, Terunaga, John a. Engler, and Morgan Sheng. 2004. "The Dynamic Turnover and Functional Roles of  $\alpha$ -Actinin in Dendritic Spines." *Neuropharmacology* 47:734–45.
- Noguchi, Jun, Masanori Matsuzaki, Graham C. R. Ellis-Davies, and Haruo Kasai. 2005. "Spine-Neck Geometry Determines NMDA Receptor-Dependent  $Ca^{2+}$  Signaling in Dendrites." *Neuron* 46:609–22.
- Nusser, Z. 1994. "Subsynaptic Segregation of Metabotropic and Ionotropic Glutamate Receptors as Revealed by Immunogold Localization." *Neuroscience* 61(3):421–27.
- Oertner, Thomas G., and Andrew Matus. 2005. "Calcium Regulation of Actin Dynamics in Dendritic Spines." *Cell Calcium* 37(December 2004):477–82.
- Okabe, Shigeo. 2007. "Molecular Anatomy of the Postsynaptic Density." *Molecular and Cellular Neuroscience* 34:503–18.
- Okamoto, Ken-Ichi, Takeharu Nagai, Atsushi Miyawaki, and Yasunori Hayashi. 2004. "Rapid and Persistent Modulation of Actin Dynamics Regulates Postsynaptic Reorganization Underlying Bidirectional Plasticity." *Nature neuroscience* 7(10):1104–12.
- Okamoto, Ken-Ichi, Radhakrishnan Narayanan, Sang H. Lee, Kazuyoshi Murata, and Yasunori Hayashi. 2007. "The Role of CaMKII as an F-Actin-Bundling Protein Crucial for Maintenance of Dendritic Spine Structure." *Proceedings of the National Academy of Sciences of the United States of America* 104:6418–23.
- Okubo-Suzuki, Reiko, Daisuke Okada, Mariko Sekiguchi, and Kaoru Inokuchi. 2008. "Synaptopodin Maintains the Neural Activity-Dependent Enlargement of Dendritic Spines in Hippocampal Neurons." *Molecular and Cellular Neuroscience* 38(2):266–76.
- Opazo, Patricio, Matthieu Sainlos, and Daniel Choquet. 2012. "Regulation of AMPA Receptor Surface Diffusion by PSD-95 Slots." *Current Opinion in Neurobiology* 22(3):453–60.
- Orth, Carlos Bas et al. 2005. "Lamina-Specific Distribution of Synaptopodin, an Actin-Associated Molecule Essential for the Spine Apparatus, in Identified Principal Cell Dendrites of the Mouse Hippocampus." *Journal of Comparative Neurology* 487(August 2004):227–39.
- Orth, Carlos Bas et al. 2007. "Loss of the Cisternal Organelle in the Axon Initial Segment of Cortical Neurons in Synaptopodin-Deficient Mice." *Journal of Comparative Neurology* 504:441–49
- Ostroff, Linnaea E., John C. Fiala, Brenda Allwardt, and Kristen M. Harris. 2002. "Polyribosomes Redistribute from Dendritic Shafts into Spines with Enlarged Synapses during LTP in Developing Rat Hippocampal Slices." *Neuron* 35:535–45.
- Ouyang, Yannan et al. 2007. "Hippocampal Seizures Cause Depolymerization of Filamentous Actin in Neurons Independent of Acute Morphological Changes." *Brain Research* 1143:238–46.

- Perroy, Julie et al. 2008. "Direct Interaction Enables Cross-Talk between Ionotropic and Group I Metabotropic Glutamate Receptors." *Journal of Biological Chemistry* 283(11):6799–6805.
- Petralia, Ronald S., Nathalie Sans, Ya Xian Wang, and Robert J. Wenthold. 2005. "Ontogeny of Postsynaptic Density Proteins at Glutamatergic Synapses." *Molecular and Cellular Neuroscience* 29:436–52.
- Petrini, Enrica Maria et al. 2009. "Endocytic Trafficking and Recycling Maintain a Pool of Mobile Surface AMPA Receptors Required for Synaptic Potentiation." *Neuron* 63(1):92–105.
- Pinaud, Fabien, Samuel Clarke, Assa Sittner, and Maxime Dahan. 2010. "Probing Cellular Events, One Quantum Dot at a Time." *Nature methods* 7(4):275–85.
- Pozo, K. et al. 2012. "3 Integrin Interacts Directly with GluA2 AMPA Receptor Subunit and Regulates AMPA Receptor Expression in Hippocampal Neurons." *Proceedings of the National Academy of Sciences* 109(4):1323–28.
- Purgert, Carolyn a et al. 2014. "Intracellular mGluR5 Can Mediate Synaptic Plasticity in the Hippocampus." *The Journal of neuroscience : the official journal of the Society for Neuroscience* 34(13):4589–98.
- Racine, Victor et al. 2007. "Visualization and Quantification of Vesicle Trafficking on a Three-Dimensional Cytoskeleton Network in Living Cells." *Journal of Microscopy* 225(December 2005):214–28.
- Ramadurai, S., a Holt, and V. V Krasnikov. 2009. "Lateral Diffusion of Membrane Proteins." *Journal of the American Chemical Society* (16):12650–56.
- Renner, Marianne et al. 2010. "Deleterious Effects of Amyloid B Oligomers Acting as an Extracellular Scaffold for mGluR5." *Neuron* 66(5):739–54.
- Renner, Marianne et al. 2011. "Lateral Diffusion on Tubular Membranes: Quantification of Measurements Bias." *PLoS ONE* 6(9).
- Renner, Marianne, Daniel Choquet, and Antoine Triller. 2009. "Control of the Postsynaptic Membrane Viscosity." *The Journal of neuroscience : the official journal of the Society for Neuroscience* 29(9):2926–37.
- Renner, Marianne, Christian G. Specht, and Antoine Triller. 2008. "Molecular Dynamics of Postsynaptic Receptors and Scaffold Proteins." *Current Opinion in Neurobiology* 18(Figure 1):532–40.
- Ribrault, C. et al. 2011. "Syntaxin1A Lateral Diffusion Reveals Transient and Local SNARE Interactions." *Journal of Neuroscience* 31(48):17590–602.
- Robison, a. J., Martha a. Bass, et al. 2005a. "Multivalent Interactions of Calcium/calmodulin-Dependent Protein Kinase II with the Postsynaptic Density Proteins NR2B, Densin-180, and  $\alpha$ -Actinin-2." *Journal of Biological Chemistry* 280(42):35329–36.
- Robison, a. J., Ryan K. Bartlett, Martha a. Bass, and Roger J. Colbran. 2005b. "Differential Modulation of Ca<sup>2+</sup>/calmodulin-Dependent Protein Kinase II Activity by Regulated Interactions with N-Methyl-D-Aspartate Receptor NR2B Subunits and  $\alpha$ -Actinin." *Journal of Biological Chemistry* 280(47):39316–23.
- Rochefort, Nathalie L., and Arthur Konnerth. 2012. "Dendritic Spines: From Structure to in Vivo Function." *EMBO reports* 13(8):699–708.
- Rostaing, Philippe et al. 2006. "Analysis of Synaptic Ultrastructure without Fixative Using High-Pressure Freezing and Tomography." *European Journal of Neuroscience* 24(October 2005):3463–74.
- Rowland, Ashley a., and Gia K. Voeltz. 2012. "Endoplasmic Reticulum–mitochondria Contacts: Function of the Junction." *Nature Reviews Molecular Cell Biology* 13(10):607–25.
- Rust, Michael J., Mark Bates, and Xiaowei Zhuang. 2006. "Sub-Diffraction-Limit Imaging by Stochastic Optical Reconstruction Microscopy (STORM)." *Nature methods* 3(10):793–95.

- Sabatini, Bernardo L., Thomas G. Oertner, and Karel Svoboda. 2002. "The Life Cycle of Ca<sup>2+</sup> Ions in Dendritic Spines." *Neuron* 33:439–52.
- Saffman, P. G., and M. Delbrück. 1975. "Brownian Motion in Biological Membranes." *Proceedings of the National Academy of Sciences of the United States of America* 72(April):3111–13.
- Saiepour, Leila et al. 2010. "Complex Role of Collybistin and Gephyrin in GABA<sub>A</sub> Receptor Clustering." *Journal of Biological Chemistry* 285(38):29623–31.
- Sala, Carlo et al. 2001. "Regulation of Dendritic Spine Morphology and Synaptic Function by Shank and Homer." *Neuron* 31:115–30.
- Sala, Carlo, and Menahem Segal. 2014. "Dendritic Spines: The Locus of Structural and Functional Plasticity." *Physiological reviews* 94:141–88.
- Sans, N. et al. 2000. "A Developmental Change in NMDA Receptor-Associated Proteins at Hippocampal Synapses." *The Journal of neuroscience : the official journal of the Society for Neuroscience* 20(3):1260–71.
- Saxton, M. J., and K. Jacobson. 1997. "Single-Particle Tracking: Applications to Membrane Dynamics." *Annual review of biophysics and biomolecular structure* 26:373–99.
- Sbalzarini, Ivo F., Arnold Hayer, Ari Helenius, and Petros Koumoutsakos. 2006. "Simulations of (an) isotropic Diffusion on Curved Biological Surfaces." *Biophysical journal* 90(February):878–85.
- Schulz, Torsten W. et al. 2004. "Actin/alpha-Actinin-Dependent Transport of AMPA Receptors in Dendritic Spines: Role of the PDZ-LIM Protein RIL." *The Journal of neuroscience : the official journal of the Society for Neuroscience* 24(39):8584–94.
- Scott, Lena et al. 2006. "Allosteric Changes of the NMDA Receptor Trap Diffusible Dopamine 1 Receptors in Spines." *Proceedings of the National Academy of Sciences of the United States of America* 103(Track II):762–67.
- Serge, Arnauld, Lawrence Fourgeaud, Agnes Hemar, and Daniel Choquet. 2003. "Active Surface Transport of Metabotropic Glutamate Receptors through Binding to Microtubules and Actin Flow." *Journal of cell science* 116:5015–22.
- Sergé, Arnauld, Lawrence Fourgeaud, Agnès Hémar, and Daniel Choquet. 2002a. "Receptor Activation and Homer Differentially Control the Lateral Mobility of Metabotropic Glutamate Receptor 5 in the Neuronal Membrane." *The Journal of neuroscience : the official journal of the Society for Neuroscience* 22(10):3910–20.
- Sergé, Arnauld, Lawrence Fourgeaud, Agnès Hémar, and Daniel Choquet. 2002b. "Receptor Activation and Homer Differentially Control the Lateral Mobility of Metabotropic Glutamate Receptor 5 in the Neuronal Membrane." *The Journal of neuroscience : the official journal of the Society for Neuroscience* 22(10):3910–20.
- Sharma, Pranav et al. 2004. "Nanoscale Organization of Multiple GPI-Anchored Proteins in Living Cell Membranes." *Cell* 116:577–89.
- Sheng, Morgan, and Casper C. Hoogenraad. 2007. "The Postsynaptic Architecture of Excitatory Synapses: A More Quantitative View." *Annual review of biochemistry* 76:823–47.
- Shipman, Seth L. et al. 2011. "Functional Dependence of Neuroligin on a New Non-PDZ Intracellular Domain." *Nature neuroscience* 14(6):718–26.
- Shirao, Tomoaki, and Christian González-Billault. 2013. "Actin Filaments and Microtubules in Dendritic Spines." *Journal of Neurochemistry* 126:155–64.
- Shrivastava, Amulya Nidhi et al. 2013. "B-Amyloid and ATP-Induced Diffusional Trapping of Astrocyte and Neuronal Metabotropic Glutamate Type-5 Receptors." *Glia*.
- Sia, Gek Ming et al. 2007. "Interaction of the N-Terminal Domain of the AMPA Receptor GluR4 Subunit with the Neuronal Pentraxin NP1 Mediates GluR4 Synaptic Recruitment." *Neuron* 55:87–102.

- Singer, S. J., and G. L. Nicolson. 1972. "The Fluid Mosaic Model of the Structure of Cell Membranes." *Science (New York, N.Y.)* 175(4023):720–31.
- Smith, Katharine R. et al. 2014. "Psychiatric Risk Factor ANK3/Ankyrin-G Nanodomains Regulate the Structure and Function of Glutamatergic Synapses." *Neuron* 84:399–415.
- Soler-Illavina, Gilberto J. et al. 2013. "Supplemental Information Leucine-Rich Repeat Transmembrane Proteins Are Essential for Maintenance of Long-Term Potentiation." *Neuron* 79:439–46.
- Spacek, J. 1985. "Three-Dimensional Analysis of Dendritic Spines. II. Spine Apparatus and Other Cytoplasmic Components." *Anatomy and embryology* 171:235–43.
- Spacek, J., and K. M. Harris. 1997. "Three-Dimensional Organization of Smooth Endoplasmic Reticulum in Hippocampal CA1 Dendrites and Dendritic Spines of the Immature and Mature Rat." *The Journal of neuroscience : the official journal of the Society for Neuroscience* 17(1):190–203.
- Specht, Christian G. et al. 2011. "Regulation of Glycine Receptor Diffusion Properties and Gephyrin Interactions by Protein Kinase C." *The EMBO journal* 30(18):3842–53.
- Specht, Christian G. et al. 2013. "Article Quantitative Nanoscopy of Inhibitory Synapses : Counting Gephyrin Molecules and Receptor Binding Sites." *Neuron* 1–14.
- Spudich, J. a. 1973. "Effects of Cytochalasin B on Actin Filaments." *Cold Spring Harbor Symposia on Quantitative Biology* 37(October):585–93.
- Star, Erin N., David J. Kwiatkowski, and Venkatesh N. Murthy. 2002. "Rapid Turnover of Actin in Dendritic Spines and Its Regulation by Activity." *Nature neuroscience* 5:239–46.
- Steward, Oswald, and Erin M. Schuman. 2003. "Compartmentalized Synthesis and Degradation of Proteins in Neurons." *Neuron* 40:347–59.
- Suzuki, Kenichi, Ken Ritchie, Eriko Kajikawa, Takahiro Fujiwara, and Akihiro Kusumi. 2005. "Rapid Hop Diffusion of a G-Protein-Coupled Receptor in the Plasma Membrane as Revealed by Single-Molecule Techniques." *Biophysical journal* 88(5):3659–80.
- Svoboda, K., D. W. Tank, and W. Denk. 1996. "Direct Measurement of Coupling between Dendritic Spines and Shafts." *Science (New York, N.Y.)* 272(18):716–19.
- Sztybel, Kinga, and Michael Tymianski. 2010. "Calcium, Ischemia and Excitotoxicity." *Cell Calcium* 47(2):122–29.
- Tada, Tomoko et al. 2007. "Role of Septin Cytoskeleton in Spine Morphogenesis and Dendrite Development in Neurons." *Current Biology* 17:1752–58.
- Tanaka, Jun-Ichi et al. 2008. "Protein Synthesis and Neurotrophin-Dependent Structural Plasticity of Single Dendritic Spines." *Science (New York, N.Y.)* 319(December):1683–87.
- Tardin, Catherine, Laurent Cognet, Cécile Bats, Brahim Lounis, and Daniel Choquet. 2003. "Direct Imaging of Lateral Movements of AMPA Receptors inside Synapses." *EMBO Journal* 22(18):4656–65.
- Thomas, Philip, Martin Mortensen, Alastair M. Hosie, and Trevor G. Smart. 2005. "Dynamic Mobility of Functional GABAA Receptors at Inhibitory Synapses." *Nature neuroscience* 8(7):889–97.
- Tomita, Susumu, Valentin Stein, Tim J. Stocker, Roger a. Nicoll, and David S. Bredt. 2005. "Bidirectional Synaptic Plasticity Regulated by Phosphorylation of Stargazin-like TARPs." *Neuron* 45:269–77.
- Tønnesen, Jan, Gergely Katona, Balázs Rózsa, and U. Valentin Nägerl. 2014. "Spine Neck Plasticity Regulates Compartmentalization of Synapses." *Nature neuroscience* 17(5):678–85.
- Tovar, K., and G. Westbrook. 2002. "Mobile NMDA Receptors at Hippocampal Synapses." *Neuron* 34:255–64.

- Tretter, Verena et al. 2008. "The Clustering of GABA(A) Receptor Subtypes at Inhibitory Synapses Is Facilitated via the Direct Binding of Receptor Alpha 2 Subunits to Gephyrin." *The Journal of neuroscience : the official journal of the Society for Neuroscience* 28(6):1356–65.
- Tretter, Verena et al. 2012. "Gephyrin, the Enigmatic Organizer at GABAergic Synapses." *Frontiers in Cellular Neuroscience* 6(May):1–16.
- Triller, Antoine, and Daniel Choquet. 2003. "Synaptic Structure and Diffusion Dynamics of Synaptic Receptors." *Biology of the Cell* 95:465–76.
- Triller, Antoine, and Daniel Choquet. 2005. "Surface Trafficking of Receptors between Synaptic and Extrasynaptic Membranes: And yet They Do Move!" *Trends in Neurosciences* 28(3):133–39.
- Triller, Antoine, and Daniel Choquet. 2008. "New Concepts in Synaptic Biology Derived from Single-Molecule Imaging." *Neuron* 59:359–74.
- Trimble, W. S., and S. Grinstein. 2015. "Barriers to the Free Diffusion of Proteins and Lipids in the Plasma Membrane." *The Journal of Cell Biology* 208(3):259–71.
- Valtschanoff, J. G., and R. J. Weinberg. 2001. "Laminar Organization of the NMDA Receptor Complex within the Postsynaptic Density." *The Journal of neuroscience : the official journal of the Society for Neuroscience* 21(4):1211–17.
- Van Zundert, Brigitte, Akira Yoshii, and Martha Constantine-Paton. 2004. "Receptor Compartmentalization and Trafficking at Glutamate Synapses: A Developmental Proposal." *Trends in neurosciences* 27(7):428–37
- Verkhratsky, Alexei. 2005. "Physiology and Pathophysiology of the Calcium Store in the Endoplasmic Reticulum of Neurons." *Physiological reviews* 85:201–79.
- Vlachos, Andreas et al. 2009. "Synaptopodin Regulates Plasticity of Dendritic Spines in Hippocampal Neurons." *The Journal of neuroscience : the official journal of the Society for Neuroscience* 29(4):1017–33.
- Vlachos, Andreas et al. 2013. "Synaptopodin Regulates Denervation-Induced Homeostatic Synaptic Plasticity."
- Waites, Clarissa L. et al. 2009. "Synaptic SAP97 Isoforms Regulate AMPA Receptor Dynamics and Access to Presynaptic Glutamate." *The Journal of neuroscience : the official journal of the Society for Neuroscience* 29(14):4332–45.
- Wyszynski, M. et al. 1997. "Competitive Binding of Alpha-Actinin and Calmodulin to the NMDA Receptor." *Nature* 385:439–42.
- Wyszynski, M. et al. 1998. "Differential Regional Expression and Ultrastructural Localization of Alpha-Actinin-2, a Putative NMDA Receptor-Anchoring Protein, in Rat Brain." *The Journal of neuroscience : the official journal of the Society for Neuroscience* 18(4):1383–92.
- Yamazaki, M., R. Matsuo, Y. Fukazawa, F. Ozawa, and K. Inokuchi. 2001. "Regulated Expression of an Actin-Associated Protein, Synaptopodin, during Long-Term Potentiation." *Journal of neurochemistry* 79(1):192–99.
- Yang, Guang, Feng Pan, and Wen-Biao Gan. 2009. "Stably Maintained Dendritic Spines Are Associated with Lifelong Memories." *Nature* 462(7275):920–24.
- Yuste, R., and W. Denk. 1995. "Dendritic Spines as Basic Functional Units of Neuronal Integration." *Nature* 375:682–84.
- Yuste, R., a Majewska, and K. Holthoff. 2000. "From Form to Function: Calcium Compartmentalization in Dendritic Spines." *Nature neuroscience* 3:653–59.
- Yuste, Rafael. 2013. "Electrical Compartmentalization in Dendritic Spines." *Annual review of neuroscience* 36:429–49.

## REFERENCES

---

- Zhang, X. -I. et al. 2013. "Essential Role for Synaptopodin in Dendritic Spine Plasticity of the Developing Hippocampus." *Journal of Neuroscience* 33(30):12510–18.
- Zhou, Qiang, Koichi J. Homma, and Mu-ming M. Poo. 2004. "Shrinkage of Dendritic Spines Associated with Long-Term Depression of Hippocampal Synapses. TL - 44." *Neuron* 44:749–57.

# **Annexes**



**Table 1. Fluorescence microscopy data.** Quantification of SP distribution in dendritic spines in hippocampal neurons.

Condition	N (spines counted)	Spines with SP				
		location	n	SD	percent (%)	SD (%)
Endo-SP	998	neck	688	14.6	68.9	1.5
		head	148	11.2	14.8	1.1
		base	32	5.6	3.2	0.6
		<b>total</b>	<b>868</b>	<b>10.6</b>	<b>87.0</b>	<b>1.1</b>
mRFP-SP	965	neck	647	14.6	67.0	1.5
		head	157	11.5	16.3	1.2
		base	33	5.6	3.4	0.6
		<b>total</b>	<b>837</b>	<b>10.5</b>	<b>86.7</b>	<b>1.1</b>

**Table 2. Fluorescence microscopy data.** Effect of 4AP on SP clusters.

Condition		n (clusters)	Mean	SEM	Median	25% quartile	75% quartile	Mann Whitney U Test (control <i>versus</i> 4AP)
SP density	control	142	3.512	0.070	3.380	2.922	4.020	p=0.442
	4AP	144	3.558	0.062	3.451	3.008	4.080	
normalized SP intensity	control	149	1.060	0.025	1	0.832	1.232	p<0.001
	4AP	151	0.886	0.024	0.824	0.696	1.010	
normalized phalloidin intensity	control	149	1.083	0.028	1	0.825	1.331	p<0.001
	4AP	151	0.864	0.031	0.793	0.658	0.970	

**Table 3. STORM/PALM data.** Distribution of SP and F-actin in the spine neck (full width at half maximum, FWHM; nm).

FWHM Condition	N (spines)	Domain	Mean	SEM	Median	25% quartile	75% quartile	Mann Whitney U Test		
								phalloidin vs SP	control vs treatment	
control	34	phalloidin	105.44	4.28	105	85	125	p<0.001	phalloidin	SP
		SP	65.58	3.41	70	50	80			
4AP	29	phalloidin	104.13	5.31	100	85	110	p<0.001	p=0.652	p=0.101
		SP	76.37	4.66	75	65	90			
Latrunculin A	33	phalloidin	100.00	4.01	100	85	115	p<0.01	p=0.373	p<0.001
		SP	84.09	3.11	85	70	95			

**Table 4. SPT data.** Diffusion coefficient  $D_{1Dlong}$  ( $\mu\text{m}^2/\text{s}$ ) of membrane constructs in spine neck.

$D_{1Dlong}$ Molecules	Area in spines	n (trajectories)	Mean	SEM	Median	25% quartile	75% quartile	Kolmogorov-Smirnov test	
								spine SP (+)	no SP area
GFP-GPI	in SP area SP (+)	164	0.247	0.0131	0.197	0.102	0.357	in vs no SP area	SP (+) vs SP (-)
	no SP area SP (+)	170	0.232	0.0107	0.216	0.097	0.306	p=0.063	p=0.118
	SP (-)	268	0.256	0.0091	0.206	0.112	0.355		
TMD-pHluorin	in SP area SP (+)	58	0.168	0.0119	0.153	0.104	0.203	p=0.551	p<0.01
	no SP area SP (+)	57	0.203	0.0180	0.17	0.132	0.241		
	SP (-)	68	0.270	0.0210	0.22	0.152	0.356		
pHluorin-mGluR5	in SP area SP (+)	123	0.070	0.0054	0.051	0.027	0.105	p<0.001	p<0.05
	no SP area SP (+)	105	0.096	0.0054	0.082	0.057	0.122		
	SP(-)	89	0.122	0.0077	0.115	0.073	0.154		

**Table 5. SPT data.** Diffusion coefficient  $D_{1Dlong}$  ( $\mu\text{m}^2/\text{s}$ ) of pHluorin-mGluR5 in control condition and pharmacological treatments.

$D_{1Dlong}$ Condition	Area in spines	n (trajectories)	Mean	SEM	Median	25% quartile	75% quartile	Kolmogorov-Smirnov test				
								spine SP (+)	no SP area	control vs treatment		spine SP (-)
control	in SP area SP (+)	123	0.070	0.0054	0.051	0.027	0.105	in vs no SP area p<0.001	no SP area SP (+) vs SP (-) p<0.05	SP (+) spine		
	no SP area SP (+)	105	0.096	0.0054	0.082	0.057	0.122			in SP	no SP	
	SP (-)	89	0.122	0.0077	0.115	0.073	0.154					
4AP	in SP area SP (+)	135	0.082	0.0045	0.072	0.044	0.108	p<0.01	p<0.001	p<0.001	p=0.275	p<0.01
	no SP area SP (+)	293	0.116	0.0049	0.091	0.056	0.146					
	SP (-)	247	0.160	0.0066	0.138	0.091	0.197					
Latrunculin A 5-10 min	in SP area SP (+)	211	0.115	0.0053	0.091	0.059	0.152	p=0.094	p<0.001	p<0.001	p=0.616	p=0.071
	no SP area SP (+)	396	0.110	0.0043	0.089	0.056	0.135					
	SP (-)	439	0.140	0.0045	0.112	0.076	0.182					
Latrunculin A 15-20 min	in SP area SP (+)	92	0.129	0.0083	0.115	0.072	0.172	p=0.309	p=0.375	p<0.001	p<0.01	p<0.05
	no SP area SP (+)	262	0.133	0.0066	0.096	0.056	0.197					
	SP (-)	359	0.137	0.0054	0.104	0.058	0.189					